UNIVERSITETET
I OSLO

Master thesis Spring 2024

Biological Effects of Organic Coatings on Carbon Black Ultrafine Particles

Susanne Croff Larsen

Toxicology and Environmental Science
60 credits
Department of Biosciences
Faculty of Mathematics and Natural Sciences

2024

Biological Effects of Organic Coatings on Carbon Black Ultrafine Particles

This project was carried out as a collaboration between the University of Oslo and Norwegian Institute of Public Health.

UNIVERSITY OF OSLO

Acknowledgements

The presented thesis was carried out at the Department of Air Pollution and Noise of the Norwegian Institute of Public Health (NIPH) as a part of the ULTRHAS research project. It was supervised by main supervisor Senior Researcher Espen Mariussen (NIPH), and co-supervisors Post Doctorial Research Fellow Vegard Sæter Grytting (NIPH) and Professor Johan Øvrevik (University of Oslo and NIPH).

First off, I would like to express my heartfelt thanks to all my supervisors for their invaluable assistance throughout this process. Your feedback and guidance have played a crucial role in shaping this thesis, and I am deeply grateful for the time and effort you have dedicated to helping me. A special gratitude goes to my “lab-aunt” Tonje Skuland for her amazing technical guidance and supervision in the laboratory; your dedication and encouragement have meant a lot to me throughout this process. I would also like to extend my thanks to Jarle Ballangby for patiently answering all my questions, no matter how silly, and to Rune Becher for generously sharing his noodles and Pepsi Max with me every Sunday. Furthermore, I would like to thank the whole department for welcoming me with open arms. I truly felt like a part of the group, whether it was playing disc golf at Holmekollen or sharing the large assortment of cakes often found in the break room. Thank you all for sharing your knowledge, good mood, and support throughout my time at NIPH, I really appreciate it!

Thank you to my family and friends for their constant support. To my mother, thank you for always believing in me throughout my life, for flying all the way to Oslo to babysit during busy periods, and for your calming words during stressful times. To my dear friend Tala, thank you for all your good advice and uplifting words.

Last but not least, thank you so much to my person in life, Carl, and our son Leon. Carl, you have been my rock throughout this period! Thank you for all the late nights you spent listening to my worries, you understand me better than anyone else, and I know I can always rely on you for anything. Your support has been invaluable throughout this process, just as it is in all aspects of our lives together. Leon, my amazing child. You are the most precious and lovable boy anyone could ever ask for, who has lifted my spirit every day. You guys’ unconditional love has given me strength and motivation to do and be my very best. Love you forever.

Abstract

Particulate matter (PM) with an aerodynamic diameter below 2.5 µm ($PM_{2.5}$) has been identified as the main contributor to the adverse health effects associated with air pollution. However, current regulations might not allow for accurate assessment of the smallest fractions of $PM_{2.5}$. These fractions, called ultrafine particles (UFP), have a massive surface area and an ability to penetrate deep into the airways and translocate into circulation. This has contributed to the concept of the "Trojan Horse effect", which suggests that UFPs derived from combustion serve as carriers for organic contaminants, enabling them access to otherwise unreachable tissues and organs. Thus, the present study aimed investigate how the organic fraction of such particles contribute to biological effects associated with UFP exposure. To achieve this, cell models representing the human respiratory system were exposed to carbon black nanoparticles, either pristine or coated with organic compounds, and relevant biomarkers for cytotoxicity, pro-inflammatory responses, and xenobiotic metabolism were used to assess and compare effects. Printex 90 (P90) was used as a model for the carbon core of ultrafine combustion particles and Benzo[a]pyrene (B[a]P) and Pyrene (Pyr) as models for the organic compounds surrounding the core. Two different 3D lung models were employed and exposed at the air-liquid interface (ALI) to simulate the bronchial and alveolar epithelium, as well as the blood-air barrier at the respiratory bronchioles and alveolar-capillary barrier. Calu-3 bronchial epithelial cells or A549 alveolar epithelial cells were grown together with THP-1 derived macrophages in the apical compartment, while vascular endothelial cells Ea.Hy926 cells were grown in the basolateral compartment. The same cell lines were also subjected for monoculture experiments. Significant differences between P90 and P90+PAH were observed in Ea.Hy monocultures, with P90+PAH inducing an overall weaker response compared to P90 alone. In 3D cultures, B[a]P significantly increased both epithelial and endothelial CYP1A1 expression. Conversely, P90+B[a]P did not affect CYP1A1 expression. The inability to induce CYP1A1 may indicate that B[a]P was not readily bioavailable when particle-bound, and did not translocate across the epithelial barrier. Furthermore, the reduced effects of PAH-coated particles relative to uncoated particles suggest that P90s toxic potential was decreased when PAH was present. These findings indicate that the chemical properties of P90+B[a]P did not allow for B[a]P release, but instead mitigated P90 toxicity, possibly by reducing its specific surface area.

Abbreviations

ALI	Air-liquid interface
B[a]P	Benzo[a]pyrene
CB	Carbon Black
Ct	Quantification threshold
D_{ae}	Aerodynamic diameter
DEP	Diesel exhaust particles
DLS	Dynamic light shattering
DPBS	Dulbecco's phosphate-buffered saline
ELISA	Enzyme linked immunosorbent assay
EROD	Ethoxyresorufin-O-deethylase
LDH	Lactate dehydrogenase
PAH	Polycyclic aromatic hydrocarbons
PM	Particulate matter
$PM_{2.5}$	PM with aerodynamic diameter less than 2.5
PM_{10}	PM with aerodynamic diameter less than 10
Pyr	Pyrene
P90	Printex90
P90+B[a]P	Benzo[a]pyrene-coated Printex90
P90+PAH	PAH-coated Printex90
P90+Pyr	Pyrene-coated Printex90
RT-qPCR	Real time Quantitative reverse transcription polymerase chain reaction
RQ	Relative quantification
UFP	Ultrafine particles
µg	Microgram
µM	Micromolar
µm	Micrometer

Table of contents

1 Introduction

1.1 Air pollution

Air pollution refers to the contamination of the environment by airborne chemical, physical or biological agents that are detrimental to human health and the environment as a whole (Landrigan et al., 2018). Primary pollutants, such as dust and industrial emissions are released directly from the source, while secondary pollutants are created by the oxidation of a primary gas-phase pollutant (Karagulian et al., 2015). Although there are natural sources for several airborne pollutants, human activity such as industry, transportation and waste burning has unquestionably increased the occurrence in the environment and contributed to a level of unhealthy contamination (Landrigan et al., 2018). In fact, fossil fuel combustion and burning of biomass is estimated to be accountable for 85% of particulate airborne pollution (Landrigan et al., 2018). Consequently, air pollution constitutes one of the most prominent environmental threats against human health and was ranked as the fourth most significant risk factor for mortality worldwide in 2020 (HEI, 2020).The Global Burden of Disease (GBD) study estimated that air pollution was responsible for a total of 6.67 million premature deaths globally, with outdoor fine particles, with an aerodynamic diameter below 2.5 μm, identified as the main contributor and responsible for approximately 4.14 million of these deaths (HEI, 2020). A significant proportion of these fatalities are associated with pulmonary and cardiovascular diseases (Cohen et al., 2017). Simultaneously, over 99% of the world's population are living in conditions not met by The World Health Organization's (WHO) air quality guidelines level (WHO, 2021). In addition, factors such as population ageing, and the increasing prevalence of non-communicable diseases (Cohen et al., 2017) in combination with the effects of climate change, increasing population numbers, expanding urbanization, and economic growth, is likely to contribute to exacerbate the burden of air pollution on a global scale (Landrigan et al., 2018). Accordingly, particulate matter (PM) has been identified as a "criteria air pollutant" by the United States Environmental Protection Agency (EPA) (EPA, 2021) and is considered as the most reliable indicator for assessing the health impacts of ambient air pollution (Burnett et al., 2014).

1.2 Particulate matter

Airborne PM is a heterogeneous mixture of solid and liquid particles, with continuous variations in both size and chemical composition across different spatial locations and time intervals (Cheung et al., 2011). The inhalation of airborne particles from various sources has been linked to the development and exacerbation of several pathological conditions, such as asthma, chronic obstructive pulmonary disease, cardiovascular disease, as well as increased susceptibility to respiratory infections and cancers (Grahame et al., 2014; Kelly & Fussell, 2011). In fact, both short-term and long-term exposure to PM has been associated with an increase in pulmonary and cardiovascular morbidity and mortality. Aditionally, long-term exposure has been associated with perinatal outcomes (Hertz-Picciotto et al., 2005; Svendsen et al., 2007) and lung cancer (Lee et al., 2022), with the latter being classified as a causal effect of PM by IARC in 2013 (IARC, 2012)

In atmospheric science, ambient particles are commonly classified according to their modes of formation, which include nucleation mode, accumulation mode, and coarse mode (Whitby, 1978). The nucleation mode consists of the smallest particles in the distribution, typically formed from gaseous molecules, with sizes <0.05 µm (Spurny, 1998). These nucleation mode particles contribute to the formation of larger particles through the condensation of various gaseous molecules and coagulation with other nucleated particles (Spurny, 1998). The accumulation mode encompasses particles ranging from 0.1 µm to 1 µm in size, which have grown as a result of emissions from fine particles and dynamic events such as condensation and coagulation (Whitby, 1978). Conversely, the coarse mode typically includes larger particles (>1 µm) released through mechanical processes (Morawska et al., 2008).

The metrics most commonly used to describe PM is based on aerodynamic diameter (d_{ae}), with PM_{10} defined by having a d_{ae} less than 10 µm, fine particles ($PM_{2.5}$), with a d_{ae} less than 2.5 µm and ultrafine particles (UFP) characterized by a d_{ae} less than 0.1 µm (Cheung et al., 2011; Kelly & Fussell, 2012). Additionally, particles with a d_{ae} ranging from 2.5-10 µm ($PM_{10-2.5}$) is commonly referred to as coarse particles (Kelly & Fussell, 2012). Historically, most regulations and air quality standards have focused on $PM_{2.5}$, leading to a significant portion of scientific studies being conducted on fine particles (Kwon et al., 2020). However, it has been proposed that the diverse dynamics of PM-generation from various sources, as well as the trimodal particle size distribution of ambient PM presents significant limitations to current

regulations focused on $PM_{2.5}$ (Kwon et al., 2020). For instance, $PM_{2.5}$ does not effectively differentiate between PM produced through combustion (nucleation and accumulation mode) and PM generated mechanically (coarse mode). Furthermore, while PM_{10} and $PM_{2.5}$ are typically defined in terms of total mass concentration, UFPs have negligible mass but represent the main proportion of the total number of particles in the atmosphere, as illustrated in Figure 1 (Hofman et al., 2016). As $PM_{2.5}$ mass concentrations do not provide information on particle number concentration (PNC) or total surface area, it has been argued that the quantification of UFPs is more accurately expressed by PNC (Kelly & Fussell, 2012; Kwon et al., 2020).

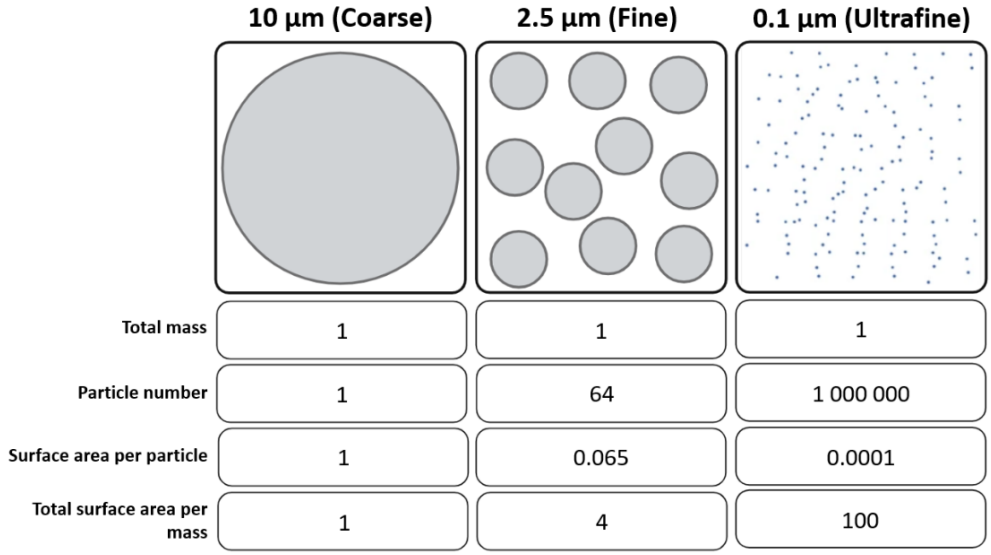

Figure 1. Comparison of particle number and surface area among particles based on total mass. The diagram operates under the assumption that all particles within each category are ideal spheres, possess uniform density, and are equally represented by mass. Coarse particles are assigned arbitrary values of 1 for mass, particle number, and surface area, serving as the reference point for comparison with other particle sizes. Adapted from Kwon et al. (2020). Created with Biorender.com.

A significant fraction of the exposure contributing to the adverse health effects of PM is concentrated within the urban areas, where there is a higher density of anthropogenic activity and emissions (Kelly & Fussell, 2011). Coarse particles in urban air tends to derive from wear-processes, such as road and tire abrasion. However, one of the greatest contributors to urban air pollution is $PM_{2.5}$ generated from combustion and transport processes (Karagulian et al., 2015). Furthermore, motor vehicles, particularly those associated with diesel engines, have been characterized as a main source of ambient UFP emissions (Kwon et al., 2020), with diesel

engine exhaust classified as a Group 1 carcinogen (carcinogenic to humans), and gasoline exhaust as a Group 2B (possibly carcinogenic to humans) by the IARC (IARC, 2013). Many primary components from vehicle exhaust and other combustion sources have short half-lives, and undergo extensive alterations through atmospheric aging processes, leading to intricate interactions between particles and gaseous components (Cassee et al., 2019). As a result, the particles to which the general population is exposed consist of dynamic and complex mixtures, including various components adsorbed to their surface areas. Moreover, particles with identical chemical composition may have very different behavior and toxic effect, depending on their size. As a particle decreases in size, its total surface area relative to mass and volume increases, which may alter its toxic potential compared to an equivalent larger particle (Renn & Roco, 2006). Consequently, the smallest fractions of particles within the $PM_{2.5}$ have a massive surface area accessible for adsorption or reactions that may increase the chemical reactivity of a given mass of the same material (Donaldson et al., 2005). Particles derived from combustion typically consist of a small carbonaceous core coated with metallic ashes and a large fraction of soluble organic constituents, and the effects of these particles are generally acknowledged to be caused by both the insoluble carbon core and the soluble organic fraction (Øvrevik et al., 2015). However, research indicates that combined exposure to combustion particles from various sources may exacerbate the adverse health effects linked to PM exposure, with lipophilic organic chemicals implicated in mediating these effects (Grytting et al., 2022; Totlandsdal et al., 2015). Due to UFPs ability to penetrate deep into the airways, it has been suggested that combustion particles mainly act as vectors for organic compounds, facilitating access to organs and cellular compartments that would otherwise be unreachable (Steiner et al., 2016). Consequently, there has been a concern that UFPs may play a significant role in many of the adverse health effects caused by PM exposure (Holme et al., 2019; Ma & Ma, 2002; Obot et al., 2002).

To account for this, determining the primary factors responsible for the adverse effects contributed by UFP exposure has been encouraged (Cassee et al., 2019; Kelly & Fussell, 2012; Kwon et al., 2020). While no single characteristic can explain all biological effects, certain factors may be more significant than others. For instance, if physical characteristics such as mass, are the main contributor to the adverse effects associated with UFPs, then specific regulations for UFPs might be necessary as current regulations do not consider PNC or total

surface area. Conversely, if UFPs from combustion mainly serve as carriers for contaminants, then PM_1 might a better measure as it more accurately targets combustion-derived particles, and their surface components, which mainly occur in the accumulation mode fraction between 0.1 and 1.0 μm (Kwon et al., 2020).

1.3 Polycyclic Aromatic Hydrocarbons

A major group of organic pollutants associated with combustion particles are polycyclic aromatic hydrocarbons (PAH). These pollutants are characterized by having two or more benzene rings fused together and are mainly generated from incomplete combustion of organic material (Bruschweiler et al., 2012; Dong et al., 2012). PAHs are generally characterized by having high melting and boiling points, low vapor pressure and low water solubility (Masih et al., 2012). When released into the atmosphere, PAHs can be found in either a gas phase or a solid phase, with the latter being associated with particles (Srogi, 2007). As the relationship between vapor pressure and size tend to correlate, PAH consisting of five or more aromatic rings tend to be sorbed onto particles, whereas PAH containing up to four aromatic rings are generally found in the gas-phase (Boström et al., 2002; Srogi, 2007). However, due to their predominant concentrations in ambient air compared to larger PAHs, three-and four ring PAHs also tend to be adsorbed to PM (Srogi, 2007). PAHs found in the gaseous phase of ambient air typically have short lifespans, lasting less than a day, thus approximately 70-90% of ambient PAHs are bound to PM (Piekarska, 2010). In contrast, PAHs associated with particles may persist for weeks and undergo long-range atmospheric transport (Singh et al., 2017; Yang et al., 2020).

PAHs have been shown to constitute a considerable proportion of the organic compound associated with urban air (Schober et al., 2006), and analysis of the surface composition of combustion particles has revealed that PAHs, such as benzo[a]pyrene (B[a]P) and pyrene (Pyr) have been detected in several urban areas (Baulig et al., 2004; Di Filippo et al., 2007; Schober et al., 2006; Westerholm et al., 1991). This is concerning, as certain PAHs is thought to have a significantly higher toxic potential compared to other substances in the organic fractions of PM (Boström et al., 2002).

The primary concern regarding PAH exposure is its association with lung cancer development. Certain PAHs contain a "bay-region" that increases susceptibility to metabolic activation (Vijayalakshmi & Suresh, 2008). Metabolization of these PAHs leads to the formation of reactive intermediates that can bind DNA, increasing the risk of mutations (Boström et al., 2002). Accordingly, the IARC has classified several PAHs as either known, likely, or possibly carcinogenic to humans (Group 1, 2A, or 2B). B[a]P is the only PAH classified as carcinogenic to humans (Group 1) (IARC, 2010), primarily due to the highly potent metabolites generated during its metabolism, such as benzo[a]pyrene-7,8-diol. These metabolites can undergo further metabolism into benzo[a]pyrene-7,8-diol-9,10-epoxides, which act on DNA, causing genotoxic and carcinogenic effects (Penning et al., 1999). Additionally, PAHs have been linked to various non-malignant health outcomes, including reduced lung function, worsened asthma symptoms, and increased morbidity and mortality associated with pulmonary and cardiovascular diseases (Cakmak et al., 2017; Horne et al., 2018; Zhang et al., 2017).

1.4 PM exposure in the respiratory tract

The human airways are continuously exposed to particles and pathogens in ambient air; thus, PM exposure primarily occurs through inhalation (Kelly & Fussell, 2012). As illustrated in Figure 2, the human respiratory tract can be divided into two distinct areas: the upper respiratory tract, consisting of the nose, pharynx, and larynx, and the lower respiratory tract, which includes the trachea, bronchial tree, and alveolar region (Patwa & Shah, 2015).

The lungs are a highly efficient system for oxygen delivery and decarboxylation, that enables gas exchange between the circulatory system and the external environment (Haddad & Sharma, 2023). Inhaled oxygen is

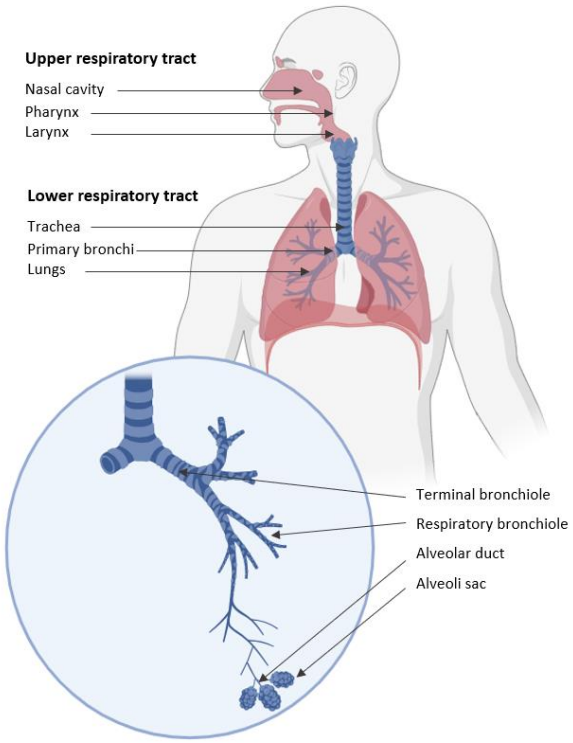

Figure 2. Schematic representation of the human respiratory tract. Adapted from Sracic (2016). Created with Biorender.com.

conducted through the bronchioles and transported to the alveolar region of the lungs (Patwa & Shah, 2015). The process of gas exchange then occurs through the functions of ventilation, which refers to the flow of air into and out of the alveoli, and perfusion, which is the flow of blood to alveolar capillaries (Haddad & Sharma, 2023).

The tracheobronchial airways are lined with a pseudostratified epithelium primarily composed of ciliated cells (Gao et al., 2015). Additionally, various other cell types, including basal progenitor cells, goblet cells, club cells, and neuroendocrine cells, are present both on the mucosal surface and within submucosal glands (Gao et al., 2015; Whitsett et al., 2010). These cells contribute to the secretion of fluids, mucins, and proteins vital for host defense (Gao et al., 2015; Whitsett et al., 2010). In contrast, the alveoli are mainly composed of epithelial cells, pneumocytes type I, covering most of the alveolar surface, and pneumocytes type II (Johnson et al., 2002). While type I cells facilitate gas exchange and maintain alveolar homeostasis, type II cells serve as secretory cells primarily tasked with synthesizing the lipid and protein constituents of pulmonary surfactant (Johnson et al., 2002).

The lung epithelium is the first line of defense against air pollutants, and the responses of the lung epithelial cells are crucial for development and aggravation of PM-induced pulmonary disorders (Carlier et al., 2021; Zhao et al., 2019). Furthermore, it has become evidently clear that endothelial responses and circulatory effects plays a crucial role in cardiovascular disorders representing a significant portion of the disease burden associated with exposure to PM (Brinchmann et al., 2018; Klein et al., 2017). A central part in protecting the underlying tissue against inhaled particles is the epithelium's ability to form tight barriers (Günther & Seyfert, 2018). The alveolar capillary barrier enables efficient gas-exchange, while simultaneously protecting the body against environmental pollutants, and prevents influx of protein-rich fluid from the blood into alveolar spaces (Günther & Seyfert, 2018). As such, the given effect of PM exposure is highly dependent on where in the respiratory tract the particles deposit.

Deposition is a process that determines the proportion of inhaled particles that becomes trapped in the respiratory tract and thereby preventing them from being expelled during exhalation (Carvalho et al., 2011; Darquenne, 2012). Deposition is influenced by several factors, including physical properties of the particles such as density, shape, solubility, and surface area, as well as individual-specific physical characteristics, such as breathing mode and

rate (Deng et al., 2019; Kim et al., 2015). However, the main contributor is widely recognized to be the particle size, with the aerodynamic diameter playing a crucial role in determining where in the respiratory tract deposition occurs (Carvalho et al., 2011; Kelly & Fussell, 2011).

Smaller particles generally tend to deposit deeper in the airways, with the exception of the smallest nanoparticles which deposit in the upper airways (Carvalho et al., 2011; Deng et al., 2019). As illustrated in Figure 3, coarse particles ($PM_{10\text{-}2.5\mu m}$), primarily deposit in the upper airways, but may reach the conducting airways and the pulmonary region to some extent. Fine particles, particularly the fraction smaller than 0.1 µm, may penetrate further into the airways and deposit in the pulmonary region, while particles between 1 and 0.1 um generally demonstrate low overall deposition. Furthermore, deposited particles tend to accumulate unevenly and preferentially settle in the branching regions of the airways. This results in significantly higher concentrations in certain areas, such as the bronchial bifurcations, compared to surrounding regions (Balashazy et al., 2003). The fate of inhaled particles further varies depending on the clearance mechanisms of the different regions of the airway. Particles deposited in the upper respiratory tract become entrapped in secreted mucus and are transported upward through the airways by the mucociliary escalator, eventually being

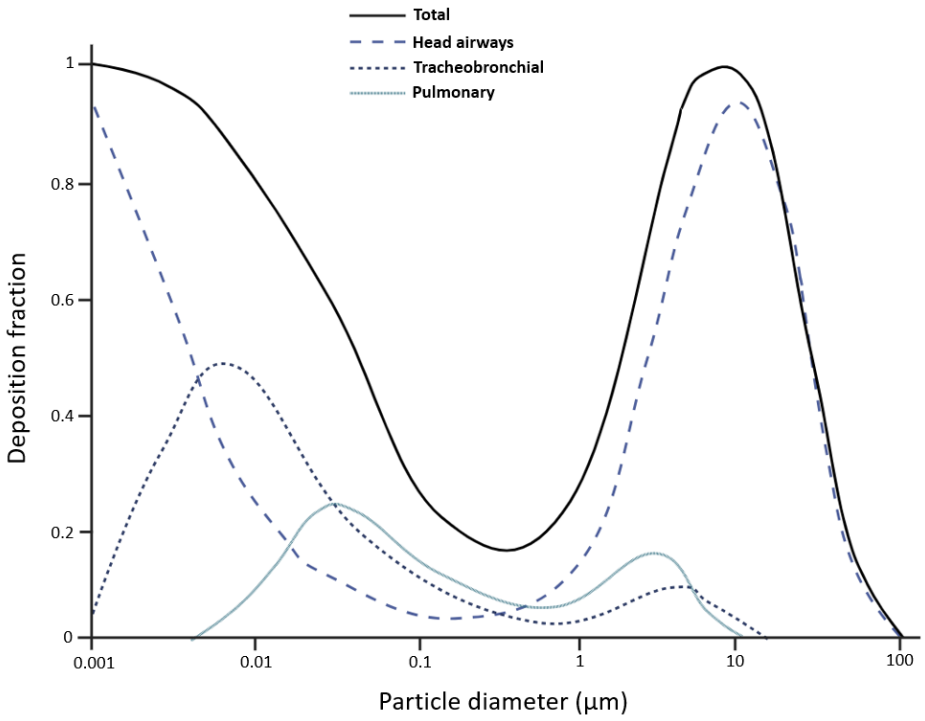

Figure 3. Predicted deposition fraction of particles in various regions of the human respiratory system based on particle size (µm). Adapted from US EPA (n.d). Created with Biorender.com.

expelled through coughing and swallowing (Bustamante-Marin & Ostrowski, 2017). In the alveolar region, where ciliated epithelial cells are absent, deposited particles are engulfed and eliminated by resident macrophages (Joshi et al., 2018).

1.5 Inflammatory responses of the lungs

There is strong evidence supporting a causal relationship between the induction of inflammatory responses in the airway mucosa and the development of respiratory diseases due to PM exposure (Aghasafari et al., 2019; Kelly & Fussell, 2011). Furthermore, as inflammatory responses in the airway can potentially trigger the release of cytokines and other pro-inflammatory mediators into the circulation, it has been theorized that this process could have a significant impact on the blood flow and progression of cardiovascular diseases (Donaldson et al., 2001; Grunig et al., 2014). Therefore, a causal association between the induction of pulmonary inflammation and the observed cardiovascular effects following PM exposure have been proposed (Grunig et al., 2014; Terzano et al., 2010)

Inflammation is the immune systems defense against harmful stimuli, such as toxic compounds and pathogens (Sherwood & Toliver-Kinsky, 2004). The inflammatory response involves a coordinated effort among numerous of cell types, and includes vasodilation, increased vascular permeability, the release of inflammatory mediators, as well as the recruitment of immune cells (Sherwood & Toliver-Kinsky, 2004). Acute inflammation is a crucial part of lungs innate defense mechanism. However, if not regulated properly, it can lead to tissue damage and disease (Chen et al., 2018). Conversely, anti-inflammatory cascades suppress the intensity of the innate response, but can cause abnormal wound repair and fibrotic diseases if left uncontrolled (Chen et al., 2018). Therefore, the progression of chronic inflammation and diseases is directly influenced by the balance between the pro- and anti-inflammatory responses (Keane & Strieter, 2002; Yamada et al., 2016). In respiratory diseases there is often found an abnormal accumulation of immune cells in the alveoli and parenchyma, indicating that perturbations in normal homeostatic control contributes to initiation and exacerbation of disease (Grommes & Soehnlein, 2011; Yamada et al., 2016).

Within the innate immune system, several studies have demonstrated that the aryl hydrocarbon receptor (AhR) is a key regulator of inflammatory responses (Beamer &

Shepherd, 2013). AhR is a highly conserved element throughout evolution and is found in most immune cell types and human tissues (Frericks et al., 2007). In the lungs, AhR serves as a regulator of the mucosal barrier and may influence immune responses by altering the gene expression, cell-cell adhesion, mucin production, and cytokine secretion (Shivanna et al., 2011; Wong et al., 2010). It plays an important role in xenobiotic metabolism and has an affinity for numerous endogenous and exogenous ligands, including various PAHs (Larigot et al., 2018; Stejskalova et al., 2011). The AhR is located in the cytosol but translocate to the nucleus upon ligand binding where it heterodimerizes with the AhR nuclear translocator (ARNT) (Larigot et al., 2018; Swanson, 2002). The AhR-ARNT complex then binds to an enhancer sequence known as dioxin response elements (DREs) and activates the transcription of genes encoding phase I and phase II metabolizing enzymes (Swanson, 2002). The human lung exhibits widespread distribution of xenobiotic metabolizing enzymes. However, CYP1A1 and CYP1B1, which are central in PAH metabolism, are particularly expressed and induced in ciliated bronchial epithelial cells and club cells, followed by alveolar type II cells and alveolar macrophages (Hakkola et al., 2020; Oesch et al., 2019). Additionally, numerous of genes involved in immune responses contain DRE sequences in their promoters and are influenced by AHR ligands, including chemokine CXCL8 (Øvrevik et al., 2014).

Cytokines and chemokines are essential components in the immune response (Turner et al., 2014). They are pleiotropic inflammatory signaling molecules and can have several effects depending on the cell type and tissue (Bukowski et al., 1994). Cytokines are key modulators in acute and chronic inflammation and participate in a complex network of interactions (Turner et al., 2014). Pro-inflammatory chemokines are primarily produced to recruit leukocytes to the site of injury or infection (Li et al., 2022). Combustion-derived particles have been shown to directly induce the release of inflammatory mediators in macrophages and lung epithelial cells, including IL-6 and CXCL8 (Hiraiwa & van Eeden, 2013; Landwehr et al., 2022; Refsnes et al., 2023) In response to cellular damage, IL-6 is rapidly and transiently generated and have been linked with numerous of inflammatory responses, including the exocytosis of macrophages and mast cells (Lacy & Stow, 2011; Murray & Stow, 2014). On the other hand, CXCL8 acts as a potent activator and chemoattractant for neutrophils, eosinophils, and T lymphocytes (Valderrama et al., 2022).

Inflammatory responses may arise directly from PM-induced release of cytokine/chemokine or indirectly through cytotoxicity, both of which appear to have a strong association with oxidative stress (Lenz et al., 2013; Li et al., 2008; Øvrevik et al., 2015). Combustion-derived particles can evidently induce the generation of reactive oxygen species (ROS) associated with such events (Donaldson et al., 2009; Øvrevik et al., 2015). Formation of ROS can be induced directly by the reactive surfaces of particles, as a result of contact with aqueous environments (Shvedova et al., 2012). Moreover, activation of intracellular signaling pathways, as well as mitochondrial disruption may instigate the production of superoxide ($O_2^{\bullet-}$) and hydrogen peroxide (H_2O_2) (Turrens, 2003). In addition, soluble organic components can generate ROS and reactive electrophilic metabolites through redox cycling and metabolic activation (Antiñolo et al., 2015). The formation of ROS may increase inflammatory responses by inducing expression of genes involved with regulating immune responses, such as various cytokines and chemokines (Liu et al., 2023; Mittal et al., 2014). Additionally, redox impairment may result in the accumulation of unfolded proteins, which in response initiates other inflammatory and stress signaling pathways (Zhang et al., 2019). At elevated levels, oxidative stress can induce toxicity, which might lead to significant cell damage and ultimately result in cellular apoptosis or necrosis (Turrens, 2003). However, while this clearly supports a link between PM exposure and inflammation, a growing body of evidence points towards PAHs and their substitutes as the causative agent for the particle-induced effects (Ho et al., 2022; Holme et al., 2019; Låg et al., 2020; Mills et al., 2011).

1.6 The “Trojan Horse” effect

The “Trojan horse effect” hypothesis suggests that combustion particles primarily act as carriers for a large fraction of soluble organics adsorbed to their surfaces, facilitating the release of these components into tissues and organs that would otherwise not be reached (Steiner et al., 2013). This has been demonstrated by Liu et al. (2021) who found that biochar fine particles enhanced the toxic effects of PAHs on the respiratory system. Their findings established an intracellular transfer of B[a]P into macrophages, where endocytosed particles acted as vectors to deliver B[a]P into the cells (Liu et al., 2021). The same study also found that biochar particles serve as long-term PAH reservoirs that continuously release B[a]P into the lung fluids. Exposure of pulmonary macrophages, epithelial cells, and local endothelial cells to

PAHs stimulates the release of pro-inflammatory mediators into the circulation, which in turn can induce systemic inflammatory responses that may amplify the pulmonary response (Øvrevik et al., 2015). Additionally, PAHs and other organic compounds have been shown to detach from PM and enter cells without the apparent endocytosis. In a study conducted by Penn et al. (2005) they found that PAHs were transferred from the particle surface and across the membrane of human bronchial epithelial cells. Their findings demonstrated that PAHs accumulated in lipid vesicles, and it was further found that the elevated concentration of PAHs resulted in potentiated PAH-toxicity upon release (Murphy et al., 2008; Penn et al., 2005). The detached PAHs may breach the epithelial barrier, where they can interfere with essential components in the bloodstream or be transported to and affect more distant cells and tissues (Boström et al., 2002). In a study by Gerde et al. (2001), it was presumed that approximately 30% of the B[a]P attached to soot particles was bioavailable when exposed to dogs. Further, they proposed that the majority of this bioavailable B[a]P would rapidly enter the bloodstream within minutes after deposition, with about 20% remaining in the bronchioles (Gerde et al., 2001). The influence of PAHs on respiratory tissues or cells may be mediated by classical AhR-dependent mechanisms, either directed through the regulation of immune responses or through the activation of Cytochrome P450 system (Larigot et al., 2018). In the latter instances, PAHs induces the expression of Cytochrome P450 enzymes (CYPs) and phase-II enzymes by binding to the AhR. This binding initiates the metabolization of PAH into reactive metabolites, a process observed to instigate the production of reactive species, including epoxides, peroxides, semiquinones, and quinones. Consequently, these reactive species contribute to the generation of ROS thereby eliciting inflammatory responses (Liu et al., 2023; Mittal et al., 2014). Importantly, while ROS are known to initiate inflammatory responses, they also participate in the regulation of cytokine gene expression. Studies suggest that ROS can exert regulatory effects on cytokine expression, potentially reducing their levels under certain condition (Morel et al., 1999).

This evidently demonstrates how PAHs and other organic components may act through their association with particles, however the “Trojan Horse” mechanisms relevance in the pathology of particle-induced disease is still not fully understood. Furthermore, the extent to which these mechanisms contribute to the biological effects associated with UFPs relative to the physical properties of the particles is still under debate. Although the reality likely falls

somewhere in between, systematically addressing these properties is essential to pave the way for more targeted regulations aimed at improving air quality and protecting public health (Figure 4).

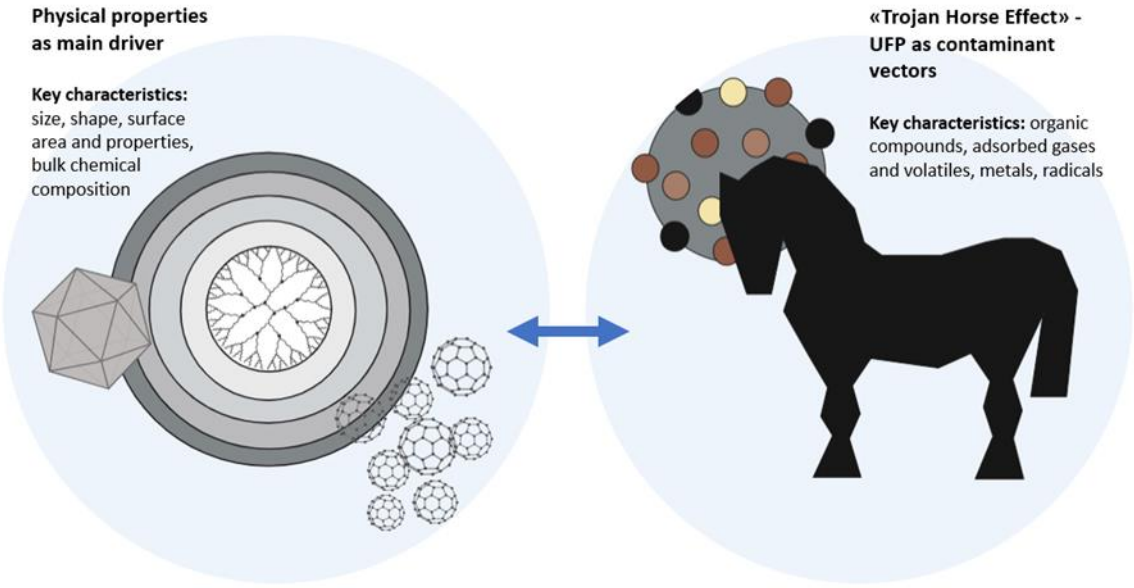

Figure 4. Physical properties vs "Trojan Horse" effect. Particle toxicity is influenced by various physical characteristics, including size, shape, and surface area, as well as chemical attributes such as soluble compounds and surface reactivity. One of the primary objectives of particle toxicology is to determine which characteristics predominantly drive the biological effects of UFPs; specifically, whether it is the physical properties of the particle, or the components adsorbed to its surface that are the main contributors to the effects. This clarification could have significant implications for the necessity of implementing specific regulations targeting UFPs. Created with Biorender.com.

1.7 Aims and Objectives

It has been suggested that a considerable portion of the adverse health effects associated with PM exposure can be attributed to the complex properties of combustion derived UFPs. These particles typically consist of a large fraction of soluble organic components adsorbed to their surfaces, which might play a central role in the PM-induced pulmonary and cardiovascular effects. To date, existing regulatory frameworks assess all PM equally, irrespective of their sources, with limit values based solely on mass concentration. However, extensive toxicological studies have demonstrated that particles originating from different sources can elicit varying health effects. Consequently, there is a need to further investigate the composition of UFPs, identifying specific compounds within the particles and gaining knowledge of how they influence these biological processes.

This study aimed to increase the understanding of the contribution of the organic fractions to the adverse effects associated with UFPs exposure, with emphasis on the "Trojan horse effect". To achieve this, the effects of exposure to combustion particles with or without the presence of PAHs were analyzed in *in vitro* cell models representing the human respiratory system. 3D lung cultures exposed at air-liquid interfaces were employed for their ability to simulate in vivo conditions more closely, while monocultures exposed in submerged conditions were utilized as a supplement to assess the biological effects. Printex 90, a sample of carbon black nanoparticles (primary particle diameter of 14 nm), was used as a model for the carbon core of ultrafine combustion particles, while Pyr and B[a]P were used to model the organic compounds surrounding the carbon core. Additionally, B[a]P was used for toxicity assays. It was hypothesized that PAH-coating of particles would increase the effects compared to the particles alone. This hypothesis was addressed through the following four overarching objectives:

1. Measure the metabolic activity and LDH release in monocultures exposed to various concentrations of Printex 90 (P90) and Printex with adsorbed PAH (P90+PAH) and PAH alone.
2. Measure the release of pro-inflammatory mediators IL-6 and CXCL8 in monocultures exposed to various concentrations of P90, P90+PAH and PAH alone.
3. Measure the CYP1A1 expression in monocultures and 3D cultures exposed to P90, P90+PAH and PAH alone.
4. Measure the IL-6 and CXCL8 expression, both protein and mRNA, in 3D cultures exposed to P90, P90+PAH and PAH alone.

2 Materials and methods

2.1 Materials

2.1.1 Ultrafine carbon black

Ultrafine carbon black P90 obtained from Degussa AG (Frankfurt, Germany) served as a model for the carbon core of ultrafine combustion particles. The primary particle size of P90 has been estimated to be 12–17 nm with a surface area of 272 m^2/g and an organic mass fraction below 1% (Stoeger et al., 2005). Notably, many of these particles have been shown to appear as parts of aggregates of various sizes when submerged in culture medium (Kang et al., 2013).

2.1.2 Polycyclic Aromatic Hydrocarbons

Benzo[a]Pyrene (B[a]P) B1760 and Pyrene (Pyr) 1885515 was acquired from Sigma-Aldrich (St. Lous, MO, USA). According to manufacturer's specification the molecular weight of B[a]P and Pyr is estimated to 252.31 and 202.25, respectively.

2.1.3 Cell lines and medium

In this study, human bronchial epithelial Calu-3 cell line, human lung carcinoma A549 cell line, endothelial cell line EA.hy926 and THP-1 macrophage-like cells was used. The cells were bought from American Type Culture Collection (ATCC) (Manassas, VA, USA). Culture medium Dulbecco's modified eagle medium (DMEM), Roswell Park Memorial Institute (RPMI) 1640 medium, Minimum Essential Medium and supplement GlutaMAX™ were obtained from Gibco (Waltham, MA, USA).

2.1.4 Reagents, chemicals and equipment used in the study

See Appendix A.

2.1.5 Solutions used in the study

See Appendix B.

2.2 Methods

2.2.1 Determination of P90 suspension

To ensure a well-dispersed and less aggregated P90 suspension initial experiments were conducted. This was done by preparing suspensions of 2 and 5 mg/mL P90 in DMEM with or without 0.05% bovine serum albumin (BSA). The suspensions were sonicated for 5 minutes (min) in a water-bath before Dynamic Light Scattering (DLS) analysis was performed.

2.2.2 Cytokine binding to particles

Carbonaceous particles have shown the ability to bind cytokines, thereby affecting the measured release of pro-inflammatory cytokines (Kocbach et al., 2008). Therefore, P90 potential to absorb CXCL8 were assessed. The procedure was conducted in a cell-free environment, with DMEM supplemented with FCS (10%) and BSA (0.05%) in order to investigate the impact of supplements on cytokine binding. Newly sonicated P90 in concentration of 0, 25 and 50 µg/ml was incubated with 800 pg/mL CXCL8 protein, diluted from ELISA standard (Invitrogen) in 1 mL medium in a humidified atmosphere at 37 ◦C and 5% CO_2. After 20 hours (h) incubation, the supernatant was collected and centrifuged for 10 min at 12000 revolutions per minute (rpm) to remove particles before cytokine analysis was performed.

2.2.3 Preparation of PAH solutions and particle suspensions

B[a]P and Pyr solutions were prepared in acetone as 0.18 mg/mL and 4 mg/mL stock solutions, respectively. Particles were coated with a given PAH as follows: a known amount of P90 was placed in a 10 ml glass vial before B[a]P and Pyr from the stock solutions was added and submerged in acetone, resulting in suspensions of 10 µg/mg particles and 100 µg/mg particles, respectively. Suspensions were then sonicated for 10 min before the vial was placed in fume hood without cover for the acetone to evaporate overnight. After evaporation of the solvent the particles were suspended in DMEM supplemented with 0.05 % BSA in a 2 mg/mL particle stock suspension and sonicated for 5 min. Prior to experiments all particle suspensions were

sonicated for an additional 5 min. The B[a]P solution used for toxicity assays was prepared in dimethyl sulfoxide (DMSO) as a 10 mM stock solution.

2.2.4 Measurement of PAH by fluorescence

To estimate the PAH concentration in supernatant relative to the nominal concentration, a semi-quantitative method was established. The method employed relied on the principle that most PAHs exhibit fluorescence, emitting characteristic wavelengths of light upon excitation which can be measured fluorometrically (Matuszewska & Czaja, 2020). As the fluorescence spectrum of each PAH is unique and depends on the number and arrangement of aromatic rings, this property can be utilized to identify different PAHs and quantify the amount present in a given sample (Matuszewska & Czaja, 2020).

After 20 h exposure, supernatants were collected from each sample, centrifuged twice at 1200 rpm and 12000 rpm to remove cells and particles, and diluted 1:20 in a solution of methanol and distilled water (50% methanol). B[a]P and Pyr stock solution were diluted in 1:1 dilution series with 50% methanol, resulting in standard curves with 8 concentrations ranging from 0-0.9 µg/mL and 0-1 µg/mL, respectively. Samples and standards were then transferred in duplicates to a black 96-well microtiter plate and fluorescence was measured using a Clariostar plate reader (BMG Labtech), with excitation and emission wavelengths at 379 and 425 nm for B[a]P, and 332 and 392 nm for Pyr. PAH concentrations were determined by linear regression of the standard curve.

2.2.5 Dynamic Light Scattering analysis

Dynamic light scattering (DLS) analysis was used to measure the hydrodynamic size of suspended particles. DLS works by detecting changes in the intensity of scattered light caused by the movement of particles in a solution. When light passes through a sample with particles, those particles scatter the light in different directions (Stetefeld et al., 2016). Because of their random motion (Brownian motion), the particles constantly change position, leading to fluctuations in scattered light intensity over time (Stetefeld et al., 2016). By studying these fluctuations, DLS can reveal the size distribution of particles in the sample. As smaller particles

diffuse more rapidly and larger particles more slowly, DLS was used to determine the size distribution between suspended particles as recommended by Stetefeld et al. (2016).

For DLS measurements, newly sonicated particle suspensions (200 µg/mL), P90, P90+B[a]P (10 µg PAH/ mg particle) and P90+Pyr (100 µg PAH/ mg particle) were transferred to disposable polystyrene cuvettes and measured at 25°C using a Zetasizer Nano system (Malvern Instrument Ltd). All data were obtained based on 3 repeated analyses of the same sample with no pause. For calculation of hydrodynamic size, the refractive (*R*i) and absorption indices (*R*s) of 1.36 and 00.10, respectively, for Printex 90 and standard optical and viscosity properties for H_2O.

2.2.6. Cultivation of cell lines

2.2.6.1 Calu-3 bronchial epithelial cells

Calu-3 is a human bronchial epithelial cell lines derived from lung adenocarcinoma and is known to form tight epithelial barriers *in vitro* (Shen et al., 1994). Calu-3 cells grown at air-liquid interface (ALI) have been shown to demonstrate many characteristics of the bronchiolar epithelium (Zhu et al., 2010).

The Calu-3 cells were maintained in Calu-3 culture medium consisting of MEM Glutamax™ with HEPES , supplemented with 10% inactivated fetal calf serum (FCS), penicillin (100 U/mL) and streptomycin (100 µg/mL) and 1 % non-essential amino acids (NEAA). The cells were cultured at 37°C in a humidified atmosphere with 5% CO_2. To ensure suitable cell culture conditions, medium was changed twice a week and cells were passaged once per week when reaching a confluency of about 70–80%. During passaging, cells were washed with Dulbecco's phosphate-buffered saline (DPBS) and detached by incubating them with 0.25 % trypsin-EDTA for approximately 5 min. Following this, trypsin stop solution consisting of DPBS with 20% Foetal bovine serum (FBS) was used to terminate the reaction.The cell suspension was then transferred to spin tubes, centrifuged at 1200 rpm for 5 min to pellet the cells, and supernatant was discarded. The pellet was resuspended in 2 mL medium, and a small aliquot of the cell suspension was mixed with 0.4% trypan blue to assess cell viability and to count the

cells. Cell counting was performed on a LUNA II automated cell counter, before $2x10^6$ cells were seeded in T75 flasks in a volume of 20 mL.

2.2.6.2 A549 alveolar epithelial cells

A549 is a human lung carcinoma cell line shown to exhibit the metabolic and transport properties consistent with alveolar type II epithelial cells in vivo (Foster et al., 1998; Lieber et al., 1976). In contrast to Calu-3, A549 cells are not able to develop tight junctions (Rothen-Rutishauser et al., 2008).

The A549 cells were cultured in A549 culture medium consisting of DMEM Glutamax™ supplemented with 10% FCS and 0.9% penicillin/streptomycin solution at 37°C in a humidified 5% CO_2 atmosphere. To secure appropriate cell culture conditions, medium was changed every other day and cells were passaged twice per week when reaching a confluency of about 70–80%. The procedure for passaging of cell culture was conducted as formerly described (see section 2.2.6.1) with minor modifications. Specifically, the cells were treated with 0.05 % trypsin-EDTA to detach the cells, and $0.5x10^6$ cells were seeded in T75 flasks on Mondays, whereas $1x10^6$ cells were seeded in 25 mL medium on Fridays.

2.2.6.3 Ea.Hy 926 endothelial cells

EA.hy926 (Ea.Hy cells) is an endothelial cell line derived by fusing human umbilical vein endothelial cells with the A549 cell line and displays features characteristic of vascular endothelial cells (Edgell et al., 1983).

The Ea.Hy cells were cultured in Ea.Hy culture medium consisting of DMEM Glutamax™ supplemented with 10% FCS, 2.75 mM Hepes and 0.9% penicillin/streptomycin solution at 37°C in a humidified 5% CO_2 atmosphere. The medium was changed every other day and cells were passaged twice per week to provide proper cell culture conditions. Passaging of the cell culture was conducted as outlined above (see section 2.2.6.1) with minor adjustments. Specifically, the cells were treated with 0.05 % trypsin-EDTA to detach the cells, and $0.75x10^6$ cells were seeded in T75 flasks on Mondays, whereas $1x10^6$ cells were seeded in 25 mL medium on Fridays.

2.2.6.4 THP-1 monocytes and preparation of THP1-derived macrophages

Phorbol myristate acetate (PMA) differentiated THP-1 cells have been shown to exhibit macrophage-like characteristics, such as an increased number of mitochondria and lysosomes (Daigneault et al., 2010).

THP-1 monocytes were maintained in THP-1 culture medium consisting of RPMI 1640 GlutaMAX™ supplemented with 10% FCS, 0.09% gentamycin solution and 1 mg/mL Na-pyruvate at 37°C in an atmosphere with 5% CO_2. To ensure proper cell culture conditions, the medium was changed every other day and cells were passaged three times per week. During passaging, cells were transferred to a spinning tube and centrifuged at 1200 rpm for 5 min. Pellet were then resuspended in THP-1 culture medium and $0.4x10^6$ cells were seeded in T75 flasks on Mondays, whereas $0.28x10^6$ cells were seeded in 25 mL on Fridays.

Differentiation into macrophage-like cells was initiated by incubating the cells in THP-1 culture medium with 32 nM PMA for 24h. The following day, the PMA containing medium was removed, cell culture was washed with DPBS, before incubated with 20 mL PMA-free THP-1 culture medium in T75 flasks for an additional 48 h.

2.2.7 Preparation and exposure of monocultures

To prepare monocultures for exposure, cells were seeded into 6-well cell culture plates at a density of $03x10^6$ cells/mL for Calu-3-, A549- or Ea.Hy cells and $0.5x10^6$ cells/mL for THP-1 derived macrophages (THP-1 macrophages) , in a total volume of 1.5 mL culture medium per well. To further ensure proper exposure conditions for monocultures, A549 and Ea.Hy cells were incubated for 48 h and Calu-3 cells and THP-1 macrophages were incubated for 72 h before exposure, with medium changed after 24 h.

Monocultures were exposed under submerged conditions in the same medium used to culture the cells. Prior to exposure, medium was replaced with fresh culture medium. Depending on the experimental protocol, monocultures were then exposed to various concentrations of newly sonicated P90, P90+B[a]P, P90+Pyr or B[a]P in a total exposure volume of 1 mL. The final exposure concentrations of particle suspensions were 12.5, 25, 50, 100 and 200 µg/mL, which corresponds to concentrations of 0, 0.125, 0.25, 0.5, 1, 2 µg/mL B[a]P and 1.25, 2.5, 5,

10 and 20 µg/mL Pyr. For B[a]P alone, the final exposure concentrations were 0.05, 0.01, 0.02, 0.6 and 2 µM. The concentration of DMSO (0.2%) and BSA (0.005%) was balanced between wells, and control received the same treatment in all experiments. Cells were then incubated for 20 h at 37°C in a humidified 5% CO_2 atmosphere.

2.2.8 Assembly of ALI 3D models

Two 3D lung models at ALI were developed utilizing either Calu-3 bronchial epithelial cell or A549 alveolar epithelial cell line. In both models, the epithelial cells were grown with a comparable quantity of THP-1 macrophages on the apical side of the permeable membrane insert, while vascular endothelial Ea.Hy cells were grown on the basolateral side of the membrane (Figure 5).

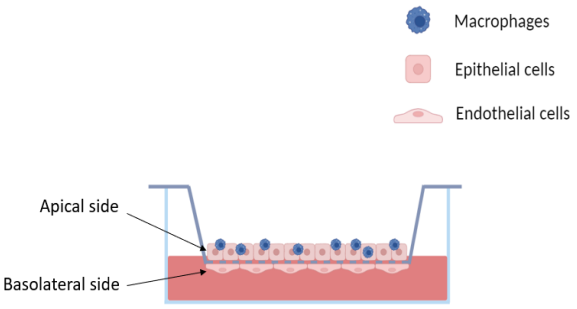

Figure 5. Assembled 3D culture at ALI, with Calu-3 or A549 epithelial cells grown together with THP macrophages on the apical side of the permeable insert, and endothelial Ea.Hy cells on the basolateral side. Created with Biorender.com.

2.2.8.1 Calu-3 model

The Calu-3 model was grown on 6-well Thincert® Cell Culture Inserts with 1 µm pores and required 10 days to prepare (Figure 6). On day 1, Ea.Hy cells were seeded onto the basolateral side of transwell inserts, at a density of $0.375x10^6$ cells/mL in a volume of 0.8 mL Ea.Hy medium ($0.3x10^6$ cells per insert) and incubated in 4 h at 37°C in a humidified 5% CO_2 atmosphere to ensure cell attachment. After incubation, medium was removed, inserts were transferred into 6-well cell culture plates and 2 mL Ea.Hy medium was added to the wells. Subsequently ,$0.2x10^6$ cells/mL Calu-3 cells were seeded into the apical compartment of the inserts, in a volume of 1.5 mL Calu-3 medium ($0.3x10^6$ cells per insert). The cell cultures were then incubated for 1 week at 37°C in a humidified atmosphere with 5% CO_2, with the medium changed twice. On day 8, the Calu-3 medium was removed, resulting in an ALI culture with the top epithelial layer exposed to air. The same day, THP-cells were seeded into T75 flasks and differentiated into macrophage-like cells incubating them with 32 nM PMA, as outlined above

(see section 2.2.6.4). After 48 h, the cell culture of THP-1 macrophages was washed twice with DPBS and detached by incubated them with 5 mL accutase for 15 min. Next, the cell culture was added 7 mL RPMI with 10% FCS, transferred to a spin tube and centrifuged at 1200 rpm for 5 min. Supernatant was discarded, and the pellet resuspended in 2mL 3D culture medium composed of equal parts DMEM:MEM:RPMI (3D culture medium). THP-1 macrophages were then added to the apical compartment at a density of $0.5x10^6$ per insert. After 4 h, the medium in the inserts were removed, 2 mL 3D culture medium was added to the basolateral comparment, and 3D culture was incubated for 24 h at 37°C in a humidified 5% CO_2 atmosphere before exposure.

2.2.8.2 A549 model

The A549 model was grown on 6-well Thincert® Cell Culture Inserts with 1 µm pores and required 6 days to prepare (Figure 6). On day 1, Ea.Hy cells were seeded on to the basolateral side of transwell inserts, at a density of $0.675x10^6$ cells/mL in a volume of 0.8 mL Ea.Hy medium ($0.54x10^6$ cells per insert) and incubated in 4 h at 37°C in a humidified 5% CO_2 atmosphere for the cells to attach. Following this, medium was removed, inserts were transferred into 6-well cell culture plates and 1.5 mL Ea.Hy medium was added to the wells. Subsequently, $0.135x10^6$ cells/mL A549 cells were seeded into the apical compartment of the inserts in a volume of 0.8 mL Ea.Hy medium ($0.108x10^6$ cells per insert). The cell culture was then incubated for 72 h at 37°C in a humidified 5% CO_2 atmosphere. On day 4, medium in both well and insert was replaced by 2 mL 3D culture medium, and THP-cells were seeded into T75 flasks and differentiated into macrophage-like cells by incubating them with 32 nM PMA, as outlined above (see section 2.2.6.4). On day 6, medium was replaced with 2 mL fresh 3D culture medium and THP-1 macrophages were detached from T75 flasks using accutase, as formerly described (see section 2.2.8.1) and seeded into the apical compartment of the inserts at a density of $0.5x10^6$ per insert. After 4 h the medium in the inserts were removed to put 3D culture in ALI and incubated for 24 h at 37°C in a humidified 5% CO_2 atmosphere before exposure.

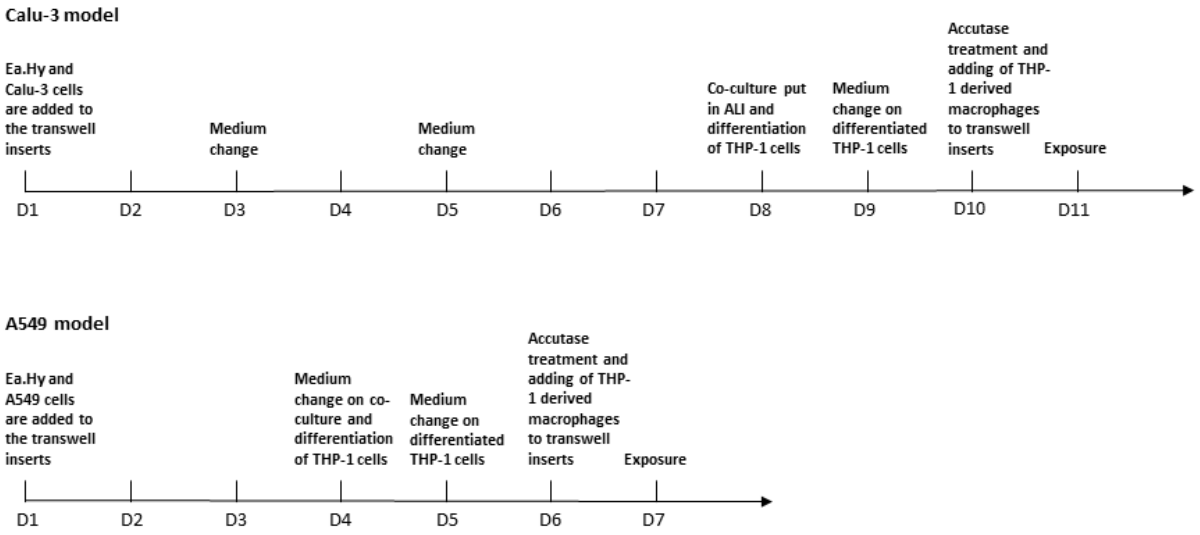

Figure 6. Timeline for ALI 3D model assembly (D = Day).

2.2.9 Exposure of 3D cultures

ALI exposure was performed using the VITROCELL® Cloud alpha 6 exposure system (VITROCELL®) equipped with a nebulizer with a droplet mass median aerodynamic diameter (MMAD) from 4-6 µm, with a recommended nebulization volume of 0.2 mL, and a Quartz Crystal Microbalance (QCM) for measuring of the deposited mass. In a Vitrocell® Cloud exposure system the suspension is converted to aerosols by the nebulizer. The generated aerosols are then introduced into the exposure module, where a homogenous mix of the aerosols is distributed evenly across the cells (Figure 7).

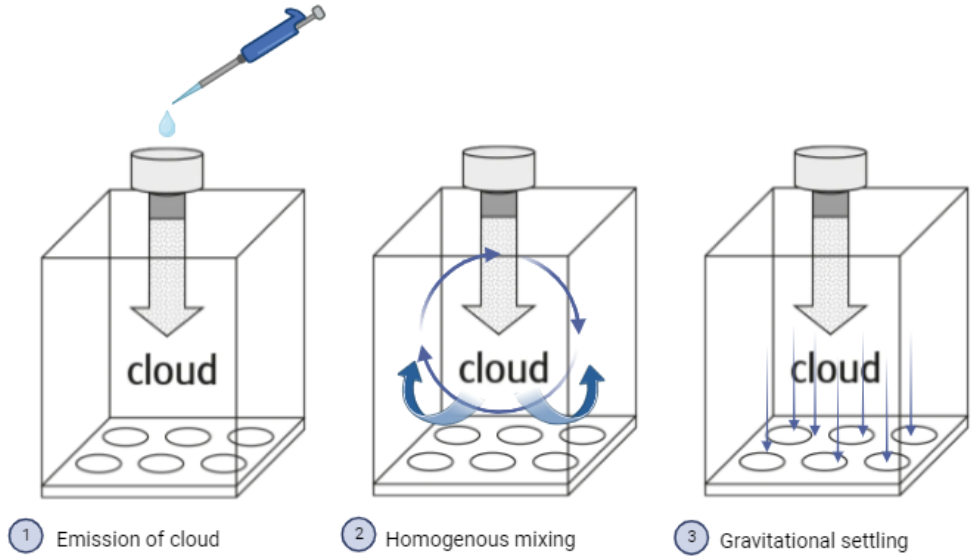

Figure 7. Three different phases to ensure that a homogenous mix of the aerosols is distributed evenly across the cells during Exposure in the Vitrocell® Cloud alpha 6 system. Adapted from VITROCELL® (n.d.). Created with Biorender.com.

Prior to experiment, nebulizer performance was determined by passing 3 x 200 µL purified water through the system. Based on the results, nebulizer throughput time was set to 1 minute. For the exposure, duplicates of transwell inserts were transferred to DPBS containing wells in the Vitrocell Cloud system which were set to hold a temperature of 37 °C. Depending on the experiment, cells were then exposed to 3 rounds of 0.167 mL purified water, P90 (2 mg/mL), P90+B[a]P (2 mg/mL with 10 µg PAH/mg particle), or B[a]P (0.08 mM), with an additional 4th exposure to 0.167 mL purified water to enhance particle throughput. The total volume was approximately 0.5 mL, corresponding to theoretical exposure concentrations of 5.2 µg/cm^2 P90 and 0.052 µg/cm^2 B[a]P with 75% deposition efficiency, which is consistent with the nominal concentration of 50 µg/mL used in monoculture experiments. Additionally, a 5-minute deposition time between each round of exposure was included to ensure gravitational settling. All procedures were conducted under a sterile fume hood, and the nebulizer was thoroughly rinsed with purified water between uses. After exposure, duplicate inserts were distributed between two new 6-well plates containing 2 mL fresh culture medium. The plates were then incubated for either 3 or 6 h at 37°C in a humidified atmosphere with 5% CO_2.

2.2.10 Estimation of cytotoxicity in monocultures

2.2.10.1 Cell viability in monocultures by AlamarBlue assay

The viability of the cells was determined using the alarmarBlue ™ assay (Invitrogen). The assay relies on the enzymatical conversion of the blue, non-fluorescent dye resazurin to the pink, fluorescent resorufin in response to cellular metabolic reduction. The reduction of resorufin can be detected fluorometrically, and allowed for quantitative measurement of cell viability. (Bopp & Lettieri, 2008).

After supernatant was harvested for the other assays, the wells were incubated for 1 h with alarmarBlue solution diluted 1:10 in culture medium. Subsequently, duplicates of 100 µL of supernatant were transferred to a 96-well microtiter plate and fluorescent was measured using a Clariostar plate reader, with excitation and emission wavelengths set to 545 and 600 nm, respectively.

2.2.10.2 LDH release in monocultures by LDH assay

The release of lactate dehydrogenase (LDH) was determined using LDH assay detection kit (Roche). LDH is a cytoplasmic enzyme released upon necrosis, and the assessment of cytotoxicity was thereby based on the LDH activity in the cell culture supernatant. To quantify LDH activity, a reaction mix comprising of diaphorase/NAD+ mixture, 2-(4-iodophenyl)-3-(4-nitrophenyl)-5-phenyl-2H-tetrazolium (INT), and sodium lactate was added to the supernatant. In the subsequent reaction, LDH catalyzed the conversion of lactate to pyruvate, generating NADH as a byproduct. NADH, in turn, reduced INT to form a red, water-soluble formazan dye that can be readily quantified by measuring its absorbance at 490 nm. Thus, the amount of formazan formed is directly proportional with the LDH activity, and correlates directly to the number of damaged cells (Kumar et al., 2018).

For LDH assay, supernatant was transferred into 1.5mL Eppendorf tubes, centrifuged twice at 1200 rpm and 12000 rpm, and diluted 1:4 in culture medium. A positive control was prepared by incubating cells for 20 min with 2% Triton-X in culture medium. To confirm cell lysis, the effect of Triton-X was investigated under a microscope. The resulting LDH max control was

then transferred to 1.5 mL Eppendorf tubes, centrifuged at 1200 rpm, to remove cells and diluted 1:5, 1:10 and 1:20 in culture medium. A standard was prepared by diluting a LDH concentrate stock to a 1000 mU/mL stock solution and diluting this further in a 1:1 dilution series, resulting in a standard curve with 8 concentrations ranging from 0-1000 mU/mL.

Samples, LDH max and standard were then transferred to a 96-well flat bottom microtiter plates in a volume of 50 µL/ well. For the reaction to start, 50 µL reaction mix consisting of catalyst (diaphorase/NAD+) and dye solution (INT and sodium lactate) was added. The plate was then incubated at room temperature in the dark for approximately 20 min until adequate color development was established. Absorbance was measured and quantified at 490 nm on a Sunrise plate reader (Tecan) equipped with dedicated software Magellan V 1.10. To relate the measured LDH concentration to cytotoxicity (% necrosis), following formula was used (Formula 1):

(1)

$$Cytotoxicity\ (\%) = \frac{ABSsample - ABSmedium}{ABSmax - ABSmedium}$$

ABSsample = absorbance for sample

ABSmedium = absorbance for medium

ABSmax = absorbance for positive control

Formula 1

2.2.11 CYP1A1-activity in monocultures by EROD assay

To estimate CYP1A1 activity in monocultures, a protocol for the ethoxyresorufin-O-deethylase (EROD) assay was established. This method relied on the AhR-mediated induction of cytochrome P450 1A family enzymes (CYP1A), which are responsible for metabolizing various PAH compounds, including B[a]P. The EROD assay measured the conversion of ethoxyresorufin to resorufin by CYP1A enzymes (Schiwy et al., 2015). This conversion produces fluorescence, allowing for quantification of CYP1A activity over time. To standardize

results, enzyme activity was normalized to the total protein content in the samples (Schiwy et al., 2015).

Prior to EROD analysis, cells were seeded into a 96-well microtiter plate, with a density of 30.000 cells/well, leaving 3 columns empty to accommodate the resorufin and protein standards for the EROD and protein assays, respectively. A549 and Ea.hy cells were exposed the following day, while Calu-3 cells were exposed after 48 h. For exposure, triplicate wells were incubated with various concentrations of B[a]P-solution (0.02, 0.05, 0.1, 0.2, 0.6, 2 µM), newly sonicated P90 or P90+B[a]P suspension (6.25, 12.5, 25, 50, 100, 200 µg/mL P90 or with 10 µg B[a]P/mg P90), in a total exposure volume of 200 µL. Culture medium with DMSO (0.2%) or BSA (0.005%) were used as controls. The plate was then incubated for 20 h at 37°C in a humidified 5% CO_2 atmosphere.

For EROD analysis, 1 µM resorufin diluted in Hank's Balanced Salt Solution (HBSS) was used to make a 1:1 dilution series resulting in a standard curve with 11 concentrations ranging from 0-1 µM. Subsequently, 7-etoxyresorufin (substrate) was diluted to 1 µM in HBSS. After exposure, cells were washed twice with DPBS before added 200 µL substrate, and standard was added to the cell-free wells. The fluorescence was then measured for approximately 80 min (70 cycles) using a Clariostar plate reader, with excitation and emission wavelengths set at 545nm and 600nm, respectively. After analysis the plate was washed twice with HBSS to remove the reagents from the EROD assay and stored at -80°C.

For the following protein assay DC™ Protein Assay Kit (BioRad) was used. The plate was thawed in room temperature and cells lysed by adding 20 µL 1% Triton in HBSS (lysis buffer). A dilution series from 40 mg/mL to 0.3125 mg/mL resorufin protein was made in lysis buffer and added to the cell-free wells. Furthermore, 25 µL of protein solution A + S (BioRad) and 200 µL of protein solution B (BioRad) was added to the wells, resulting in a total volume of 245 µL/well. The plate was then incubated in the dark for approximately 15 min. To prevent interference from particle residues, the plate was centrifuged at 4000 rpm and samples were transferred to a new 96-well microtiter plate. Absorbance was measured at 750 nm by using a Sunrise plate reader and Magellan software (V 1.10) was used to estimate total protein concentration from the standard curve.

2.2.12 Estimation of cytokine release by ELISA

To measure the release of IL-6 and CXCL8 in cell culture supernatant, sandwich enzyme-linked immunosorbent assay (ELISA) cytosets (Invitrogen) were used. In sandwiched ELISA, the protein of interest becomes sandwiched between two layers of antibodies, the pre-coated capture antibody, and the second (detection) antibody (Lakshmipriya et al., 2016). In this study, the amount of IL-6 and CXCL8 protein was quantified by adding a substrate solution containing Streptavidin horseradish peroxidase (HRP), which reacted with the enzyme-antibody-target complex to produce a color change. This color was then measured spectrophotometrically, with the intensity of the color being directly proportional to the concentration of IL-6 and CXCL8 present in the sample (Tabatabaei & Ahmed, 2022)

For solutions used in ELISA, see Appendix B.

Prior to ELISA, a 96-well microtiter plate was coated with a capture antibody solution for the respective targeted protein, covered, and incubated at 4°C overnight. The following day, the plates were washed in plate washer and Blocking solution was added before the plate was covered and incubated at room temperature for 1 h. Simultaneously, samples were thawed in room temperature and diluted in Diluent buffer. Standards were prepared by diluting IL-6 or CXCL8 concentrate in a 1:1 dilution series, resulting in seven-point standard curves with concentrations ranging from 0-1000 pg/mL and 0-800 pg/mL, respectively.

The plate was washed before duplicates of each sample and standard were added to the wells and incubated with detection antibody for 2 hours. Following this, the plate was incubated for 30 minutes with an HRP solution. Then, the plate was incubated with TMB solution, awaiting color change. Throughout the process, all incubation steps were performed on the microplate shaker in the dark, and the plate was washed between each addition of reagent. When adequate color development was reached, the reaction was stopped with Stop solution. The absorbance was measured at 450 nm on a Sunrise plate reader, and the concentration (pg/mL) estimated from the standard curve using Magellan software (V 1.10).

2.2.13 RNA isolation of 3D cultures

Prior to RNA isolation, cells from the apical and basolateral sides of inserts were washed twice with DPBS before lysed with RLT lysis buffer (Qiagen) with 1% mercaptoethanol. To homogenize the cells and reduce viscosity, the cell suspensions were transferred to QIA-Shredder tubes and centrifuged at 12000 rpm. After centrifugation, filters were disposed, and the tubes were stored at -70°C for subsequent processing.

RNA was isolated using the RNeasy miniprep kit (Qiagen). Cell lysates were thawed in a water bath and diluted 1:1 in water with 70% ethanol. The resulting mixture was transferred to RNeasy spin columns and centrifuged at 12000 relative centrifugal force (g) to remove contaminants. Subsequently, the columns were washed with RW1 buffer (Qiagen) before treated with DNase for 15 min, to destroy bound DNA. After incubation at room temperature, column filters were washed with RW1 buffer (Qiagen) and RPE buffer (Qiagen). Note that the samples were centrifuged at 12000 g and the filtrate was removed between each step. After the washing process, the column filters were transferred to 1.5 mL Eppendorf PCR tubes and RNA eluted with elution buffer by centrifugation. The quantity and quality of the isolated RNA were then measured at 230, 260 and 280 nm with micro spectrophotometer NanoDrop200 (Thermo Fisher Scientific Inc.), before samples were stored at -80°C.

2.2.14 Gene expression in 3D cultures

Real time quantitative reverse transcription polymerase chain reaction (RT-qPCR) was used to detect and quantify RNA. In this process, RNA was first reversed transcribed to generate complementary DNA (cDNA), which served as the template for the qPCR. In RT-qPCR, the target gene was copied by adding forward and reverse primers specific to that gene. In addition to primers, a probe centrally positioned in the gene sequence was introduced. During transcription, this probe dissociates, triggering a detectable change in light intensity. For each copy, the amount of DNA increases, and thus the light intensity increases (Wong et al., 2015). Based on this, fluorescence was utilized to measure the quantity of amplification product in each cycle. The quantification cycle (Ct) in a qPCR amplification reaction is then used to determine the fractional number of cycles required for the fluorescence signal to surpass a predetermined quantification threshold. This threshold is dependent on the initial

concentration of the target gene in the sample; higher concentrations result in lower Ct values, as the fluorescence reaches the threshold earlier in the amplification process (Bustin et al., 2009).

2.2.14.1 cDNA synthesis

The RNA was reversed transcribed into complementary DNA (cDNA) using a High-Capacity cDNA Reverse Transcription kit (Applied Biosystems). Prior to the cDNA synthesis, a master mix (see Appendix B) containing reverse buffer, deoxynucleotide triphosphate (dNTP), random primers, multiscript reverse transcriptase and nuclease-free water was made and 12.5 µL distributed to PCR tubes. RNA (1000 ng) from each sample were transferred to the tubes, resulting in a total volume of 25 µL per tube. The PCR strips were then spun down, and the cDNA synthesis was performed in a CFX96 Touch Real-Time PCR Detection System (BioRad) at 37° C for 2 h. Samples were stored in the refrigerator overnight, or at -80°C for longer periods.

2.2.14.2 Real Time qPCR

The gene expression of glyceraldehyde 3-phosphate dehydrogenase (GAPDH), IL6, CXCL8 and cytochrome P450 1A1 (CYP1A1) was determined using RT- qPCR. Analysis was performed on duplicate samples, with Taqmans primers/probes and PCR universal Master Mix. Prior to analysis, real time master mix was made by mixing PCR universal master mix and respective primer, and cDNA was diluted to 1 ng/mL with RNase free water. Subsequently, 11 µL of the various master mixes and internal control was the transferred to a PCR plate before 9 µL cDNA (1ng/mL) was added, resulting in a total volume of 20 µL per well. The plate was then sealed with an optical adhesive cover centrifuged at 300 g for 1 min and transferred to a CFX96 Touch Real-Time PCR Detection System where the standard 7500 PCR mode was run with following temperature and time setting:

50°C	2 min	
95 °C	10 min	
95 °C	15 sec	40 cycles
60 °C	1 min.	
4 °C		

The relative change in gene expression compared with to control was determined using the normalized Ct values (ΔCt) and expressed as fold increase compared with control with GAPDH serving as the reference gene. Software CFX Maestro (Version 2.2) was used to calculate the fold-change in expression of the target gene relative to the reference gene, i.e., the relative quantification (RQ), with following formula (Formula 2):

(2)

$$RQ = 2^{-\Delta\Delta Ct},\ \Delta\Delta Ct = (Ct_{target\ gene} - Ct_{GAPDH})\ exposed - (Ct_{target\ gene} - Ct_{GAPDH})\ control$$

$Ct_{target\ gene}$ = Ct value for target gene

Ct_{GAPDH} = Ct value for reference gene

Control = unexposed cells

Formula 2

2.2.15 Statistical analysis

All statistical analyses were performed in GraphPad Prism software (version 9.0.0). Two-way ANOVA was used to determine the differences between groups. If the row or column factors were significant, respective Dunnett's or Šídák's post-tests were performed. One-way ANOVA was used to investigate the influence of B[a]P compared to control. P-values below 0.05 were considered to reflect significant differences. To evaluate the distribution of the residuals, QQ-plots and Spearman's tests were used. Log-transformation was performed if the data did not meet model assumptions of normality and homoscedasticity. For qPCR measurements, statistical analysis was conducted using the mean ΔCt values of 3 experiments (see Appendix C7). The ΔCt value represents the difference in quantification

cycle (Ct) values between the target gene and a reference gene, serving as a measure of relative expression and was calculated using following formula (Formula 3):

(3)

$$\Delta Ct = (Ct_{target\ gene} - Ct_{GAPDH})$$

$Ct_{target\ gene}$ = Ct value for target gene

Ct_{GAPDH} = Ct value for reference gene

Formula 3

3 Results

For an overview of data presented in the figures, see Appendix C.

3.1 Characterization of Printex suspension

Concentrations of 2 and 5 mg/mL P90 were suspended in DMEM with or without 0.05% BSA. Size (mean ± SD) of particles in the suspensions were determined by using DLS analysis. The hydrodynamic diameter of the particles in the various stock suspensions were as follows; 2 mg/mL with BSA: 0.715 ± 0.021 µm, 2 mg/mL without BSA: 2.698 ± 0.119µm, 5 mg/mL with BSA: 1.181 ± 0.364µm and 5 mg/mL without BSA: 2.625 ± 0.228µm.

Analysis showed that 2 mg/ml P90 in medium added 0.05% BSA had the most suitable homogenous size distribution and were therefore chosen as the prime stock suspension used in the experiments. Furthermore, the P90 stocks ability to bind cytokine was assessed. The result demonstrated that P90 does not bind CXCL8 under the employed conditions (Table 1).

Table 1. CXCL8 concentration was measured in cell-free system exposed to various concentrations of P90 for 20 h. The nominal CXCL8 concentration was 800 pg/mL per sample. The results are presented as the measured mean ± SD CXCL8 concentration of 1 experiment.

Table 1 IL-8 concentrations (pg/mL) in samples (mean ± SD)

P90 (µg/mL)	IL-8 concentration
0	757.02 ± 99.99
50	766.27 ± 114.50
100	792.62 ± 175.76

Throughout the study, the particle size distribution in P90, P90+Pyr and P90+B[a]P was determined by DLS. The hydrodynamic diameter (mean ± SD) of the particles in the various stock suspensions were as follows; P90: 0.459 ± 0.019 µm, P90+Pyr: 0.239 ± 0.004 µm and P90+B[a]P: 0.237 ± 0.043 µm. Notably, the particles in newly made P90 stock were estimated to be 1.297 ± 0.081 µm.

3.2 PAH concentrations in exposure medium

The nominal concentration of Pyr was largely present in the medium post-exposure of all cell types (Table 2), with the exception of the highest concentrations, which were approximately halved. Conversely, no B[a]P were found in the supernatants (Table 3).

Table 2. Pyr was measured fluorometrically in medium of Calu-3, Ea.Hy and THP-1 monocultures exposed to various concentrations of P90+Pyr for 20 h. Pyr concentrations of 0, 1.25, 2.5, 5, 10, 20 µg/mL corresponds to the 0-200 µg/mL concentrations of P90+Pyr. The results are presented as mean ± SD for 3 experiments, with limit of quantification (LOQ) = 0.015.

Table 2 Pyr concentrations (µg/mL) in samples (mean ± SD)

Nominal [Pyr] (µg/mL)	Calu-3	Ea.Hy	THP-1
0	< 0.015	0.182 ± 1.010	0.342 ± 0.563
1.25	2.253 ± 1.381	2.016 ± 1.428	3.133 ± 0.521
2.5	3.763 ± 1.017	2.567 ± 1.247	4.599 ± 0.412
5	5.319 ± 1.193	5.779 ± 1.558	4.702 ± 1.040
10	6.728 ± 1.228	8.383 ± 1.317	6.980 ± 1.700
20	8.845 ± 1.655	11.464 ± 1.418	10.588 ± 0.222

Table 3. B[a]P was measured fluorometrically in medium of Calu-3, Ea.Hy and THP-1 monocultures exposed to various concentrations of P90+B[a]P for 20 h. B[a]P concentrations of 0, 0.125, 0.25, 0.5, 1, 2 µg/mL corresponds to the 0-200 µg/mL concentrations of P90+B[a]P. The results are presented as mean ± SD for 3 experiments, with LOQ = 0.014.

Table 3 B[a]P concentrations (µg/mL) in samples (mean ± SD)

Nominal [B[a]P] (µg/mL)	Calu-3	Ea.Hy	THP-1
0	< 0.014	0.012 ± 0.829	< 0.014
0.125	< 0.014	< 0.014	< 0.014
0.25	< 0.014	< 0.014	< 0.014
0.5	< 0.014	0.002 ± 0.660	< 0.014
1	< 0.014	0.302 ± 0.846	< 0.014
2	< 0.014	< 0.014	< 0.014

3.4 Determination of cytotoxicity in monocultures

The cell viability of monocultures following exposure was determined by using AlamarBlue™ assay. A significant decrease in cell viability relative to control was found in all monocultures exposed to 200 µg/mL P90, except the Calu-3 cells (Figure 8).

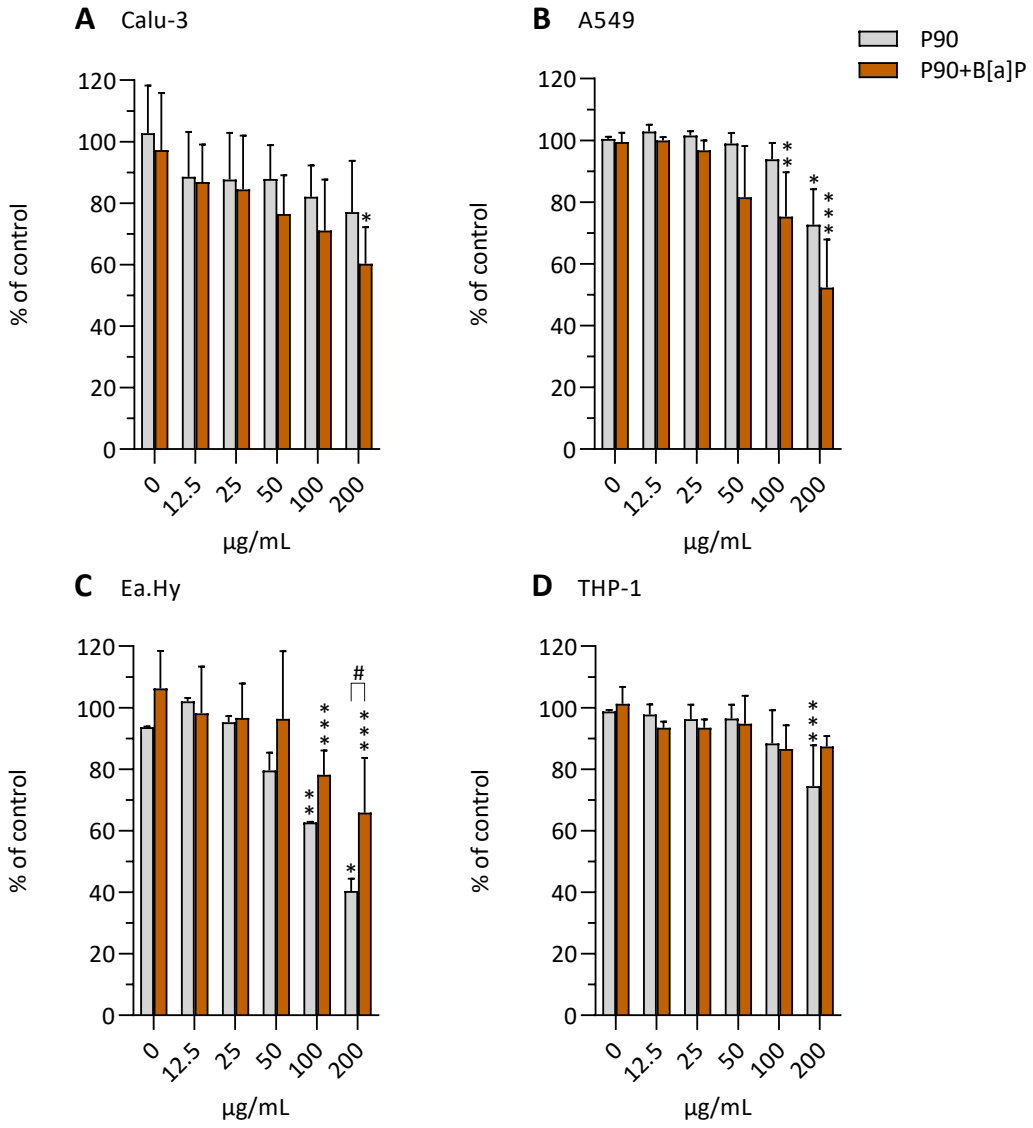

Figure 8. The relative cells viability of monocultures measured after 20 h exposure to 0-200 µg/mL P90 (light grey bars) or P90+B[a]P (orange bars) with 10 µg PAH/mg particle. The cell viability of (**A)** Calu-3, (**B)** A549, (**C)** Ea.Hy and (**D)** THP-1 monocultures was determined using the AlarmarBlue™ assay. The data is presented as the mean ± SD percentage (%) of mean P90 and P90+B[a]P control of 3 experiments. Statistical analysis was performed by two-way ANOVA with Dunnett's or Šídák's multiple comparisons test. Significantly different compared with control, *****p<0.05; ****** p<0.01;******* p<0.001. Significant difference between P90 and P90+B[a]P **#** p<0.05; **##** p<0.01, **###** p<0.001.

Particularly, Ea.Hy cells exhibited the highest responsiveness to P90 treatment, and a significant alteration of cell viability was detected from 100 µg/mL P90, with a 50% decrease in cell viability for the highest concentration of P90 compared with control (Figure 8C). Similar results were observed for monocultures exposed to P90+B[a]P, where a significant response was predominantly observed for cells treated with the highest concentrations. The most pronounced effect of P90+B[a]P exposure was observed in A549 and Ea.Hy cells, with a significant decrease in cell viability detected from 100 µg/mL P90+B[a]P, resulting in a 30-40% decrease in cell viability at the highest concentration relative to control (Figure 8B and C). Nevertheless, a significant difference in cell viability was observed between Ea.Hy cells treated with 200 µg/mL P90 compared with P90+B[a]P. Specifically, cell viability decreased by 20% for cells exposed to P90 relative to P90+B[a]P (Figure 8C). No significant effects on cell viability were detected upon B[a]P exposure alone (Figure 9). Similar results were observed for exposure to P90+Pyr, where no significant alteration of cell viability was found (Figure 10). Correspondingly, significant differences between cells exposed to P90 and P90+Pyr was detected from 100 µg/mL (Figure 10B).

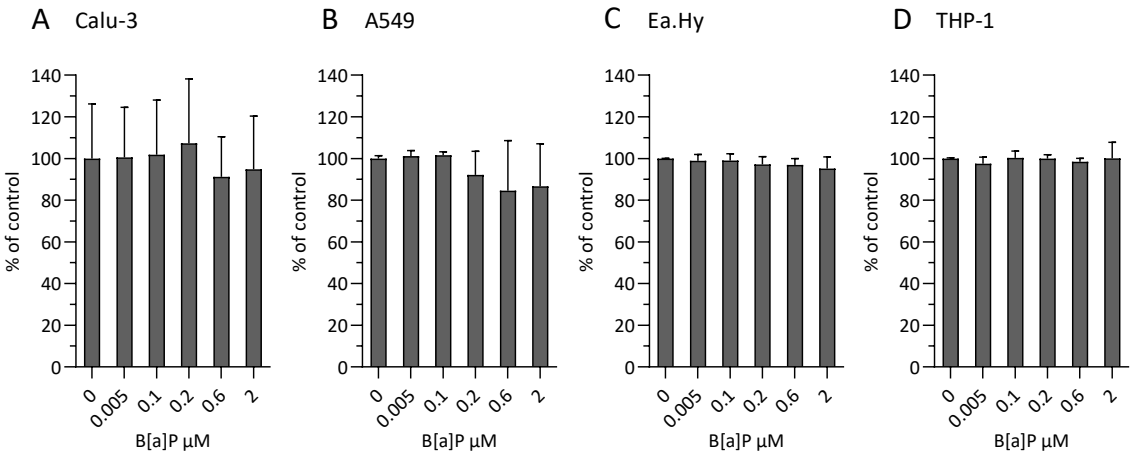

Figure 9. The relative cells viability of monocultures measured after 20 h exposure to concentrations from 0-2 µM B[a]P. The cell viability of (**A)** Calu-3, (**B)** A549, (**C)** Ea.Hy and (**D)** THP-1 monocultures was analyzed by using AlarmarBlue™ assay. The data is presented as the mean±SD percentage (%) of the mean control of 3 experiments. Statistical analysis was performed by one-way ANOVA with Dunnett's multiple comparisons test. Significantly different compared with control, *****p<0.05; ****** p<0.01; ******* p<0.001.

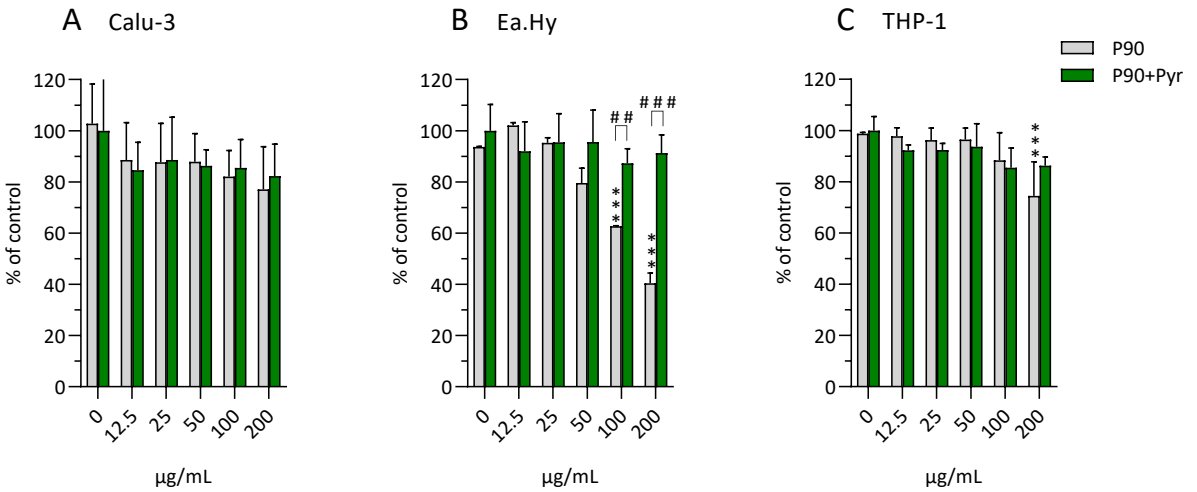

Figure 10. The relative cells viability of monocultures measured after 20 h exposure to 0-200 µg/mL P90 (light grey bars) or P90+Pyr (green bars) with 100 µg PAH/mg particle. The cell viability of (**A)** Calu-3, (**B)** Ea.Hy and (**C)** THP-1 monocultures was determined using the AlarmarBlue™ assay. The data is presented as the mean ± SD percentage (%) of mean P90 and P90+Pyr control of 3 experiments. Statistical analysis was performed by two-way ANOVA with Dunnett's or Šídák's multiple comparisons test. Significantly different compared with control, *****p<0.05; ****** p<0.01;******* p<0.001. Significant difference between P90 and P90+B[a]P **#** p<0.05; **##** p<0.01, **###** p<0.001.

To further investigate the relationship between exposure and cytotoxicity, the release of LDH in monoculture supernatant was measured post-exposure by using LDH assay (Figure 11). Consistent with the effect on cell viability, significant increases in LDH release were detected in A549 and Ea.hy cells exposed to 200 µg/mL P90 (Figure 11B and C), with a 30% increase in response compared with control in Ea.Hy cells. Similarly, a significant induction of LDH release was only found at the highest concentrations of P90+B[a]P in A549 and Ea.Hy cells. Similar to the results from AlarmarBlue assay, P90 appeared to induce a stronger cytotoxic effect compared to P90+B[a]P in Ea.Hy cells, and a clear trend of increased LDH release for exposure to P90 was detected (Figure 11C). No increase in LDH release was observed in Calu-3 cells, regardless of treatment. This is contrasting to the effects measured by AlarmarBlue, where cell viability significantly decreased 40% at 200 µg/mL P90+B[a]P. There was no detected increase in LDH release in THP-1 macrophages, regardless of a significant decrease in cell viability observed at 200 µg/mL P90. Note that a cytotoxicity rate of 60% was determined for the control group within the THP-1 monoculture (Figure 11C), potentially attributable to challenges encountered in acquiring an LDH maximum control.

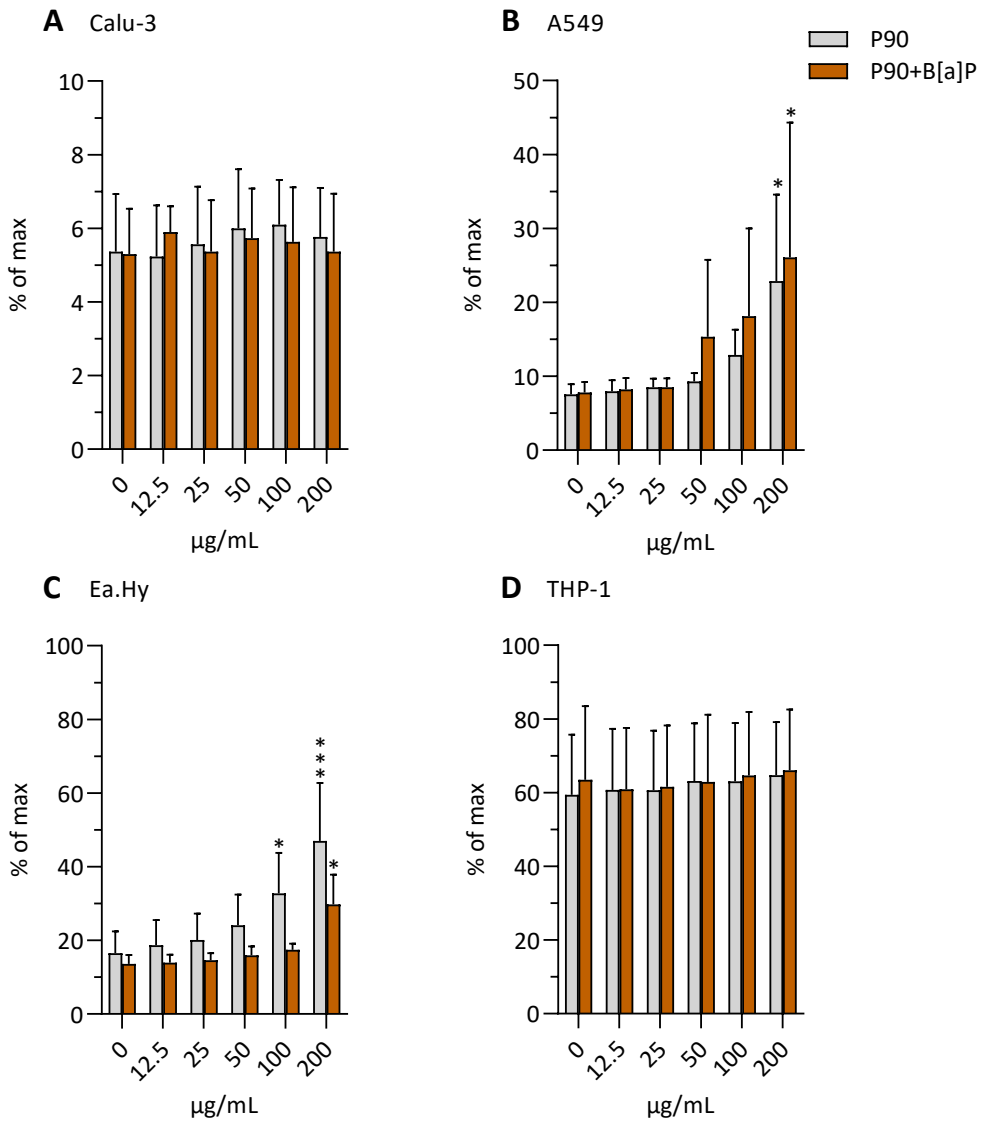

Figure 11. The relative LDH concentration of monocultures measured after 20 h exposure to 0-200 µg/mL P90 (light grey bars) or P90+B[a]P (orange bars) with 10 µg PAH/mg particle. The LDH concentration in (**A)** Calu-3, (**B)** A549, (**C)** Ea.Hy and (**D)** THP-1 monocultures was analyzed by using LDH Cytotoxicity Detection assay. The data is presented as the mean±SD percentage (%) of the positive control (2% triton X100) of 3 experiments. Statistical analysis was performed by two-way ANOVA with Dunnett's or Šídák's multiple comparisons test. Significantly different compared with control, *p<0.05; ** p<0.01;*** p<0.001. Significantly difference between P90 and P90+B[a]P **#** p<0.05; **##** p<0.01, **###** p<0.001.

B[a]P did not induce an increase in LDH release in any of the monocultures (Figure 12). As observed from Alarmarblue assay, exposure to P90+Pyr did not appear to induce cytotoxicity and no induced release of LDH was detected (Figure 13). Thus, Ea.hy cells treated with P90+Pyr exhibited significantly lower LDH response from those exposed to P90 from 100 µg/mL (Figure 13B).

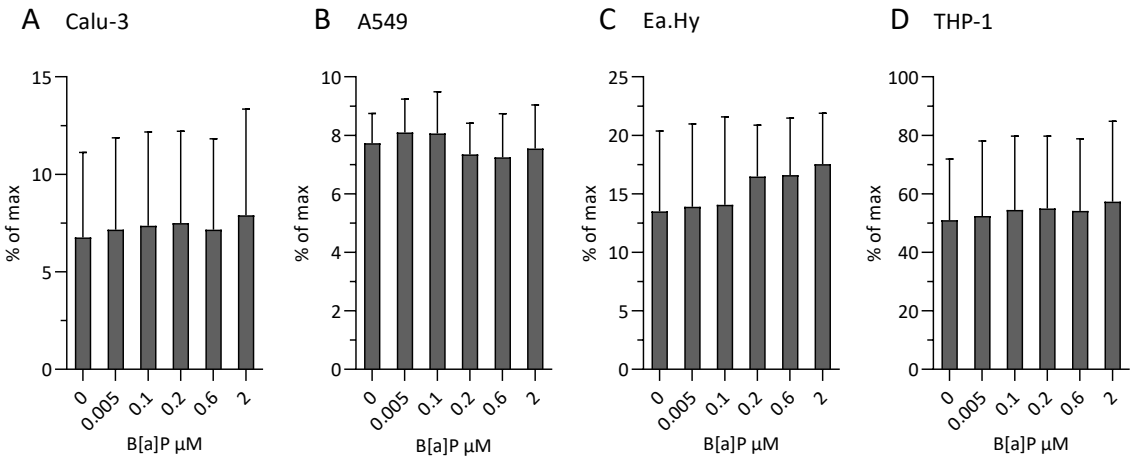

Figure 12. The relative concentration of LDH measured in monocultures after 20 h exposure to concentrations from 0-2 µM B[a]P. The LDH concentration in (**A)** Calu-3, (**B)** A549, (**C)** Ea.Hy and (**D)** THP-1 monocultures was analyzed by using LDH Cytotoxicity Detection assay.The data is represented as the mean±SD percentage (%) of the positive control (2% triton X100) of 3 experiments. Statistical analysis was performed by one-way ANOVA with Dunnett's multiple comparisons test. Significantly different compared with control, *****p<0.05; ****** p<0.01;******* p<0.001.

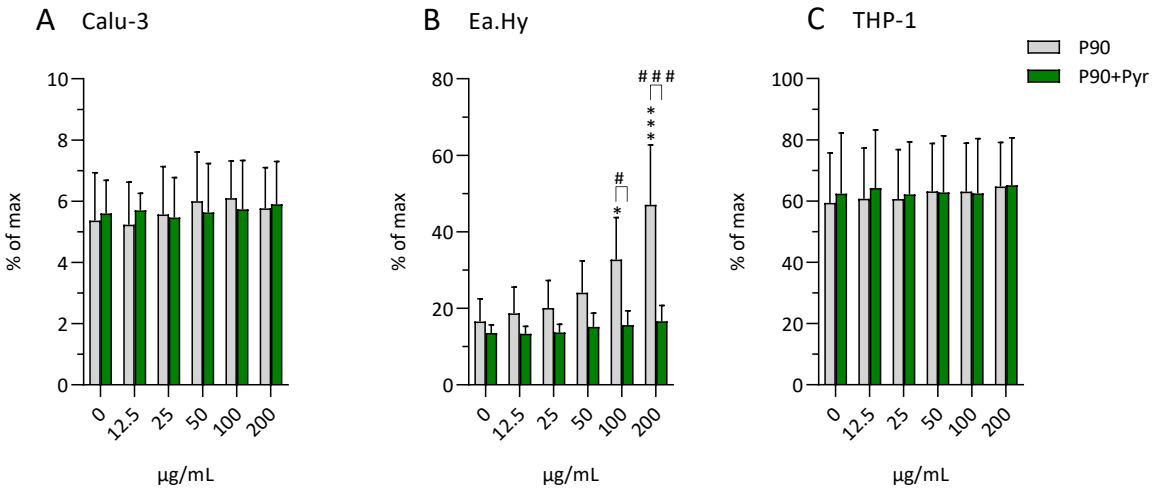

Figure 13. The relative LDH concentration of monocultures measured after 20 h exposure to 0-200 µg/mL P90 (light grey bars) or P90+Pyr (green bars) with 100 µg PAH/mg particle. The LDH concentration in (**A)** Calu-3, (**B)** Ea.Hy and (**C)** THP-1 monocultures was analyzed by using LDH Cytotoxicity Detection assay. The data is presented as the mean±SD percentage (%) of the positive control (2% triton X100) of 3 experiments. Statistical analysis was performed by two-way ANOVA with Dunnett's or Šídák's multiple comparisons test. Significantly different compared with control, *****p<0.05; ****** p<0.01;******* p<0.001. Significantly difference between P90 and P90+B[a]P **#** p<0.05; **##** p<0.01, **###** p<0.001.

3.5 Release of pro-inflammatory cytokines in monocultures

The release of pro-inflammatory mediators IL-6 and CXCL8 in exposure medium were estimated by ELISA. In Ea.Hy cells, P90 induced a concentration-dependent increase in IL-6 release, which was significantly different from control from 25 µg/mL (Figure 14C). Conversely, P90 did not induce a significant increase in IL-6 release in Calu-3 and A549 cells. The responsiveness to P90+B[a]P treatment was generally low in all monocultures, with the exception of a modest, but significant increase observed in Ea.Hy cells exposed to 200 µg/mL (Figure 14C). Accordingly, significant differences in IL-6 release between exposure to P90 and P90+B[a]P was observed from 100 µg/mL in Ea.Hy cells and 200 µg/mL in A549 cells (Figure 14B and C).

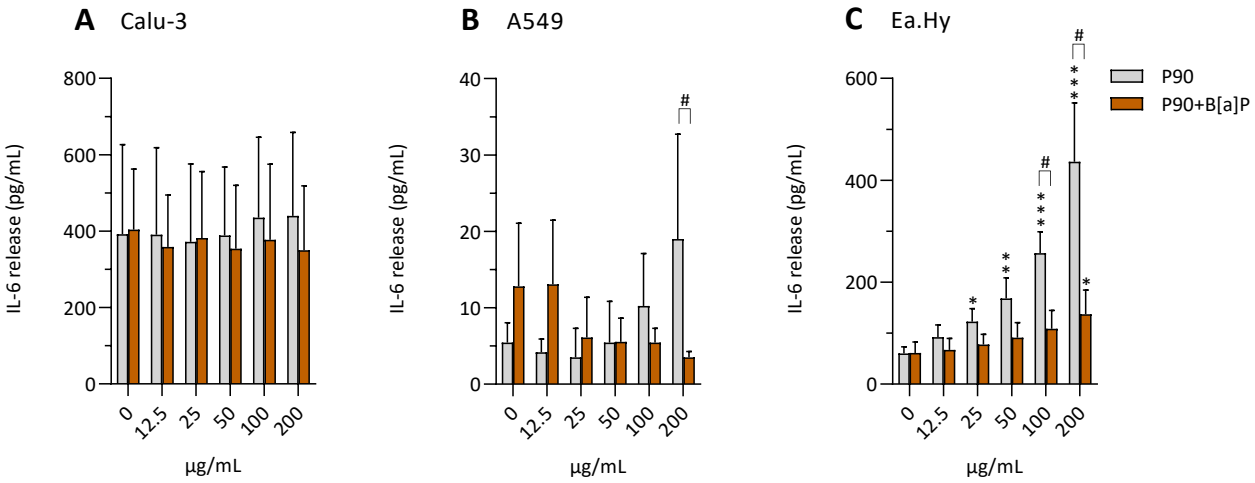

Figure 14. The relative IL-6 concentration of monocultures measured after 20 h exposure to 0-200 µg/mL P90 (light grey bars) or P90+B[a]P (orange bars) with 10 µg PAH/mg particle. The IL-6 concentration in (**A)** Calu-3, (**B)** A549 and (**C)** Ea.Hy monocultures was analyzed by using analyzed by using ELISA. The data represent the mean±SD concentration (pg/mL) of 3 experiments. Statistical analysis was performed by two-way ANOVA with Dunnett's or Šídák's multiple comparisons test. Significantly different compared with control, *p<0.05; ** p<0.01;*** p<0.001. Significantly difference between P90 and P90+B[a]P **#** p<0.05; **##** p<0.01, **###** p<0.001.

While particles did not induce IL-6 responses in Calu-3 cells (Figure 14A), exposure to B[a]P alone appeared to elicit an elevated response relative to concentration, which were significant at 2 µM (Figure 15A). In contrast, no effect of B[a]P was detected in the A549 and Ea.Hy cells (Figure 15B and C).

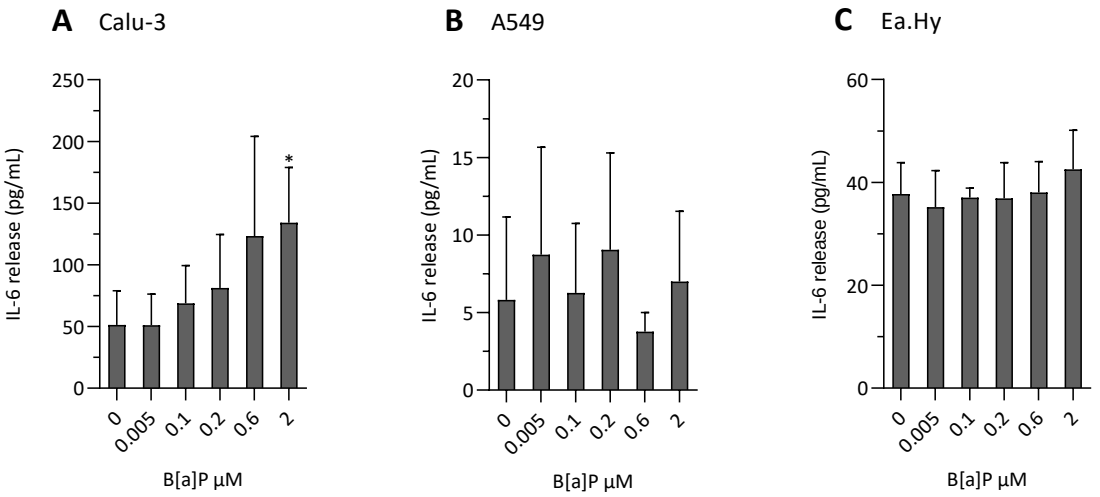

Figure 15 The relative IL-6 concentration in monocultures after exposure 20 h to concentrations from 0-2 µM B[a]P. The IL-6 concentration in (**A)** Calu-3, (**B)** A549 and (**C)** Ea.Hy monocultures was analyzed by using ELISA. The data represent the mean±SD concentration (pg/mL) of 3 experiments. Statistical analysis was performed by one-way ANOVA with Dunnett's multiple comparisons test. Significantly different compared with control, *p<0.05; ** p<0.01;*** p<0.001.

P90+Pyr did not induce an increased release of IL-6 in Calu-3 or Ea.Hy cells (Figure 16). Significant differences in IL-6 response between Ea.Hy cells exposed to P90 and P90+Pyr were detected from 50 µg/mL (Figure 16B).

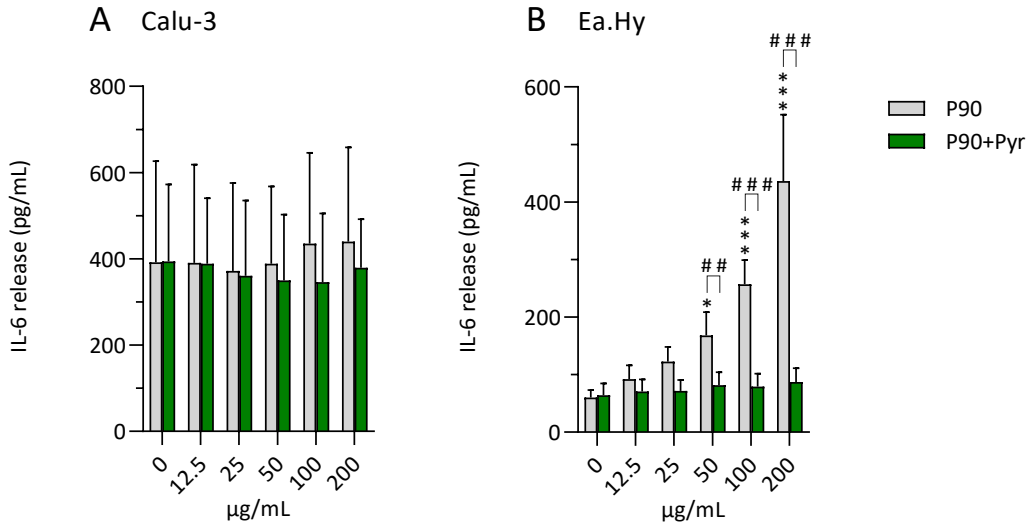

Figure 16 The relative IL-6 concentration of monocultures measured after 20 h exposure to 0-200 µg/mL P90 (light grey bars) or P90+Pyr (green bars) with 100 µg PAH/mg particle. The IL-6 concentration in (**A)** Calu-3 and (**B)** Ea.Hy monocultures was analyzed by using analyzed by using ELISA. The data represent the mean±SD concentration (pg/mL) of 3 experiments. Statistical analysis was performed by two-way ANOVA with Dunnett's or Šídák's multiple comparisons test. Significantly different compared with control, *p<0.05; ** p<0.01;*** p<0.001. Significantly difference between P90 and P90+B[a]P **#** p<0.05; **##** p<0.01, **###** p<0.001.

The pro-inflammatory potential of P90 on Ea.Hy cell were further supported by a clear concentration-dependent increase in CXCL8 release, significant from 25 µg/mL P90 (Figure 17C). A significant increase in CXCL8 release was also detected in the A549 cells with 200 µg/mL P90 (Figure 17B). Similar to the results from IL-6 analysis, P90+B[a]P treatment did not induce an increased release of CXCL8 in monocultures, except for a minor but significant increase in Ea.Hy cells exposed to 200 µg/mL (Figure 17C).

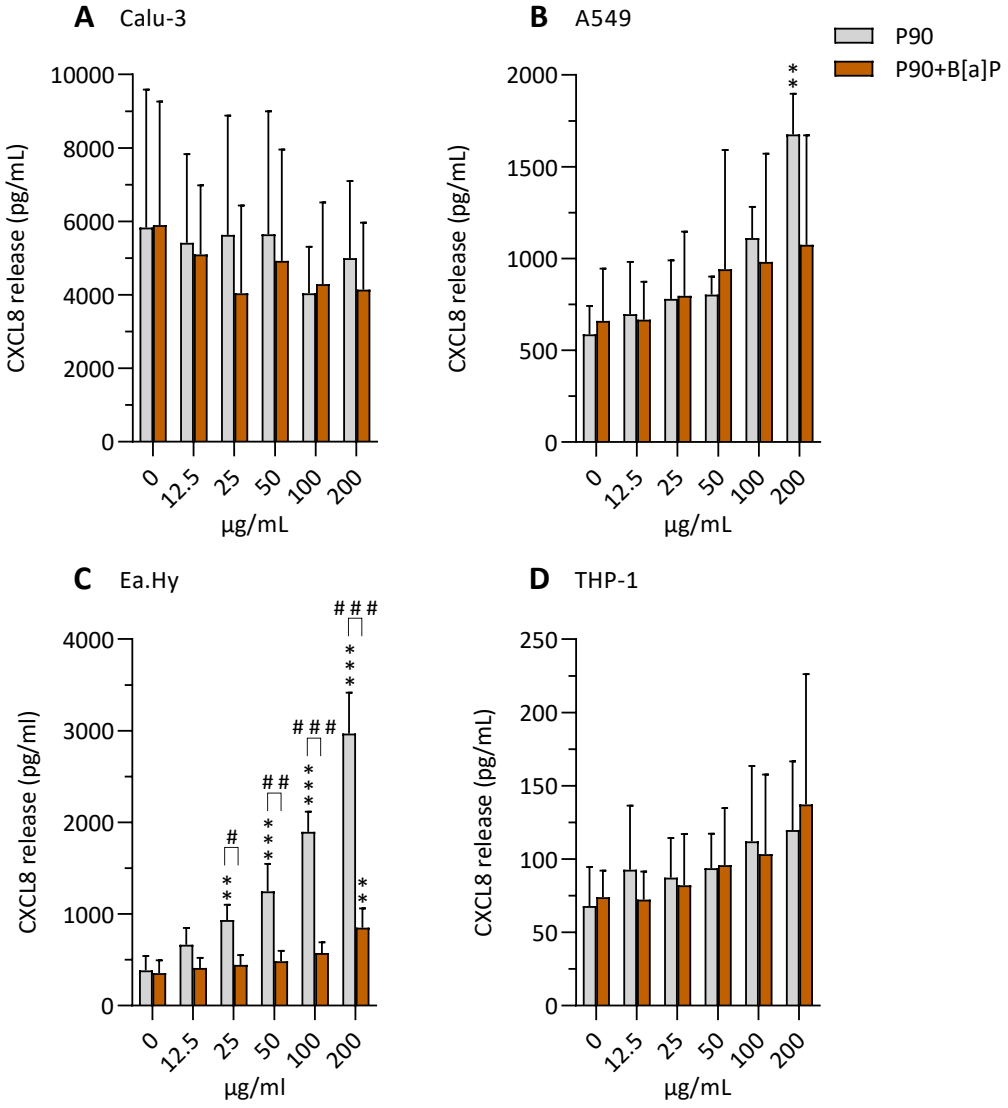

Figure 17. The relative CXCL8 concentration of monocultures measured after 20 h exposure to 0-200 µg/mL P90 (light grey bars) or P90+B[a]P (orange bars) with 10 µg PAH/mg particle. The CXCL8 concentration in **(A)** Calu-3, **(B)** A549, **(C)** Ea.Hy and **(D)** THP-1 monocultures was analyzed by using ELISA. The data represent the mean±SD concentration (pg/mL) of 3 experiments. Statistical analysis was performed by two-way ANOVA with Dunnett's or Šídák's multiple comparisons test. Significantly different compared with control, *****p<0.05; ****** p<0.01;******* p<0.001. Significantly difference between P90 and P90+B[a]P **#** p<0.05; **##** p<0.01, **###** p<0.001.

Correspondingly, significant differences between exposure to P90 and P90+B[a]P were detected in Ea.Hy cells from 25 µg/mL (Figure 17C). No significant increases in CXCL8 release compared with control was detected for cells exposed to B[a]P (Figure 18).

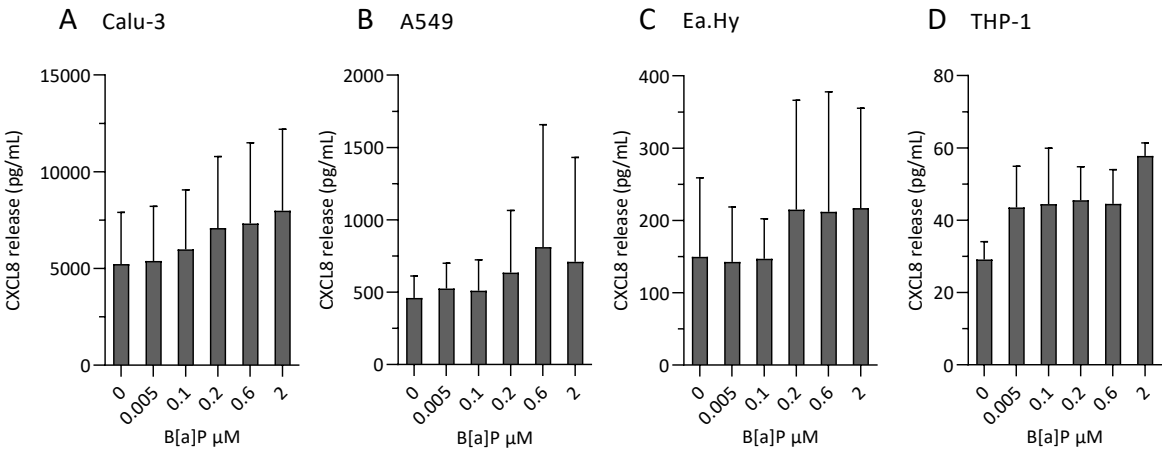

Figure 18 A Concentration-dependent cytokine responses in monocultures after exposure to B[a]P. The cells were exposed to concentrations from 0-2 µM for 24 h. The CXCL8 concentration in (**A)** Calu-3, (**B)** A549, (**C)** Ea.Hy and (**D)** THP-1 monocultures was analyzed by using ELISA. The data represent the mean±SD concentration (pg/mL) of 3 experiments. Statistical analysis was performed by one-way ANOVA with Dunnett's multiple comparisons test. Significantly different compared with control, *p<0.05; ** p<0.01;*** p<0.001.

The same trend was exhibited upon P90+Pyr exposure, with differences in the detected CXCL8 response between Ea.Hy cells treated with P90 and P90+B[a]P significant from 25 µg/mL (Figure 19B).

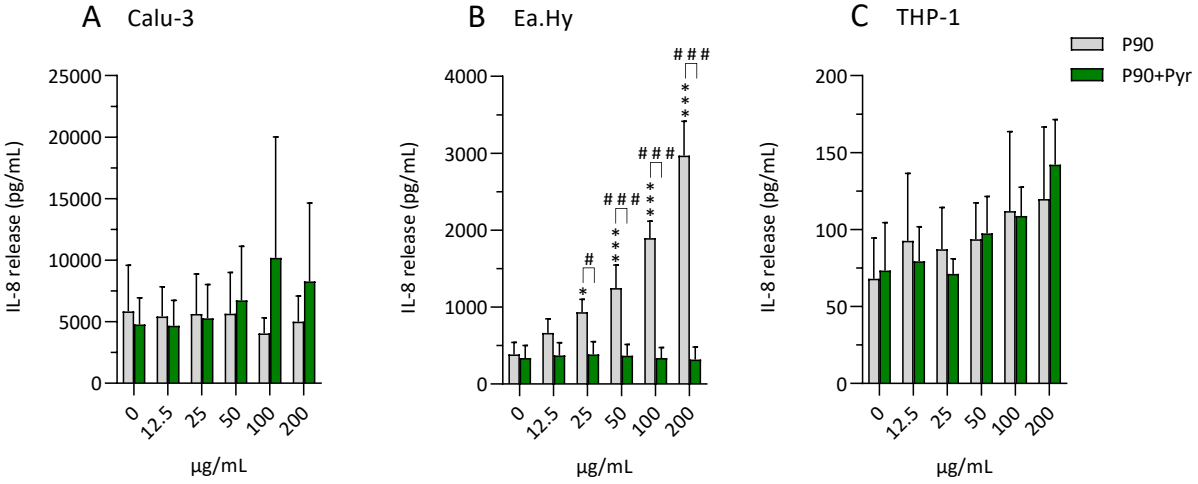

Figure 19 The relative CXCL8 concentration of monocultures measured after 20 h exposure to 0-200 µg/mL P90 (light grey bars) or P90+Pyr (green bars) with 100 µg PAH/mg particle. The CXCL8 concentration in (**A)** Calu-3, (**B)** Ea.Hy and (**C)** THP-1 monocultures was analyzed by using ELISA. The data represent the mean±SD concentration (pg/mL) of 3 experiments. Statistical analysis was performed by two-way ANOVA with Dunnett's or Šídák's multiple comparisons test. Significantly different compared with control, *p<0.05; ** p<0.01;*** p<0.001. Significantly difference between P90 and P90+B[a]P **#** p<0.05; **##** p<0.01, **###** p<0.001.

3.6 Estimated CYP1A1 activity in monocultures

EROD assay was used to estimate the CYP1A1 activity in monocultures after exposure. Enzyme activity was only detected in Calu-3 monocultures exposed to various concentrations of B[a]P (Table 4). No induced enzyme activity was found after exposure to particle suspensions (P90 and P90+B[a]P) or in the other cell lines (data not shown). Pyr-induced CYP1A1 activity was not measured.

Table 4. Shows the estimated CYP1A1 activity in Calu-3 cells exposed to various concentrations of B[a]P (0-2µM) for 20 h. The conversion of 7-etoxyresorufin to resorufin was estimated by EROD assay, and normalized with the total amount of protein in the samples. The produced Resorufin (pmol)/mg protein/min presented (mean ± SD) is proportional with CYP1A1 activity, and was used to estimate concentration dependent CYP1A1 activity after approximately 80 min (70 cycles).

Table 4 Resorufin (pmol)/mg protein/min (mean ± SD)

B[a]P µM	Resorufin(pmol)/mg protein/min
0.02	-0.002 ± 0.005
0.05	0.079 ± 0.033
0.1	0.147 ± 0.049
0.2	0.351 ± 0.128
0.6	2.855 ± 0.449
2	7.452 ± 0.656

3.7 Release of pro-inflammatory cytokines in 3D cultures

Although not significant, the Calu-3 model exhibited an increase in IL-6 release upon B[a]P exposure (Figure 20A and C). Conversely, exposure to P90 or P90+B[a]P appeared to have no effect on IL-6 response compared to control. Similar results were obtained from the A549 model, with no significant induction of IL-6 detected (Figure 20B and D). Furthermore, no increase in CXCL8-release were observed in 3D cultures (Figure 21). However, generally higher levels of CXCL8 were detected in the basolateral compartment relative to the apical compartment in both models. The CXCL8 release also appeared to be increasing over time, as higher levels were detected after 6 h compared to 3 h exposure.

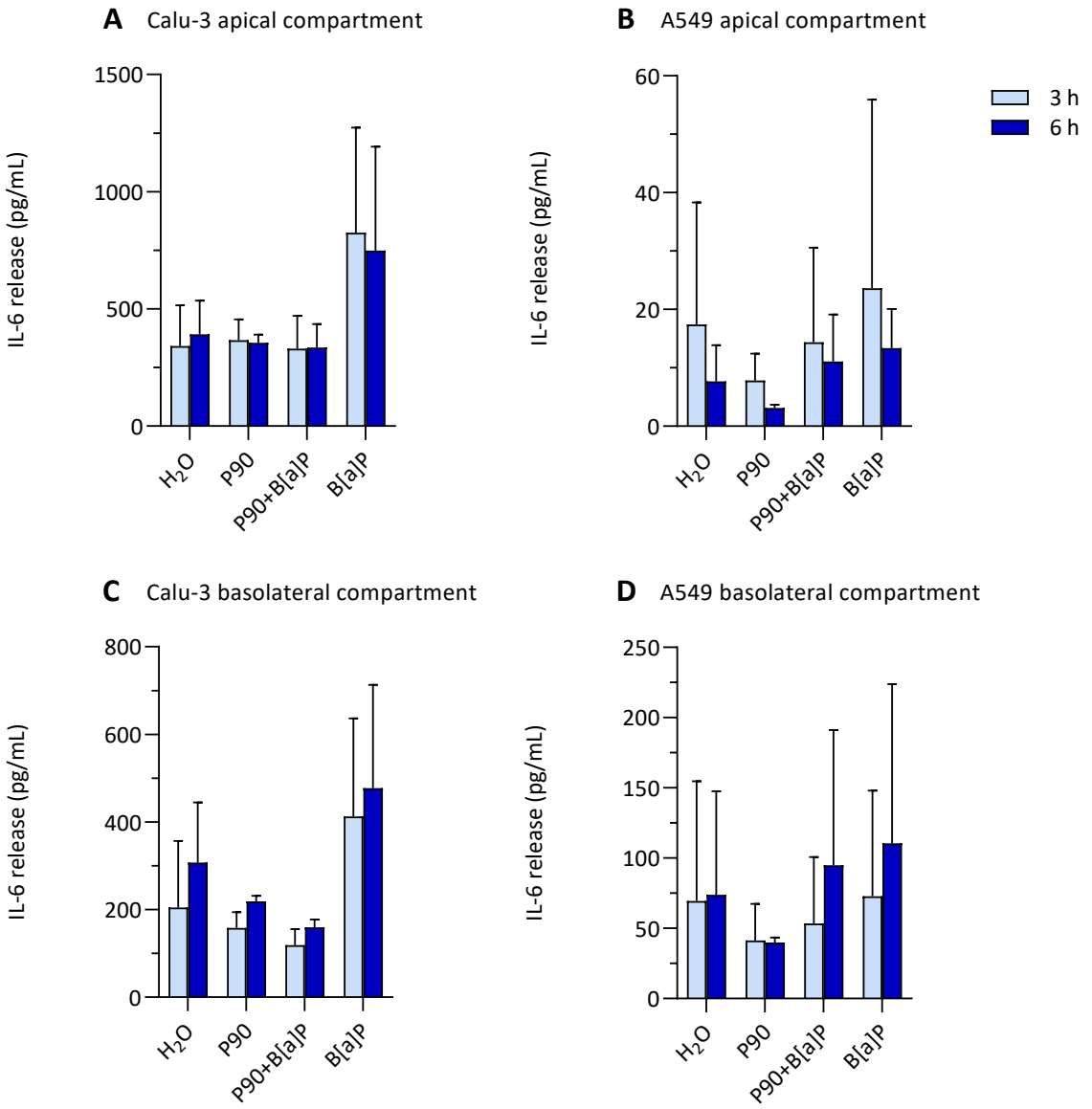

Figure 20. Cytokine responses in ALI 3D cultures after exposure to H_2O (control), P90, P90+B[a]P and B[a]P for 3 (light blue bars) and 6 h (dark blue bars). Response in apical epithelial cells (Calu-3 or A549) with THP-1 macrophages and basolateral endothelial Ea.Hy cells was measured using ELISA. **A**-**B** Calu-3 model; **C-D** A549 model. The data represent the mean±SD concentration (pg/mL) of 3 experiments. Statistical analysis was performed by two-way ANOVA with Dunnett's or Šídák's multiple comparisons test. Significantly different compared with control, *p<0.05; ** p<0.01;*** p<0.001. Significantly difference between 3 h and 6 h, **#** p<0.05; **##** p<0.01, **###** p<0.001.

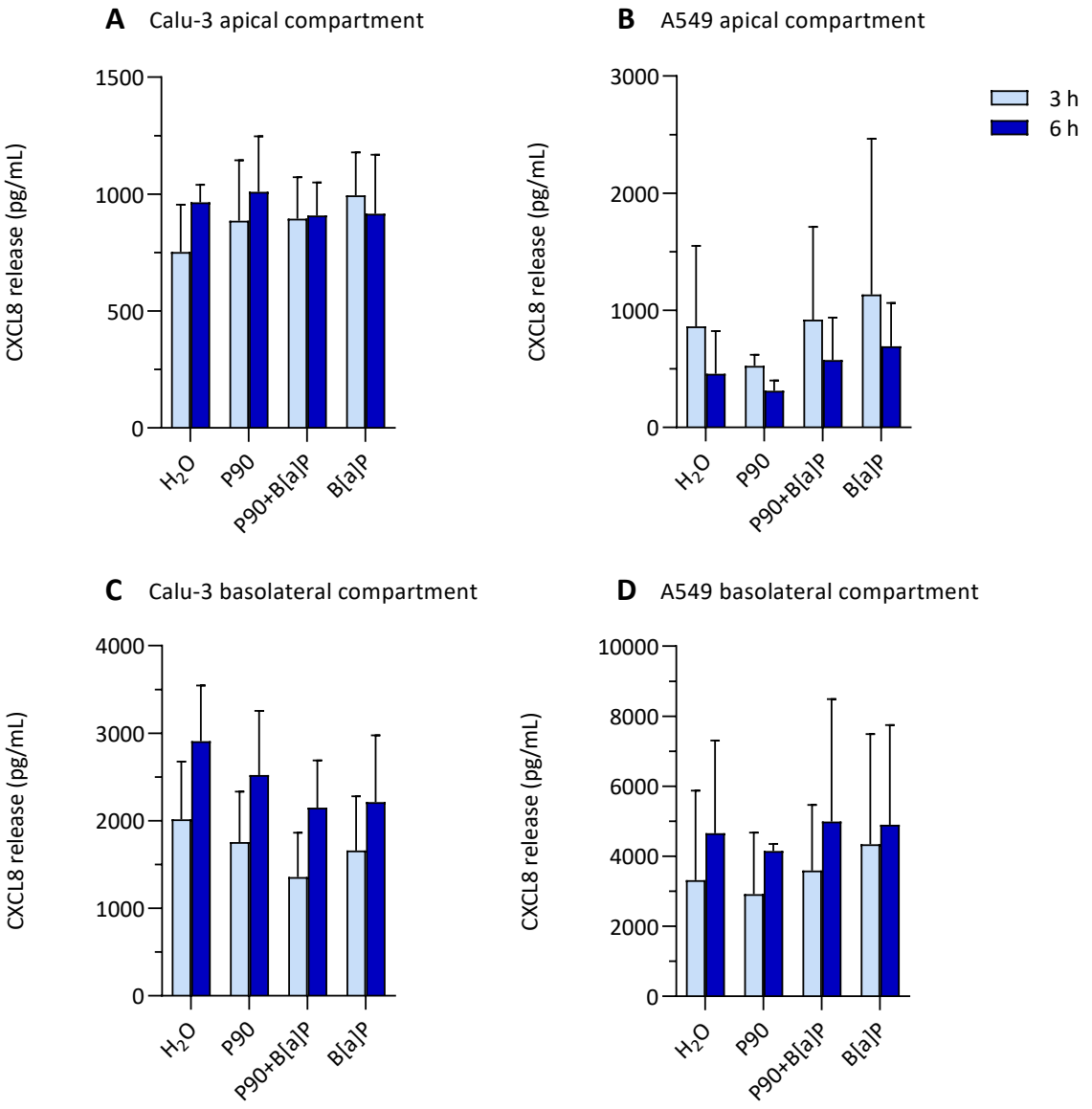

Figure 21. Cytokine responses in ALI 3D cultures after exposure to H_2O (control), P90, P90+B[a]P and B[a]P for 3 (light blue bars) and 6 h (dark blue bars). Response in apical epithelial cells (Calu-3 or A549) with THP-1 macrophages and basolateral endothelial Ea.Hy cells was measured using ELISA. **A**-**B** Calu-3 model; **C-D** A549 model. The data represent the mean±SD concentration (pg/mL) of 3 experiments. Statistical analysis was performed by two-way ANOVA with Dunnett's or Šídák's multiple comparisons test. Significantly different compared with control, *p<0.05; ** p<0.01;*** p<0.001. Significantly difference between 3 h and 6 h, **#** p<0.05; **##** p<0.01, **###** p<0.001.

3.8 Gene expression linked to inflammatory responses and PAH metabolism in 3D cultures

The expression of genes related to inflammatory responses and xenobiotic metabolism, IL-6, CXCL8 and CYP1A1, was analyzed by using RT-qPCR. In line with the measured protein release, no significant induction of IL-6 or CXCL8 expression was observed (Figure 22 and 23). The

absence of IL-6 expression further corroborated with the high Ct values observed in both models, particularly on the apical side of the A549 model, where a Ct value greater than 35 was recorded. Conversely, the Ct values indicated an overall higher level of CXCL8 expression, with both the apical and basolateral cell layers in the A549 model exhibiting Ct values below 27.

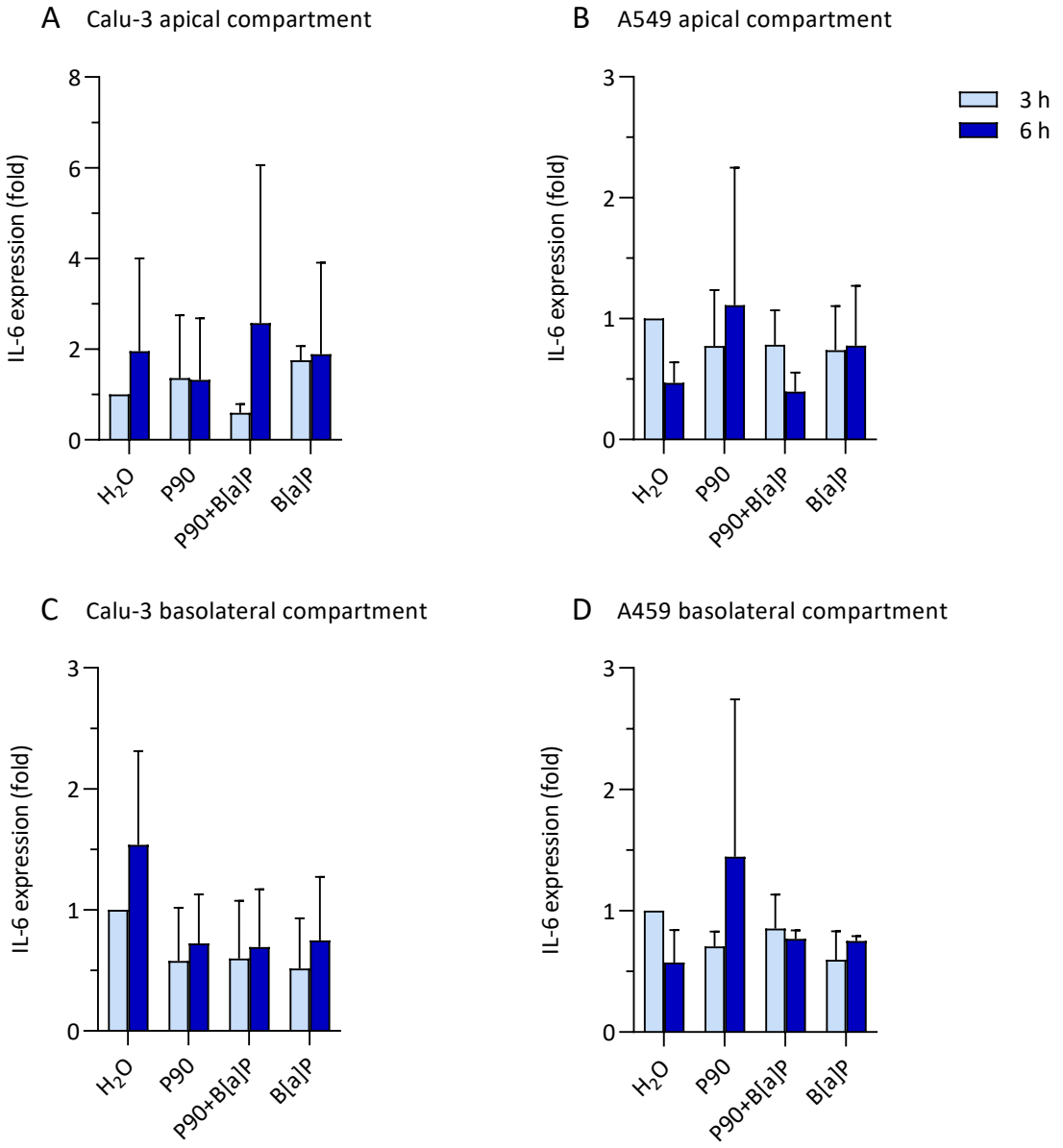

Figure 22. IL-6 gene expression in ALI 3D cultures after exposure to H_2O (control), P90, P90+B[a]P and B[a]P for 3 (light blue bars) and 6 h (dark blue bars). Expression in apical epithelial cells (Calu-3 or A549) with THP-1 macrophages and basolateral endothelial Ea.Hy cells was measured using RT-qPCR. **A**-**B** Calu-3 model; **C**-**D** A549 model. The data represent the fold increase compared with control (3 h exposure to H_2O) of 3 experiments. Statistical analysis was done using the calculated Δcq values and performed by two-way ANOVA with Dunnett's or Šídák's multiple comparisons test. Significantly different compared with control, *p<0.05; ** p<0.01;*** p<0.001. Significantly difference between 3 h and 6 h, # p<0.05; ## p<0.01, ### p<0.001.

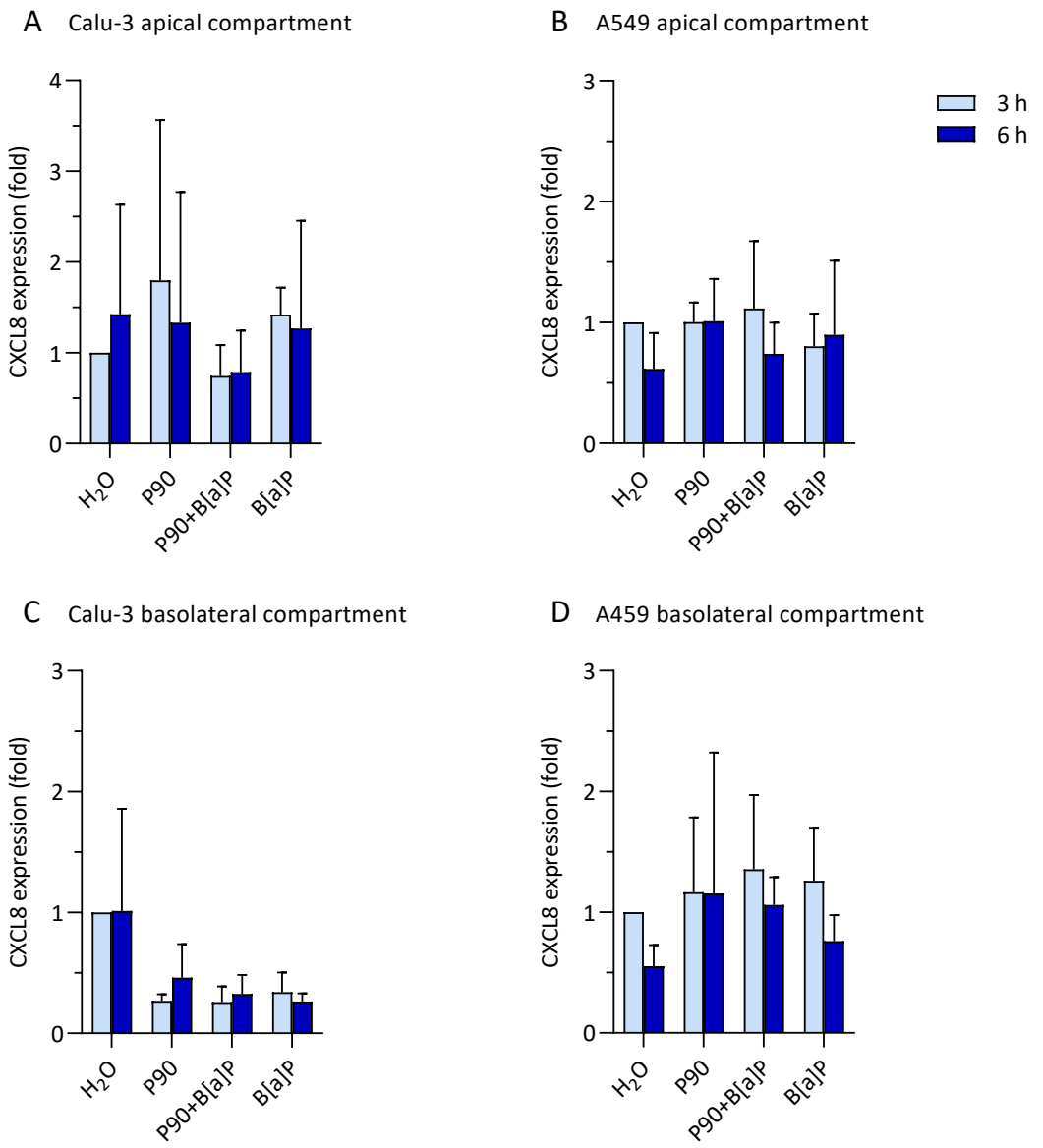

Figure 23. CXCL8 gene expression in ALI 3D cultures after exposure to H_2O (control), P90, P90+B[a]P and B[a]P for 3 (light blue bars) and 6 h (dark blue bars). Expression in apical epithelial cells (Calu-3 or A549) with THP-1 macrophages and basolateral endothelial Ea.Hy cells was measured using RT-qPCR. **A**-**B** Calu-3 model; **C**-**D** A549 model. The data represent the fold increase compared with control (3 h exposure to H_2O) of 3 experiments. Statistical analysis was done using the calculated Δcq values and performed by two-way ANOVA with Dunnett's or Šídák's multiple comparisons test. Significantly different compared with control, *p<0.05; ** p<0.01;*** p<0.00. Significantly difference between 3 h and 6 h, **#** p<0.05; **##** p<0.01, **###** p<0.001.

B[a]P induced a significant CYP1A1 expression in 3D cultures, and the B[a]P-induced apical CYP1A1 expression was approximately 500 times greater relative to control after 3 h in both models (Figure 24A and B). The basolateral response was much weaker compared to the apical response. However, a significant basolateral induction of CYP1A1 expression was detected in the Calu-3 model (Figure 24C). Although not significant, the same tendency was observed in

the A549 model. Furthermore, a significantly decreased induction of CYP1A1 expression was detected in the basolateral compartment in the Calu-3 model from 3 h to 6 h exposure (Figure 24C). Notably, the Ct values indicated a higher level of CYP1A1 expression in the Calu-3 cells compared to the A549 cells, which had a Ct > 35. This finding is consistent with the results from the EROD assay. Notably, P90+B[a]P did not induce CYP1A1 expression (Figure 24).

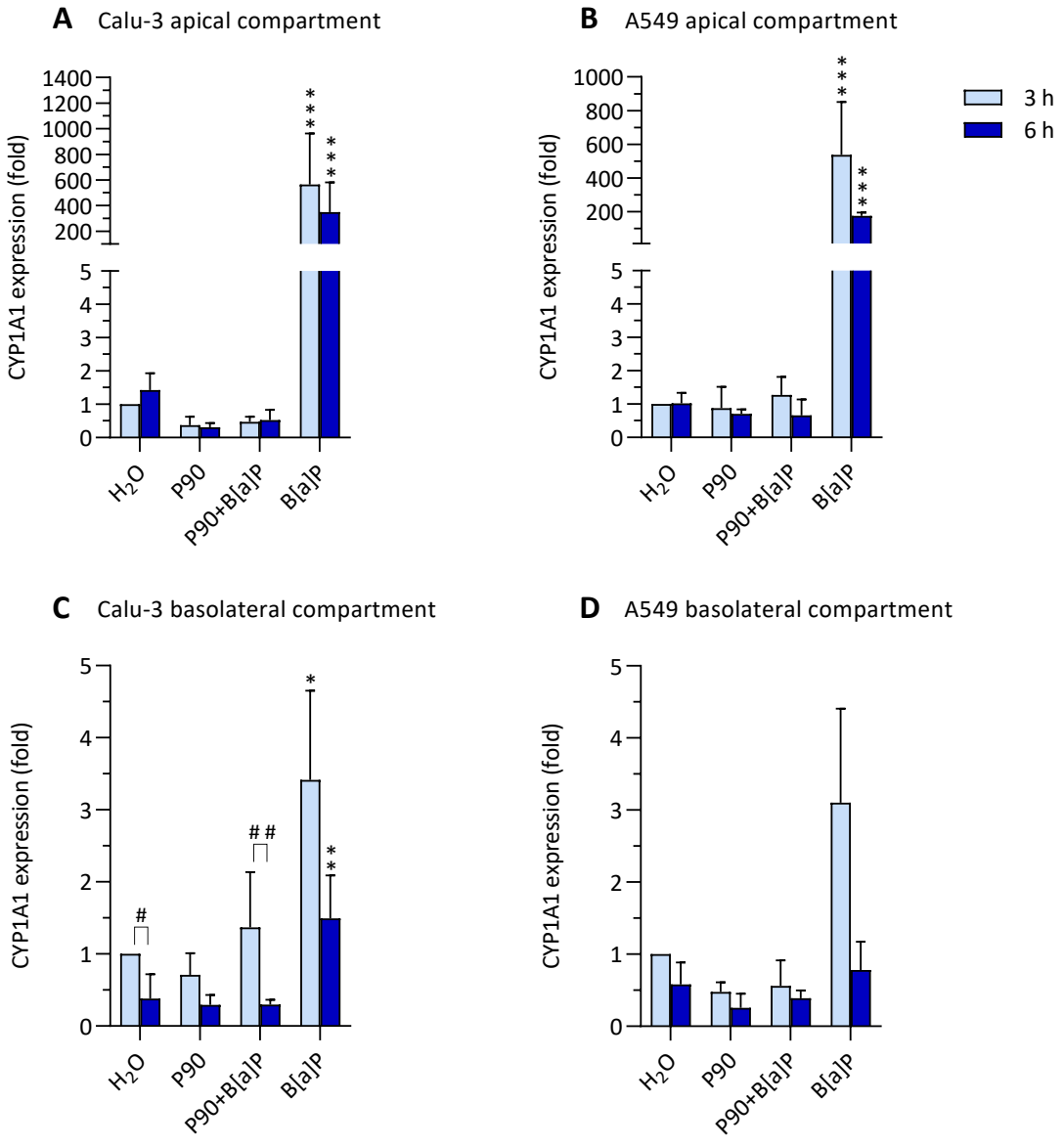

Figure 24. CYP1A1 gene expression in ALI 3D cultures after exposure to H_2O (control), P90, P90+B[a]P and B[a]P for 3 (light grey bars) and 6 h (dark grey bars). Expression in apical epithelial cells (Calu-3 or A549) with THP-1 macrophages and basolateral endothelial Ea.Hy cells was measured using RT-qPCR. **A**-**B** Calu-3 model; **C**-**D** A549 model. The data represent the fold increase compared with control (3 h exposure to H_2O) of 3 experiments. Statistical analysis was done using the calculated ΔCq values and performed by two-way ANOVA with Dunnett's or Šídák's multiple comparisons test. Significantly different compared with control, *p<0.05; ** p<0.01;*** p<0.001. Significantly difference between 3 h and 6 h, # p<0.05; ## p<0.01, ### p<0.001.

4 Discussion

The present study aimed to increase the understanding of factors driving the biological effects associated with UFPs exposure, and specifically to investigate UFPs ability to act as carriers for organic components indicative of a "Trojan horse" mechanism. Two different ALI 3D lung models with varying epithelial barrier capacities were established. The response of Calu-3 bronchial epithelial cells or A549 alveolar epithelial cells grown together with THP-1 macrophages were used to simulate responses of the human lung epithelium. Vascular endothelial Ea.hy cells grown in the basolateral compartment was employed to assess the endothelial response. The same cell lines were used in submerged conditions in monoculture experiments.

Monocultures and 3D cultures were exposed to carbon black nanoparticles and selected PAHs, both alone and in combination, and relevant biomarkers were used to evaluate and compare effects. P90 was used as a model for the carbon core of ultrafine combustion particles and B[a]P and Pyr as models for the organic compounds surrounding the core. For monocultures, cytotoxicity was assessed by AlarmarBlue and LDH assay, pro-inflammatory responses were estimated by ELISA, while CYP1A1 activity was determined using EROD assay. In 3D cultures, the protein levels and mRNA expression of IL-6 and CXCL8 was determined by ELISA and RT-qPCR, respectively. In addition, RT-qPCR was used to determine the induced CYP1A1 expression.

The results showed that Ea.Hy cells were more responsive to exposure compared to the other monocultures. In these cells the overall toxic potential of P90 alone appeared to be higher compared to P90+PAH, and significant differences in effects was observed from 25 µg/mL P90. For the 3D cultures, B[a]P induced a significant increase in CYP1A1 expression in the epithelial cell layer of both models. However, B[a]P-coated P90 failed to induce CYP1A1 expression in both monocultures and in 3D cultures, indicating its inability to activate AhR.

4.1 Particle suspension and PAH measurements

In this study, particle suspensions containing heightened levels of B[a]P and Pyr was utilized in *in vitro* experiments. In urban air, pyrene is typically more abundant compared to B[a]P, and

have been reported to surpass B[a]P levels by a factor of 2 to 10 (Boström et al., 2002; Lovinsky-Desir et al., 2016). Furthermore, when measuring the PAH-content of diesel exhaust particles (DEP), Totlandsdal et al. (2014) estimated the concentration of B[a]P to be 10 µg/g and Pyr to 80 µg/g. To reflect these proportions, Pyr concentrations employed were 10 times higher compared to that of B[a]P in P90+PAH suspension.

P90 suspensions were made throughout the study, including P90+Pyr and P90+B[a]P stocks. DLS analysis showed that the P90 stock solution consisted of particles with a larger hydrodynamic diameter (0.45 ± 0.11 µm) compared to the P90+Pyr (0.25 ± 0.01 µm) and P90+B[a]P (0.24 ± 0.02 µm) stock solutions. It is important to note that these measurements reflect the particles hydrodynamic diameter, which refers to how a particle diffuses within fluid, rather than the primary diameter of the particle. The discrepancy in size observed between the suspensions may be attributed to potential alterations in the physical properties of the particles due to PAH-coating. Moreover, the acetone treatment applied to the P90+PAH suspension might have impacted the particles differently compared to the untreated P90 suspension. Additionally, particles in freshly prepared P90 stock exhibited a hydrodynamic diameter close to 1.25 µm, contrasting with older suspensions. This variance could be due to the repeated sonication and mixing of older suspensions, or it might indicate that the suspension required time to stabilize.

To estimate the PAH concentration in the samples relative to the nominal concentration, a semi-quantitative method was established. The method employed relied on the principle that different PAHs exhibit specific fluorescent features at different wavelengths upon excitation, which can be measured fluorometrically (Matuszewska & Czaja, 2020; Qazi et al., 2021). When measuring PAH concentrations in the medium after 20 h exposure to P90+PAH, no release of B[a]P was detected. On the contrary, the detected Pyr concentration was comparable to the nominal concentration. A possible explanation for this observation could be that the higher concentration of Pyr relative to B[a]P employed in the particle suspensions caused a saturation of the binding sites on the P90 particles. While P90+B[a]P had a nominal PAH concentration of 10 µg/mg P90, P90+Pyr had a nominal Pyr concentration of 100 µg/mg P90. Given that PAH release from carbon particles is highly dependent on the proportion of PAH adsorbed to the particle (Bevan & Worrell, 1985; Gerde et al., 2001), it is possible that the disproportionate relationship between the PAH concentrations could have affected the results. Furthermore,

the method only gave an approximate estimate of the PAH concentrations, and the limit of detection most likely affected the reliability of the measurements.

To prevent underestimation of cytokine release, P90s potential to adsorb CXCL8 was estimated in the culture medium used in the assays. The results showed that CXCL8 did not bind to P90. The binding of IL-6 was not assessed, however findings from previous studies, with comparable concentrations of P90 and additives, indicate that IL-6 adsorption to P90 is prevented under the aforementioned conditions. For instance, Kocbach et al. (2008) found that incubation of P90 with FBS for 24h significantly reduced the binding of CXCL8 and prevented the binding for IL-6 completely. Moreover, the study also found that incubation for 24 h with 0.1% BSA prevented cytokine binding for all cytokines tested.

4.2 Effects in Monocultures

4.2.1 The cytotoxic effect of uncoated and PAH-coated P90, and B[a]P

Significant alteration of cell viability measured by AlamarBlue was only observed for the highest concentrations of P90 and P90+B[a]P in monocultures, and no effect was observed for exposure to P90+Pyr or B[a]P alone. Similarly, the measured LDH release was modest in all monocultures, with no effect observed for exposure to B[a]P alone. Compared to the other monocultures, Ea.Hy cells exhibited an enhanced response, with significant cytotoxicity observed when exposed to both P90 and P90+B[a]P at concentrations of 100 µg/mL. Furthermore, P90 induced more pronounced cytotoxic effects compared to P90+PAH in the Ea.Hy cells, and significant differences in cell viability between coated and uncoated particles were observed from 100 µg/mL. These results are in alignment with a study conducted by Goulaouic et al. (2008), who found no reduction in cell viability when THP-1 macrophages were exposed to 50 µg/mL P90 particles alone or with adsorbed PAHs. Thus, the result indicates that P90 and P90+PAH only induce cytotoxic effects above concentrations of 50 µg/mL. Consequently, the results from the present study also suggest that P90 has a higher cytotoxic potential than P90+PAH, thereby indicating that PAH coating onto particles decrease the cytotoxicity relative to the particle itself. Similarly, in a study by Ryu et al. (2023), it was also found that PAH-coated particles induced less cytotoxic effects compared to uncoated particles when exposing A549 cells to CB particles of various sizes, with or without B[a]P

coating. However, the authors attributed the difference in cytotoxic potential solely to an increase in particle size caused by B[a]P adsorption (Ryu et al., 2023). Particle size did not however seem to contribute to the cytotoxic effect in the present study as P90 particles were actually estimated to be larger compared to P90+PAH particles. Notably, the different methods for particle formation, i.e., Ryu et al. (2023) employed a spray drying method, might have affected this difference in particle size.

It has been shown that UFPs have the ability to interact with the culture medium, thereby having their surfaces modified by protein (or other molecules) coronas, which may significantly impact the particle-induced toxicity (Liu et al., 2020; Rothen-Rutishauser et al., 2023; Stoeger et al., 2005). Pan et al. (2022) reported that the cytotoxic effect of P90+Pyr can be influenced by BSA to a greater extent than uncoated P90. The study found that BSA could bind with P90+Pyr, leading to a decrease in cytotoxicity by forming P90+Pyr/protein conjugates (Pan et al., 2022). However, it is worth noting that their study employed considerably higher concentrations of BSA (5%) compared to the present study, thus limiting the comparability of the formation of protein coronas. It is also worth noting that the study conducted by Pan et al. (2022), evaluated cytotoxicity up to 50 µg/mL, which is below the concentration where significant differences between P90 and P90+PAH were detected in the present study.

Exposure to B[a]P alone appeared to have no cytotoxic effects on monocultures, indicating that PAHs in the employed concentrations had a low cytotoxic potential. This finding aligns with a previous study which demonstrated that B[a]P treatment did not affect cell viability of primary macrophages up to 10 µM (Podechard et al., 2008). Moreover, in a study assessing the cytotoxic potential of Pyr, it was found that incubating A549 cells with Pyr concentration up to 9506 µM did not induce cell death (Bömmel et al., 2003). Collectively, this indicates that the proportions of PAHs adsorbed to P90 did not contribute to the observed cytotoxicity, and that the observed effect were due to the increasing concentration of particles, and not the presence of PAH. The results obtained in the present study therefore indicates that the difference in effects between uncoated and coated particles is attributed to the chemical alteration of the PAH-coated particles, rather than particle size.

4.2.2 The effect of uncoated and PAH-coated P90, and B[a]P on IL-6 and CXCL8 release

The contrasting results of P90 and P90+PAH exposure was also evident in the assessment of pro-inflammatory cytokines. A concentration-dependent release of both IL-6 and CXCL8 was detected in Ea.Hy cells exposed to P90, whereas exposure to P90+PAH only induced modest responses. The pro-inflammatory potential of P90 has been well established in previous studies (Totlandsdal et al., 2010; Totlandsdal et al., 2008). Therefore, the reduced effect of P90+PAH might indicate that PAH-coating have an inhibitory effect on P90-induced pro-inflammatory responses. This finding aligns with a previous study by Lindner et al. (2017), who found that B[a]P coating prevented the P90-induced increase of CXCL8 expression in A549 cells. The study suggested that this was due to the reduction of P90s specific surface area, demonstrating that B[a]P adsorption decreased P90 surface area by one-third in a suspension containing of 0.25 µg B[a]P per mg P90 (Lindner et al., 2017). In comparison, the present study employed a considerably higher concentration of B[a]P per mg P90 (10 µg/ mg P90), suggesting that P90s specific surface might have been even more reduced, which could possibly explain the apparent inhibitory effect of PAH-coating.

Goulaouic et al. (2008) attributed the reduced effect of PAH-coated particles to a decrease in PAH bioavailability when investigating the CXCL8 release following exposure to 50 µg/mL P90 with or without PAH-coating and PAH alone in THP-1 macrophages. They found that exposure to both P90 and P90 with B[a]P adsorbed (0.01 µg/ mg particle) only induced modest CXCL8 responses. However, exposure to the same amount of B[a]P alone significantly surpassed these responses, indicating that B[a]P-coating diminished the PAHs pro-inflammatory effects (Goulaouic et al., 2008). These findings do not align with the result obtained from the present study, where exposure to B[a]P did not induce CXCL8, thus suggesting that PAH-coating mitigated the pro-inflammatory effects of P90 and not the opposite.

The relevance of particle size in pro-inflammatory effects has also been assessed in previous studies. For instance, Goulaouic et al. (2008) found the effect of PAH-coated P90 to be considerably weaker than the effect of larger particles (Huber 990 carbon black, diameter: 260.3 nm) with same amount of PAH absorbed. On the other hand, Ryu et al. (2023) presented contrasting results and found that smaller particles were predominant in inducing inflammatory response in A549 cells, regardless of the presence of PAH. In the present study, the size of the P90+B[a]P sample was nearly halved compared to P90 alone, but still exhibited

significantly decreased effects compared to the larger, uncoated particles. Thus, the most likely interpretation of the results seems to be that PAH surface coating reduces the toxic potential of P90 by influencing their chemical properties, possibly by decreasing their specific surface area.

The findings from the present study indicate that the impact of the organic fraction of UFP is minimal compared to the particle itself. However, the importance of the organic components for the proinflammatory effects of particles has been previously demonstrated. Totlandsdal et al. (2012) reported a significant increase in IL-6 release in human bronchial epithelial BEAS-2B when exposed to both DEP and its organic extract, while exposure to DEP residuals representing the carbon core, did not elicit a similar response. Furthermore, it has been reported that DEP samples with higher PAH and lower metal content was a more potent inducer of pro-inflammatory responses compared to DEP samples characterized by lower PAH levels and higher metal content, indicating the potential inflammatory influence of organic constituents (Totlandsdal et al., 2015).

It has also been reported that the organic fraction might influence the various pro-inflammatory pathways (Fuentes-Mattei et al., 2010; Longhin et al., 2018). Longhin et al. (2018) found that urban $PM_{2.5}$, generated from combustion of organic materials, including carbon particles with adsorbed PAHs, induced the release of IL-6 in BEAS-2B cells, but not CXCL8. Their results demonstrated an accumulation of CXCL8 in intracellular vehicles accompanied by changes in the organization of actin filament, thus indicating that $PM_{2.5}$ decreased the delivery of CXCL8 vesicles to the plasma membrane. However, the same study found that PM_{10} mainly consisting of mineral particles with high content of metals and endotoxins induced the release of both IL-6 and CXCL8, and further speculated whether the inhibition of CXCL8 release was caused by the organic components of the combustion particles (Longhin et al., 2018). This finding further highlights how the inflammatory potential of different PMs is highly variable, and strongly dependent on the specific composition of the adsorbed component.

The overall findings suggest that B[a]P exhibits low toxicity under the conditions of this study, and a significant increase in IL-6 release was observed only in Calu-3 cells, with no effect detected on CXCL8 response. This contrasts with previous studies, where even lower concentrations of B[a]P have been found to induce significant pro-inflammatory responses in

both THP-1 macrophages and vascular endothelial cells (Goulaouic et al., 2008; Shi et al., 2021). In a study by Podechard et al. (2008) it was reported a significant increase in CXCL8 release relative to control in primary macrophages exposed to concentrations as low as 1 µM B[a]P. The study further attributed this increase to B[a]P's activation of AhR, as demonstrated by reduced CXCL8 induction following AhR knock-down (Podechard et al., 2008). In the present study, CYP1A1 activity measured by EROD, typically indicative of AhR activation, was not detected in monocultures, except in Calu-3 cells. While speculative, this finding raises the possibility that the variability in pro-inflammatory effect from B[a]P exposure between the monocultures may have been influenced by this differential AhR activation.

4.2.3 The effect of P90+B[a]P and B[a]P on CYP1A1 activity

CYP1A1 activity measured with EROD assay was only detected in Calu-3 cells exposed to B[a]P. Conversely, P90+B[a]P did not appear to induce CYP1A1 activity. The inability to induce CYP1A1 activity indicates that B[a]P was unable to bind to AhR, thus suggesting that B[a]P is not bioavailable when adsorbed to P90. Furthermore, the lack of observed CYP1A1 activity in other monocultures exposed to B[a]P could indicate that the CYP1A1 is not sufficiently expressed in these cells. There is however compelling evidence supporting AhRs involvement in cytokine responses (Gargaro et al., 2021; Liu et al., 2017; Martins et al., 2022; Shi et al., 2021). For instance, exposure to P90+B[a]P did not trigger CYP1A1 activity in Ea.Hy cells but significantly increased CXCL8 release, which could potentially inhibit CYP1A1 activity according to previous research by Totlandsdal et al. (2010). Conversely, B[a]P induced CYP1A1 activity in Calu-3 cells but did not induce a CXCL8 response in the present study. AhR activity has been shown to suppress pro-inflammatory responses, which may explain the lack of cytokine response in Calu-3 cells, as demonstrated by Øvrevik et al. (2014). However, it is important to note that these explanations are speculative and further research is needed to elucidate the mechanisms underlying these observations.

4.3 Effects in 3D cultures

4.3.1 The effect of uncoated and B[a]P-coated P90, and B[a]P on IL-6 and CXCL8 expression

Exposure to P90, P90+B[a]P or B[a]P did not have a significant effect on the cytokine response in 3D cultures. The lack of P90-induced endothelial response was unexpected as P90 gave a significant increase in cytokine release in Ea.Hy monoculture. However, because the Ea.Hy cells in the 3D cultures were indirectly affected by aerosol exposure, the response is likely to be considerably dampened by the epithelial barrier. In addition, the difference in incubation time after exposure is likely to have contributed to the observed response. While monocultures were exposed for 20 h, 3D cultures were only exposed for 3 and 6 h. The detected endothelial cytokine release is thereby dependent on the amount of P90 that is translocated into the basolateral compartment of the 3D models in 3 and 6 h. In a study investigating translocation of nanoparticles (NPs) across epithelial barrier, George et al. (2015) found that silica NPs translocated respectively at 3% and 35% across the Calu-3 and A549 cells during 24 h exposure.

In this study, a nominal exposure concentration of 5.2 μg/cm^2 of P90 was used. Assuming a translocation capacity of 35%, the theoretical concentration reaching endothelial cells would be approximately 1.87 μg/cm^2 in the A549 model, and significantly less in the Calu-3 model. In contrast, monocultures were directly exposed to P90 concentrations from 1.30-20.83 μg/cm^2. Therefore, the most likely interpretation of these findings is that particles were not translocated into the endothelial layer of the 3D models. Similarly, a relatively low rate of particle translocation have been demonstrated *in vivo*. Miller et al. (2017) only found 0.02% of the inhaled dose of nanoparticles to be translocated into the bloodstream after 24 h in humans.

Although not a significant finding, the results indicated higher levels of cytokines in the basolateral compartment relative to the apical compartment in the A549 model compared to the Calu-3 model. This is likely due to the Calu-3 cells ability to form a tight epithelial barrier, which limits the passage of secreted cytokines and other water-soluble molecules across the transwell insert (Cooney & Hickey, 2011). The 3D cultures also exhibited some differences in the overall cytokine release, apical and basolateral compartment combined. The basal and B[a]P-induced IL-6 release was considerably higher in the Calu-3 model compared to the A549

model. This might be due to a higher basal IL-6 release in the Calu-3 cells relative to that of A549 cells, as detected in monocultures. Conversely, the total CXCL8 release was similar for the two models. In A549 monoculture, P90 induced a significant increased CXCL8 response at 200 µg/mL, which were not reflected in the 3D cultures. This indicates that the exposure concentration used for 3D cultures, corresponding to approximately 50 µg/mL, was not sufficient to induce an effect. Furthermore, the exposure time could have affected the relative protein concentration detected in supernatant. Although both IL-6 and CXCL8 can be rapidly produced and released by cells in response to various stimuli, their levels may continue to increase over time as part of a sustained inflammatory reaction (Longhin et al., 2018). Additionally, the release of both IL-6 and CXCL8 appears to be increasing from 3 to 6 h. Therefore, longer exposure times may provide a more comprehensive understanding of the kinetics of cytokine release and the extent of the inflammatory response. Nevertheless, as outlined above (see section 4.2.2), there are numerous factors that may potentially affect particle-induced inflammatory responses.

4.3.2 The effect of P90+B[a]P and B[a]P on CYP1A1 expression

A substantial increase in CYP1A1 expression relative to control was observed in both 3D cultures in the apical cells when exposed to B[a]P. This was expected as one of the most recognized modes of action for B[a]P is the association with AhR and the following upregulation of CYP enzymes, where CYP1A1 is highly involved in B[a]P metabolism (Shiizaki et al., 2017). These results are consistent with findings from previous studies (Jiang et al., 2007; Totlandsdal et al., 2012). Notably, a high C_t value (>35) in the apical compartment of the A549 model indicates that CYP1A1 is expressed to a lesser degree in the A549 cells compared to Calu-3 cells. This is also consistent with the findings from the estimation of CYP1A1 activity in monocultures, where enzyme activity was only observed in Calu-3 cells, and not in A549 cells.

The CYP1A1 expression was considerably weaker in the basolateral Ea.Hy cells compared to the apical compartments. However, the comparable induction of CYP1A1 expression in Ea.Hy cells in both 3D cultures suggest that the different barrier capacity of epithelial cells did not influence the B[a]P throughput, indicating that B[a]P passively diffused through the lipid

bilayer of calu-3 and A549 cell layer to reach the endothelial cells. This is consistent with B[a]Ps lipophilic nature, as reported by previous studies (Fu et al., 2022; Miller & Ramos, 2001). On the contrary, no CYP1A1 activity was detected in Ea.Hy monocultures measured by EROD assay. The presence of CYP1A1 expression in cocultured Ea.Hy cells suggests active gene transcription, however the absence of detectable enzyme activity in monoculture indicates minimal protein expression. The difference in CYP1A1 expression between ALI culture and submerged monoculture exposure implies variations in cellular environment and metabolic activities between the two methods. This discrepancy may lead to different intracellular levels of CYP1A1, possibly influenced by factors such as cell quantity and medium volume. Further investigation would be needed to understand the underlying contributing mechanisms.

P90+B[a]P did not induce CYP1A1 gene expression. This was unexpected as other studies have shown that the organic components of PM are capable of initiating AhR-dependent pathways (Baulig et al., 2003; Juarez Facio et al., 2022). The inability to induce CYP1A1 expression indicates that P90+B[a]P were not able to associate with AhR. This is contrasting to the findings of other studies with comparable 3D cultures. In a study by Klein et al. (2017) it was found a significant induction of CYP1A1 expression in endothelial cells when exposing 3D cultures to a relative low amount (80 ng/cm^2) of DEP. Similarly, Brinchmann et al. (2018) demonstrated that exposure to DEP increased the expression of AhR-related genes. This effect was observed both when cells were exposed to DEP directly and when they were exposed to lipophilic organic extracts of DEP (Brinchmann et al., 2018). These findings demonstrate that the organic compounds of DEP, containing AhR agonists, reach the endothelial cells after exposure of the epithelial cells at the apical side. This implies their availability for cellular interaction, emphasizing the potential role of organic compounds in the effects induced by PM. The significance of the organic fraction has also been demonstrated by Mills et al. (2011), who found that exposure to DEP induced direct vascular dysfunction, while exposure to pure carbon nanoparticles did not, suggesting that vascular dysfunction was driven by the soluble fractions present on the particle surface rather than the particle itself. Furthermore, Keebaugh et al. (2015) found that removing organic components from concentrated ambient $PM_{0.18}$ significantly reduced atherosclerotic plaque size and lipid content in genetically modified mice predisposed to atherosclerosis, suggesting that atherosclerotic effects of $PM_{2.5}$ is due to the organic constituents attached to the particles.

In contrast, the results obtained in the present study suggest that B[a]P adsorbed to P90 was not readily bioavailable and thus did not translocate across the epithelial barrier. This suggests that the absence of P90+B[a]P-induced CYP1A1 expression is likely due to the chemical properties of the particles, which inhibit B[a]P from binding to AhR. In such a scenario, its reasonable that CYP1A1 expression is not induced, as P90 alone lacks this capability. This has been demonstrated by Takano et al. (2002), who found that mice intratracheally instilled with DEP exhibited a dose-dependent increase in CYP1A1 expression, while no such effect was observed with CB particles (Takano et al., 2002).

4.4 P90+B[a]P as a model for combustion particles

It has been proposed that CB particles may not accurately represent typical ambient PM or traffic emissions due to their unrealistic chemical composition, including a higher content of elemental carbon (EC) (Farahani et al., 2021; Long et al., 2013). In the present study, particles were coated with 10 µg B[a]P or 100 µg Pyr per mg P90. Given that all of these PAHs were adsorbed onto the particles, the resulting EC proportion for P90+BaP and P90+Pyr would be 99.9% and 99%, respectively. For comparison, standardized DEPs have less than 40% EC (Farahani et al., 2021). Furthermore, real exhaust particles and UFPs from traffic contain very little carbon and predominantly consist of highly soluble organic matter, with the proportion of EC collected in various US cities ranging from 8-17% (Farahani et al., 2021). Consequently, the EC concentration represented in this study is significantly higher than those encountered in real-world exposure, which essentially are particles consisting of a liquid mass surrounding a small carbon core. As a result, these particles contain a significant amount of soluble organic carbon (including PAHs), which can be easily released into cells. In contrast, the thin layer of PAHs coated on P90 particles in this study appeared to bind strongly and was not readily released. This aligns with well with observation from previous studies (Bevan & Yonda, 1985; Borm et al., 2005). For instance, Bevan and Worrell (1985) demonstrated that reducing the B[a]P concentration on CB particles decreased both the rate and extent of elution. The study used phospholipid vesicles in an in vitro setting to simulate the release pattern and found that B[a]P at high concentrations (100-fold higher than the natural level of these CBs) was released in two phases, with some remaining unreleased (Bevan & Worrell, 1985). A similar pattern of biphasic elution of B[a]P was observed when diesel particles loaded with a high concentration

of B[a]P were administered to living organisms (Gerde et al., 2001). In the study they absorbed B[a]P, corresponding to 25% of the surface, onto denuded diesel soot and administrated it to dogs. While they demonstrated that 36% of the B[a]P was rapidly released from the particles, they found the remaining 64% of B[a]P to be strongly particle-bound and retained in the lungs up to 5.6 months (Gerde et al., 2001). These observations implies that the release of B[a]P from carbon particles depends on the proportion of B[a]P adsorbed to the particle. Specifically, when the percentage of PAHs adsorbed to the particles is below a certain threshold, their strong binding to the particles drastically decreases their bioavailability. This is in agreement with observations from the present study, and further supports that the low proportion of B[a]P relative to the large amount of P90, did not allow for B[a]P release. Collectively, this indicates that the employed model for organic combustion particles, i.e., B[a]P-coated P90, poses significant limitation in the evaluation of the “Trojan horse” effect. Primarily because the model employed does not seem to facilitate the disassociation of B[a]P, thereby limiting its bioavailability, as well as diminishing the observed effects attributed to the particles themselves.

5 Conclusion

The present study found that P90 and P90+PAH induced cytotoxicity in monocultures only at the highest exposure concentrations (>100 µg/mL). However, a significant difference between the cytotoxic potential of P90 and P90+PAH was observed in Ea.Hy cells, with P90-induced cytotoxicity significantly surpassing that of P90+PAH from a concentration of 100 µg/mL. Together with the lacking effects of PAH exposure, this suggests that the cytotoxic effect observed from P90+PAH exposure was driven by the increase in P90 concentration, rather than the increasing concentration of PAHs. The findings from the assessment of the pro-inflammatory effect were similarly interpreted. However, the pro-inflammatory potential of P90 was significantly higher compared to P90+PAH at lower concentrations (>25 µg/mL). This further indicates that PAH-coating had an inhibitory effect on the overall toxicity of P90 by influencing its chemical properties, possibly by decreasing its specific surface area. Although Ea.Hy monoculture exhibited a significant increase in P90-induced IL-6 and CXCL8 release, the same effect was not observed when assessing the endothelial response in 3D cultures. These findings suggest that the Ea.Hy cells in the basolateral compartment were not exposed to sufficient concentrations, possibly due to the lack of particle translocation. Furthermore, P90+B[a]P failed to induce CYP1A1 expression in both monocultures and in 3D cultures. This indicates that B[a]P associated with P90 was not able to bind to AhR, which further suggests that B[a]P was not readily bioavailable. This was most likely due to the low amount of B[a]P (10 µg per mg P90) relative to the large fraction of elemental carbon (P90), not allowing for B[a]P release. This may contrast a real-life scenario, where particles often consist of a small carbon core surrounded by a liquid mass, which can be readily released in cells. Therefore, this study was not able to demonstrate an increased effect of PAH-coating on particles relative to pristine particles. Instead, the PAH-coating appeared to mitigate the toxicity elicited by the particles themselves, in addition to inhibiting PAH toxicity. Thus, constrained by the experimental conditions utilized, the present study was unable to definitively determine the organic fractions contribution to the biological effects of combustion derived UFPs, and how this relates to the “Trojan Horse” effect. Accordingly, further investigation is encouraged to gain a deeper understanding of the relevance of “Trojan Horse” mechanisms in the progression of particle-induced diseases.

6 Future perspectives

The results presented in this study indicated that PAH-coating of P90 altered the toxicity of the particles by mitigating the effects of the particles themselves and preventing PAH toxicity. While this finding would be interesting to further investigate, particularly the apparent dual inhibitory effects of PAH-coatings on P90, it highly limited the assessment of the "Trojan Horse" mechanism. The thin PAH-coating seemed to impede B[a]P release, suggesting that the proportion of the organic fraction relative to the carbon core did not accurately represent ambient combustion particles. Therefore, adjusting the proportion of PAH-coating relative to the carbon core in future studies would be central for a more realistic model. One potential approach could involve testing various concentration ratios between P90 and PAHs to identify an optimal concentration. For instance, fluorescence measurements of PAHs could be conducted to evaluate their distribution and concentration within the particles. Moreover, incorporating the Brunauer-Emmett-Teller (BET) method to measure the specific surface area of the particles could provide further understanding of their physicochemical properties and their influence on biological responses. However, exploring alternative particle models, such as cast particles, may offer a more realistic representation of combustion particles. This approach could involve comparing particles with varying organic compound contents and evaluating differences between particle extracts and residues to gain valuable insights into their biological effects.

This study used DLS to estimate the particle size distribution in particle suspension. It would be beneficial to combine this with transmission electron microscopy (TEM) to increase reliability when determining size and particle agglomeration. This could also aid in determining the occurrence of particle endocytosis, and provide a more accurate assessment of the effective concentration of particles/PAHs taken up by the cells.

In this study, the employed methods exclusively evaluated endpoints. Although such methods allow for an estimation of the overall effects of exposure, they do not provide any information about the mechanisms driving these effects. Gaining a deeper understanding of central pathways, such as those involving AhR and ROS mechanisms, would indeed aid in the investigation of the "Trojan Horse" effect. Thus, assessing the effect of various inhibitors and/or including a broader spectrum of relevant genes could prove valuable.

In further studies, it would be advantageous to evaluate the toxic potential of Pyr, as well as determine the PAH concentration in the stock suspensions. PAH measurement showed that Pyr was present in the exposure medium at almost nominal concentrations, which limited the assessment of this PAH in this study. Utilizing saturation experiments would therefore enhance the reliability and accuracy of further investigations. Furthermore, it would be favorable for 3D cultures be exposed to Pyr to compare with B[a]P effects, as well as results from monoculture experiments. Additionally, increasing the number of experiments would aid in enhancing the biological significance of the results and gaining statistical power.

7 References

Aghasafari, P., George, U., & Pidaparti, R. (2019). A review of inflammatory mechanism in airway diseases. *Inflammation Research*, *68*(1), 59-74. https://doi.org/10.1007/s00011-018-1191-2

Antiñolo, M., Willis, M. D., Zhou, S., & Abbatt, J. P. (2015). Connecting the oxidation of soot to its redox cycling abilities. *Nature communications*, *6*, 6812. https://doi.org/10.1038/ncomms7812

Balashazy, I., Hofmann, W., & Heistracher, T. (2003). Local particle deposition patterns may play a key role in the development of lung cancer. *Journal of applied physiology*, *94*(5), 1719-1725. https://doi.org/10.1152/japplphysiol.00527.2002

Baulig, A., Garlatti, M., Bonvallot, V., Marchand, A., Barouki, R., Marano, F., & Baeza-Squiban, A. (2003). Involvement of reactive oxygen species in the metabolic pathways triggered by diesel exhaust particles in human airway epithelial cells. *American journal of physiology*, *285*(3), L671-679. https://doi.org/10.1152/ajplung.00419.2002

Baulig, A., Poirault, J. J., Ausset, P., Schins, R., Shi, T., Baralle, D., Dorlhene, P., Meyer, M., Lefevre, R., Baeza-Squiban, A., & Marano, F. (2004). Physicochemical characteristics and biological activities of seasonal atmospheric particulate matter sampling in two locations of Paris. *Environmental Science & Technology*, *38*(22), 5985-5992. https://doi.org/10.1021/es049476z

Beamer, C. A., & Shepherd, D. M. (2013). Role of the aryl hydrocarbon receptor (AhR) in lung inflammation. *Springer seminars in immunopathology*, *35*(6), 693-704. https://doi.org/10.1007/s00281-013-0391-7

Bevan, D. R., & Worrell, W. J. (1985). Elution of benzo[a]pyrene from carbon blacks into biomembranes in vitro. *Journal of Toxicology and Environmental Health Sciences*, *15*(5), 697-710. https://doi.org/10.1080/15287398509530697

Bevan, D. R., & Yonda, N. T. (1985). Elution of polycyclic aromatic hydrocarbons from carbon blacks into biomembranes in vitro. *Toxicology and Industrial Health*, *1*(1), 57-67. https://doi.org/10.1177/074823378500100106

Bopp, S. K., & Lettieri, T. (2008). Comparison of four different colorimetric and fluorometric cytotoxicity assays in a zebrafish liver cell line. *BioMed Central Pharmacology*, *8*, 8. https://doi.org/10.1186/1471-2210-8-8

Borm, P. J., Cakmak, G., Jermann, E., Weishaupt, C., Kempers, P., van Schooten, F. J., Oberdörster, G., & Schins, R. P. (2005). Formation of PAH-DNA adducts after in vivo and vitro exposure of rats and lung cells to different commercial carbon blacks. *Toxicology and Applied Pharmacology*, *205*(2), 157-167. https://doi.org/10.1016/j.taap.2004.10.020

Boström, C. E., Gerde, P., Hanberg, A., Jernström, B., Johansson, C., Kyrklund, T., Rannug, A., Törnqvist, M., Victorin, K., & Westerholm, R. (2002). Cancer risk assessment, indicators, and guidelines for polycyclic aromatic hydrocarbons in the ambient air. *Environmental Health Perspectives*, *110(*3), 451-488. https://doi.org/10.1289/ehp.110-1241197

Brinchmann, B. C., Skuland, T., Rambøl, M. H., Szoke, K., Brinchmann, J. E., Gutleb, A. C., Moschini, E., Kubátová, A., Kukowski, K., Le Ferrec, E., Lagadic-Gossmann, D., Schwarze, P. E., Låg, M., Refsnes, M., Øvrevik, J., & Holme, J. A. (2018). Lipophilic components of diesel exhaust particles induce pro-inflammatory responses in human endothelial cells through AhR dependent pathway(s). *Particle and Fibre Toxicology*, *15*(1), 21. https://doi.org/10.1186/s12989-018-0257-1

Bruschweiler, E. D., Danuser, B., Huynh, C. K., Wild, P., Schupfer, P., Vernez, D., Boiteux, P., & Hopf, N. B. (2012). Generation of polycyclic aromatic hydrocarbons (PAHs) during woodworking operations. *Frontiers in Oncology*, *2*, 148. https://doi.org/10.3389/fonc.2012.00148

Bukowski, R. M., Olencki, T., McLain, D., & Finke, J. H. (1994). Pleiotropic effects of cytokines: clinical and preclinical studies. *Stem Cells*, *12*, 129-140;140-121.

Burnett, R. T., Pope, C. A., 3rd, Ezzati, M., Olives, C., Lim, S. S., Mehta, S., Shin, H. H., Singh, G., Hubbell, B., Brauer, M., Anderson, H. R., Smith, K. R., Balmes, J. R., Bruce, N. G., Kan, H., Laden, F., Prüss-Ustün, A., Turner, M. C., Gapstur, S. M., . . . Cohen, A. (2014). An integrated risk function for estimating the global burden of disease attributable to ambient fine particulate matter exposure. *Environmental Health Perspectives*, *122*(4), 397-403. https://doi.org/10.1289/ehp.1307049

Bustamante-Marin, X. M., & Ostrowski, L. E. (2017). Cilia and Mucociliary Clearance. *Cold Spring Harbor Perspectives in Biology*, *9*(4). https://doi.org/10.1101/cshperspect.a028241

Bustin, S. A., Benes, V., Garson, J. A., Hellemans, J., Huggett, J., Kubista, M., Mueller, R., Nolan, T., Pfaffl, M. W., Shipley, G. L., Vandesompele, J., & Wittwer, C. T. (2009). The MIQE guidelines: minimum information for publication of quantitative real-time PCR experiments. *Clinical Chemistry*, *55*(4), 611-622. https://doi.org/10.1373/clinchem.2008.112797

Bömmel, H., Haake, M., Luft, P., Horejs-Hoeck, J., Hein, H., Bartels, J., Schauer, C., Pöschl, U., Kracht, M., & Duschl, A. (2003). The diesel exhaust component pyrene induces expression of IL-8 but not of eotaxin. *International Immunopharmacology*, *3*(10-11), 1371-1379. https://doi.org/10.1016/s1567-5769(03)00135-8

Cakmak, S., Hebbern, C., Cakmak, J. D., & Dales, R. E. (2017). The influence of polycyclic aromatic hydrocarbons on lung function in a representative sample of the Canadian population. *Environmental Pollution*, *228*, 1-7. https://doi.org/10.1016/j.envpol.2017.05.013

Carlier, F. M., de Fays, C., & Pilette, C. (2021). Epithelial Barrier Dysfunction in Chronic Respiratory Diseases. *Frontiers in Physiology*, *12*, 691227. https://doi.org/10.3389/fphys.2021.691227

Carvalho, T. C., Peters, J. I., & Williams, R. O., 3rd. (2011). Influence of particle size on regional lung deposition--what evidence is there? *International Journal of Pharmaceutics*, *406*(1-2), 1-10. https://doi.org/10.1016/j.ijpharm.2010.12.040

Cassee, F., Morawska, L., Peters, A., Wierzbicka, A., Buonanno, G., Cyrys, J., SchnelleKreis, J., Kowalski, M., Riediker, M., Birmili, W., Querol, X., Yildirim, A. Ö., Elder, A., Yu, I. J., Øvrevik, J., Hougaard, K. S., Loft, S., Schmid, O., Schwarze, P. E., ... Aurelio, T. (2019). *White Paper: Ambient ultrafine particles: evidence for policy makers*. https://efca.net/files/WHITE%20PAPER-UFP%20evidence%20for%20policy%20makers%20(25%20OCT).pdf

Chen, L., Deng, H., Cui, H., Fang, J., Zuo, Z., Deng, J., Li, Y., Wang, X., & Zhao, L. (2018). Inflammatory responses and inflammation-associated diseases in organs. *Oncotarget*, *9*(6), 7204-7218. https://doi.org/10.18632/oncotarget.23208

Cheung, K., Daher, N., Kam, W., Shafer, M. M., Ning, Z., Schauer, J. J., & Sioutas, C. (2011). Spatial and temporal variation of chemical composition and mass closure of ambient coarse particulate matter (PM10–2.5) in the Los Angeles area. *Atmospheric Environment*, *45*(16), 2651-2662. https://doi.org/https://doi.org/10.1016/j.atmosenv.2011.02.066

Cohen, A. J., Brauer, M., Burnett, R., Anderson, H. R., Frostad, J., Estep, K., Balakrishnan, K., Brunekreef, B., Dandona, L., Dandona, R., Feigin, V., Freedman, G., Hubbell, B., Jobling, A., Kan, H., Knibbs, L., Liu, Y., Martin, R., Morawska, L., . . . Forouzanfar, M. H. (2017). Estimates and 25-year trends of the global burden of disease attributable to ambient air pollution: an analysis of data from the Global Burden of Diseases Study 2015. *Lancet*, *389*(10082), 1907-1918. https://doi.org/10.1016/s0140-6736(17)30505-6

Cooney, D. J., & Hickey, A. J. (2011). Cellular response to the deposition of diesel exhaust particle aerosols onto human lung cells grown at the air-liquid interface by inertial impaction. *Toxicology in Vitro*, *25*(8), 1953-1965. https://doi.org/10.1016/j.tiv.2011.06.019

Daigneault, M., Preston, J. A., Marriott, H. M., Whyte, M. K., & Dockrell, D. H. (2010). The identification of markers of macrophage differentiation in PMA-stimulated THP-1 cells and monocyte-derived macrophages. *PLoS One*, *5*(1), e8668. https://doi.org/10.1371/journal.pone.0008668

Darquenne, C. (2012). Aerosol deposition in health and disease. *Journal of Aerosol Medicine and Pulmonary Drug Delivery*, *25*(3), 140-147. https://doi.org/10.1089/jamp.2011.0916

Deng, Q., Deng, L., Miao, Y., Guo, X., & Li, Y. (2019). Particle deposition in the human lung: Health implications of particulate matter from different sources. *Environmental Research*, *169*, 237-245. https://doi.org/10.1016/j.envres.2018.11.014

Di Filippo, P., Riccardi, C., Gariazzo, C., Incoronato, F., Pomata, D., Spicaglia, S., & Cecinato, A. (2007). Air pollutants and the characterization of the organic content of aerosol particles in a mixed industrial/semi-rural area in central Italy. *Journal of Environmental Monitoring*, *9*(3), 275-282. https://doi.org/10.1039/b615118c

Donaldson, K., Borm, P. J., Castranova, V., & Gulumian, M. (2009). The limits of testing particle-mediated oxidative stress in vitro in predicting diverse pathologies; relevance for testing of nanoparticles. *Particle and Fibre Toxicology*, *6*, 13. https://doi.org/10.1186/1743-8977-6-13

Donaldson, K., Stone, V., Seaton, A., & MacNee, W. (2001). Ambient particle inhalation and the cardiovascular system: potential mechanisms. *Environmental Health Perspectives*, *109*(4), 523-527. https://doi.org/10.1289/ehp.01109s4523

Donaldson, K., Tran, L., Jimenez, L. A., Duffin, R., Newby, D. E., Mills, N., MacNee, W., & Stone, V. (2005). Combustion-derived nanoparticles: a review of their toxicology following inhalation exposure. *Particle and Fibre Toxicology*, *2*, 10. https://doi.org/10.1186/1743-8977-2-10

Dong, J., Li, F., & Xie, K. (2012). Study on the source of polycyclic aromatic hydrocarbons (PAHs) during coal pyrolysis by PY–GC–MS. *Journal of Hazardous Materials*, *243*, 80-85. https://doi.org/https://doi.org/10.1016/j.jhazmat.2012.09.073

Edgell, C. J., McDonald, C. C., & Graham, J. B. (1983). Permanent cell line expressing human factor VIII-related antigen established by hybridization. *Proceedings of the National Academy of Sciences of the United States of America*, *80*(12), 3734-3737. https://doi.org/10.1073/pnas.80.12.3734

Environmental Protection Agency. (2021). *Our Nation's Air* https://gispub.epa.gov/air/trendsreport/2022/#home

Environmental Protection Agency. (n.d.). *Particle Pollution Exposure. Particle Pollution and Your Patient's Health* https://www.epa.gov/pmcourse/particle-pollution-exposure

Farahani, V. J., Pirhadi, M., & Sioutas, C. (2021). Are standardized diesel exhaust particles (DEP) representative of ambient particles in air pollution toxicological studies? *The Science of The Total Environment*, *788*, 147854. https://doi.org/https://doi.org/10.1016/j.scitotenv.2021.147854

Foster, K. A., Oster, C. G., Mayer, M. M., Avery, M. L., & Audus, K. L. (1998). Characterization of the A549 cell line as a type II pulmonary epithelial cell model for drug metabolism. *Experimental Cell Research*, *243*(2), 359-366. https://doi.org/10.1006/excr.1998.4172

Frericks, M., Meissner, M., & Esser, C. (2007). Microarray analysis of the AHR system: tissue-specific flexibility in signal and target genes. *Toxicology and Applied Pharmacology*, *220*(3), 320-332. https://doi.org/10.1016/j.taap.2007.01.014

Fu, C., Li, Y., Xi, H., Niu, Z., Chen, N., Wang, R., Yan, Y., Gan, X., Wang, M., Zhang, W., Zhang, Y., & Lv, P. (2022). Benzo(a)pyrene and cardiovascular diseases: An overview of pre-clinical studies focused on the underlying molecular mechanism. *Frontiers in Nutrition*, *9*, 978475. https://doi.org/10.3389/fnut.2022.978475

Fuentes-Mattei, E., Rivera, E., Gioda, A., Sanchez-Rivera, D., Roman-Velazquez, F. R., & Jimenez-Velez, B. D. (2010). Use of human bronchial epithelial cells (BEAS-2B) to study immunological markers resulting from exposure to PM(2.5) organic extract from Puerto Rico. *Toxicology and Applied Pharmacology*, *243*(3), 381-389. https://doi.org/10.1016/j.taap.2009.12.009

Gao, W., Li, L., Wang, Y., Zhang, S., Adcock, I. M., Barnes, P. J., Huang, M., & Yao, X. (2015). Bronchial epithelial cells: The key effector cells in the pathogenesis of chronic obstructive pulmonary disease? *Respirology*, *20*(5), 722-729. https://doi.org/10.1111/resp.12542

Gargaro, M., Scalisi, G., Manni, G., Mondanelli, G., Grohmann, U., & Fallarino, F. (2021). The Landscape of AhR Regulators and Coregulators to Fine-Tune AhR Functions. *International Journal of Molecular Sciences*, *22*(2). https://doi.org/10.3390/ijms22020757

George, I., Vranic, S., Boland, S., Courtois, A., & Baeza-Squiban, A. (2015). Development of an in vitro model of human bronchial epithelial barrier to study nanoparticle translocation. *Toxicology in Vitro*, *29*(1), 51-58. https://doi.org/https://doi.org/10.1016/j.tiv.2014.08.003

Gerde, P., Muggenburg, B. A., Lundborg, M., & Dahl, A. R. (2001). The rapid alveolar absorption of diesel soot-adsorbed benzo[a]pyrene: bioavailability, metabolism and dosimetry of an inhaled particle-borne carcinogen. *Carcinogenesis*, *22*(5), 741-749. https://doi.org/10.1093/carcin/22.5.741

Goulaouic, S., Foucaud, L., Bennasroune, A., Laval-Gilly, P., & Falla, J. (2008). Effect of polycyclic aromatic hydrocarbons and carbon black particles on pro-inflammatory cytokine secretion: impact of PAH coating onto particles. *Journal of Immunotoxicology*, *5*(3), 337-345. https://doi.org/10.1080/15476910802371016

Grahame, T. J., Klemm, R., & Schlesinger, R. B. (2014). Public health and components of particulate matter: the changing assessment of black carbon. *Journal of the Air & Waste Management Association*, *64*(6), 620-660. https://doi.org/10.1080/10962247.2014.912692

Grommes, J., & Soehnlein, O. (2011). Contribution of neutrophils to acute lung injury. *Molecular Medicine*, *17*(3-4), 293-307. https://doi.org/10.2119/molmed.2010.00138

Grunig, G., Marsh, L. M., Esmaeil, N., Jackson, K., Gordon, T., Reibman, J., Kwapiszewska, G., & Park, S. H. (2014). Perspective: ambient air pollution: inflammatory response and effects on the lung's vasculature. *Pulmonary Circulation*, *4*(1), 25-35. https://doi.org/10.1086/674902

Grytting, V. S., Chand, P., Låg, M., Øvrevik, J., & Refsnes, M. (2022). The pro-inflammatory effects of combined exposure to diesel exhaust particles and mineral particles in human bronchial epithelial cells. *Particle and Fibre Toxicology*, *19*(1), 14. https://doi.org/10.1186/s12989-022-00455-0

Günther, J., & Seyfert, H. M. (2018). The first line of defence: insights into mechanisms and relevance of phagocytosis in epithelial cells. *Seminars in Immunopathology*, *40*(6), 555-565. https://doi.org/10.1007/s00281-018-0701-1

Haddad, M., & Sharma, S. (2023). *Physiology, Lung*. StatPearls Publishing. https://www-ncbi-nlm-nih-gov.ezproxy.uio.no/books/NBK545177/

Hakkola, J., Hukkanen, J., Turpeinen, M., & Pelkonen, O. (2020). Inhibition and induction of CYP enzymes in humans: an update. *Archives of Toxicology*, *94*(11), 3671-3722. https://doi.org/10.1007/s00204-020-02936-7

Health Effects Institute. (2020). *State of Global Air 2020* https://www.stateofglobalair.org/resources/report/state-global-air-report-2020

Hertz-Picciotto, I., Herr, C. E., Yap, P. S., Dostál, M., Shumway, R. H., Ashwood, P., Lipsett, M., Joad, J. P., Pinkerton, K. E., & Srám, R. J. (2005). Air pollution and lymphocyte phenotype proportions in cord blood. *Environmental Health Perspectives*, *113*(10), 1391-1398. https://doi.org/10.1289/ehp.7610

Hiraiwa, K., & van Eeden, S. F. (2013). Contribution of lung macrophages to the inflammatory responses induced by exposure to air pollutants. *Mediators of Inflammation*, *2013*, 619523. https://doi.org/10.1155/2013/619523

Ho, C. C., Wu, W. T., Lin, Y. J., Weng, C. Y., Tsai, M. H., Tsai, H. T., Chen, Y. C., Yet, S. F., & Lin, P. (2022). Aryl hydrocarbon receptor activation-mediated vascular toxicity of ambient fine particulate matter: contribution of polycyclic aromatic hydrocarbons and osteopontin as a biomarker. *Particle and Fibre Toxicology*, *19*(1), 43. https://doi.org/10.1186/s12989-022-00482-x

Hofman, J., Staelens, J., Cordell, R., Stroobants, C., Zikova, N., Hama, S. M. L., Wyche, K. P., Kos, G. P. A., Van Der Zee, S., Smallbone, K. L., Weijers, E. P., Monks, P. S., & Roekens, E. (2016). Ultrafine particles in four European urban environments: Results from a new continuous long-term monitoring network. *Atmospheric Environment*, *136*, 68-81. https://doi.org/https://doi.org/10.1016/j.atmosenv.2016.04.010

Holme, J. A., Brinchmann, B. C., Le Ferrec, E., Lagadic-Gossmann, D., & Øvrevik, J. (2019). Combustion Particle-Induced Changes in Calcium Homeostasis: A Contributing Factor to Vascular Disease? *Cardiovascular Toxicology*, *19*(3), 198-209. https://doi.org/10.1007/s12012-019-09518-9

Holme, J. A., Brinchmann, B. C., Refsnes, M., Låg, M., & Øvrevik, J. (2019). Potential role of polycyclic aromatic hydrocarbons as mediators of cardiovascular effects from combustion particles. *Environmental Health*, *18*(1), 74. https://doi.org/10.1186/s12940-019-0514-2

Horne, B. D., Joy, E. A., Hofmann, M. G., Gesteland, P. H., Cannon, J. B., Lefler, J. S., Blagev, D. P., Korgenski, E. K., Torosyan, N., Hansen, G. I., Kartchner, D., & Pope, C. A., 3rd. (2018). Short-Term Elevation of Fine Particulate Matter Air Pollution and Acute Lower Respiratory Infection. *American Journal of Respiratory and Critical Care Medicine*, *198*(6), 759-766. https://doi.org/10.1164/rccm.201709-1883OC

International Agency for Reseach on Cancer. (2010). *Some non-heterocyclic polycyclic aromatic hydrocarbons and some related exposures* (Vol. 92). International Agency for Reseach on Cancer. https://publications.iarc.fr/110

International Agency for Reseach on Cancer. (2012). *Personal Habits and Indoor Combustions* (Vol. 100E). International Agency for Research on Cancer. https://publications.iarc.fr/122

International Agency for Research on Cancer. (2013). *Diesel and Gasoline Engine Exhausts and Some Nitroarenes* (Vol. 105). International Agency for Research on Cancer. https://publications.iarc.fr/129

Jiang, H., Gelhaus, S. L., Mangal, D., Harvey, R. G., Blair, I. A., & Penning, T. M. (2007). Metabolism of benzo[a]pyrene in human bronchoalveolar H358 cells using liquid chromatography-mass spectrometry. *Chemical Research in Toxicology*, *20*(9), 1331-1341. https://doi.org/10.1021/tx700107z

Johnson, M. D., Widdicombe, J. H., Allen, L., Barbry, P., & Dobbs, L. G. (2002). Alveolar epithelial type I cells contain transport proteins and transport sodium, supporting an active role for type I cells in regulation of lung liquid homeostasis. *Proceedings of the National Academy of Sciences of the United States of America*, *99*(4), 1966-1971. https://doi.org/10.1073/pnas.042689399

Joshi, N., Walter, J. M., & Misharin, A. V. (2018). Alveolar Macrophages. *Cellular Immunology*, *330*, 86-90. https://doi.org/10.1016/j.cellimm.2018.01.005

Juarez Facio, A. T., Yon, J., Corbière, C., Rogez-Florent, T., Castilla, C., Lavanant, H., Mignot, M., Devouge-Boyer, C., Logie, C., Chevalier, L., Vaugeois, J. M., & Monteil, C. (2022). Toxicological impact of organic ultrafine particles (UFPs) in human bronchial epithelial BEAS-2B cells at air-liquid interface. *Toxicology in Vitro*, *78*, 105258. https://doi.org/10.1016/j.tiv.2021.105258

Kang, M., Lim, C. H., & Han, J. H. (2013). Comparison of toxicity and deposition of nano-sized carbon black aerosol prepared with or without dispersing sonication. *Toxicological Research*, *29*(2), 121-127. https://doi.org/10.5487/tr.2013.29.2.121

Karagulian, F., Belis, C. A., Dora, C. F. C., Prüss-Ustün, A. M., Bonjour, S., Adair-Rohani, H., & Amann, M. (2015). Contributions to cities' ambient particulate matter (PM): A systematic review of local source contributions at global level. *Atmospheric Environment*, *120*, 475-483. https://doi.org/https://doi.org/10.1016/j.atmosenv.2015.08.087

Keane, M. P., & Strieter, R. M. (2002). The importance of balanced pro-inflammatory and anti-inflammatory mechanisms in diffuse lung disease. *Respiratory Research*, *3*(1), 5. https://doi.org/10.1186/rr177

Kelly, F. J., & Fussell, J. C. (2011). Air pollution and airway disease. *Journal of the British Society for Allergy and Clinical Immunology*, *41*(8), 1059-1071. https://doi.org/10.1111/j.1365-2222.2011.03776.x

Kelly, F. J., & Fussell, J. C. (2012). Size, source and chemical composition as determinants of toxicity attributable to ambient particulate matter. *Atmospheric Environment*, *60*, 504-526. https://doi.org/https://doi.org/10.1016/j.atmosenv.2012.06.039

Kim, K. H., Kabir, E., & Kabir, S. (2015). A review on the human health impact of airborne particulate matter. *Environment International*, *74*, 136-143. https://doi.org/10.1016/j.envint.2014.10.005

Klein, S. G., Cambier, S., Hennen, J., Legay, S., Serchi, T., Nelissen, I., Chary, A., Moschini, E., Krein, A., Blömeke, B., & Gutleb, A. C. (2017). Endothelial responses of the alveolar barrier in vitro in a dose-controlled exposure to diesel exhaust particulate matter. *Particle and Fibre Toxicology*, *14*(1), 7. https://doi.org/10.1186/s12989-017-0186-4

Kocbach, A., Totlandsdal, A. I., Låg, M., Refsnes, M., & Schwarze, P. E. (2008). Differential binding of cytokines to environmentally relevant particles: a possible source for misinterpretation of in vitro results? *Toxicology Letters*, *176*(2), 131-137. https://doi.org/10.1016/j.toxlet.2007.10.014

Kumar, P., Nagarajan, A., & Uchil, P. D. (2018). Analysis of Cell Viability by the Lactate Dehydrogenase Assay. *Cold Spring Harbor protocols*, *2018*(6). https://doi.org/10.1101/pdb.prot095497

Kwon, H. S., Ryu, M. H., & Carlsten, C. (2020). Ultrafine particles: unique physicochemical properties relevant to health and disease. *Experimental & Molecular Medicine*, *52*(3), 318-328. https://doi.org/10.1038/s12276-020-0405-1

Lacy, P., & Stow, J. L. (2011). Cytokine release from innate immune cells: association with diverse membrane trafficking pathways. *Blood*, *118*(1), 9-18. https://doi.org/10.1182/blood-2010-08-265892

Lakshmipriya, T., Gopinath, S. C., & Tang, T. H. (2016). Biotin-Streptavidin Competition Mediates Sensitive Detection of Biomolecules in Enzyme Linked Immunosorbent Assay. *PLoS One*, *11*(3), e0151153. https://doi.org/10.1371/journal.pone.0151153

Landrigan, P. J., Fuller, R., Acosta, N. J. R., Adeyi, O., Arnold, R., Basu, N. N., Baldé, A. B., Bertollini, R., Bose-O'Reilly, S., Boufford, J. I., Breysse, P. N., Chiles, T., Mahidol, C., Coll-Seck, A. M., Cropper, M. L., Fobil, J., Fuster, V., Greenstone, M., Haines, A., . . . Zhong, M. (2018). The Lancet Commission on pollution and health. *Lancet*, *391*(10119), 462-512. https://doi.org/10.1016/s0140-6736(17)32345-0

Landwehr, K. R., Hillas, J., Mead-Hunter, R., King, A., O'Leary, R. A., Kicic, A., Mullins, B. J., & Larcombe, A. N. (2022). Toxicity of different biodiesel exhausts in primary human airway epithelial cells grown at air-liquid interface. *The Science of The Total Environment*, *832*, 155016. https://doi.org/10.1016/j.scitotenv.2022.155016

Larigot, L., Juricek, L., Dairou, J., & Coumoul, X. (2018). AhR signaling pathways and regulatory functions. *Biochim Open*, *7*, 1-9. https://doi.org/10.1016/j.biopen.2018.05.001

Lee, H. W., Kang, S. C., Kim, S. Y., Cho, Y. J., & Hwang, S. (2022). Long-term Exposure to PM10 Increases Lung Cancer Risks: A Cohort Analysis. *Cancer Research and Treatment*, *54*(4), 1030-1037. https://doi.org/10.4143/crt.2021.1030

Lenz, A. G., Karg, E., Brendel, E., Hinze-Heyn, H., Maier, K. L., Eickelberg, O., Stoeger, T., & Schmid, O. (2013). Inflammatory and oxidative stress responses of an alveolar epithelial cell line to airborne zinc oxide nanoparticles at the air-liquid interface: a comparison with conventional, submerged cell-culture conditions. *BioMed Research International*, *2013*, 652632. https://doi.org/10.1155/2013/652632

Li, H., Wu, M., & Zhao, X. (2022). Role of chemokine systems in cancer and inflammatory diseases. *MedComm*, *3*(2), e147. https://doi.org/10.1002/mco2.147

Li, N., Xia, T., & Nel, A. E. (2008). The role of oxidative stress in ambient particulate matter-induced lung diseases and its implications in the toxicity of engineered nanoparticles. *Free Radical Biology & Medicine*, *44*(9), 1689-1699. https://doi.org/10.1016/j.freeradbiomed.2008.01.028

Lieber, M., Smith, B., Szakal, A., Nelson-Rees, W., & Todaro, G. (1976). A continuous tumor-cell line from a human lung carcinoma with properties of type II alveolar epithelial cells. *International Journal of Cancer*, *17*(1), 62-70. https://doi.org/10.1002/ijc.2910170110

Lindner, K., Ströbele, M., Schlick, S., Webering, S., Jenckel, A., Kopf, J., Danov, O., Sewald, K., Buj, C., Creutzenberg, O., Tillmann, T., Pohlmann, G., Ernst, H., Ziemann, C., Hüttmann, G., Heine, H., Bockhorn, H., Hansen, T., König, P., & Fehrenbach, H. (2017). Biological effects of carbon black nanoparticles are changed by surface coating with polycyclic aromatic hydrocarbons. *Particle and Fibre Toxicology*, *14*(1), 8. https://doi.org/10.1186/s12989-017-0189-1

Liu, J., Han, X., Zhang, T., Tian, K., Li, Z., & Luo, F. (2023). Reactive oxygen species (ROS) scavenging biomaterials for anti-inflammatory diseases: from mechanism to therapy. *Journal of Hematology & Oncology*, *16*(1), 116. https://doi.org/10.1186/s13045-023-01512-7

Liu, N., Tang, M., & Ding, J. (2020). The interaction between nanoparticles-protein corona complex and cells and its toxic effect on cells. *Chemosphere*, *245*, 125624. https://doi.org/https://doi.org/10.1016/j.chemosphere.2019.125624

Liu, T., Zhang, L., Joo, D., & Sun, S.-C. (2017). NF-κB signaling in inflammation. *Signal Transduction and Targeted Therapy*, *2*(1), 17023. https://doi.org/10.1038/sigtrans.2017.23

Liu, X., Ma, J., Ji, R., Wang, S., Zhang, Q., Zhang, C., Liu, S., & Chen, W. (2021). Biochar Fine Particles Enhance Uptake of Benzo(a)pyrene to Macrophages and Epithelial Cells via Different Mechanisms. *Environmental Science & Technology Letters*, *8*(3), 218-223. https://doi.org/10.1021/acs.estlett.0c00900

Long, C. M., Nascarella, M. A., & Valberg, P. A. (2013). Carbon black vs. black carbon and other airborne materials containing elemental carbon: Physical and chemical distinctions. *Environmental Pollution*, *181*, 271-286. https://doi.org/https://doi.org/10.1016/j.envpol.2013.06.009

Longhin, E., Holme, J. A., Gualtieri, M., Camatini, M., & Øvrevik, J. (2018). Milan winter fine particulate matter (wPM2.5) induces IL-6 and IL-8 synthesis in human bronchial BEAS-2B cells, but specifically impairs IL-8 release. *Toxicol In Vitro*, *52*, 365-373. https://doi.org/10.1016/j.tiv.2018.07.016

Lovinsky-Desir, S., Miller, R. L., Bautista, J., Gil, E. N., Chillrud, S. N., Yan, B., Camann, D., Perera, F. P., & Jung, K. H. (2016). Differences in Ambient Polycyclic Aromatic Hydrocarbon Concentrations between Streets and Alleys in New York City: Open Space vs. Semi-Closed Space. *International Journal of Environmental Research and Public Health*, *13*(1). https://doi.org/10.3390/ijerph13010127

Låg, M., Øvrevik, J., Refsnes, M., & Holme, J. A. (2020). Potential role of polycyclic aromatic hydrocarbons in air pollution-induced non-malignant respiratory diseases. *Respiratory Research*, *21*(1), 299. https://doi.org/10.1186/s12931-020-01563-1

Ma, J. Y., & Ma, J. K. (2002). The dual effect of the particulate and organic components of diesel exhaust particles on the alteration of pulmonary immune/inflammatory responses and metabolic enzymes. *Environmental Carcinogenesis & Ecotoxicology Reviews*, *20*(2), 117-147. https://doi.org/10.1081/gnc-120016202

Martins, L. R. L., Grzech-Leśniak, K., Castro Dos Santos, N., Suárez, L. J., Giro, G., Bastos, M. F., & Shibli, J. A. (2022). Transcription Factor AhR, Cytokines IL-6 and IL-22 in Subjects with and

without Peri-Implantitis: A Case Control-Study. *International Journal of Environmental Research and Public Health*, *19*(12). https://doi.org/10.3390/ijerph19127434

Masih, J., Singhvi, R., Kumar, K., Jain, V. K., & Taneja, A. (2012). Seasonal Variation and Sources of Polycyclic Aromatic Hydrocarbons (PAHs) in Indoor and Outdoor Air in a Semi Arid Tract of Northern India. *Aerosol and Air Quality Research*, *12*(4), 515-525. https://doi.org/10.4209/aaqr.2011.11.0192

Matuszewska, A., & Czaja, M. (2020). The Use of Synchronous Fluorescence Technique in Environmental Investigations of Polycyclic Aromatic Hydrocarbons in Airborne Particulate Matter from an Industrial Region in Poland. In V. Richard (Ed.), *Environmental Emissions* (pp. Ch. 7). IntechOpen. https://doi.org/10.5772/intechopen.92402

Miller, K. P., & Ramos, K. S. (2001). Impact of cellular metabolism on the biological effects of benzo[a]pyrene and related hydrocarbons. *Drug Metabolism Reviews*, *33*(1), 1-35. https://doi.org/10.1081/dmr-100000138

Miller, M. R., Raftis, J. B., Langrish, J. P., McLean, S. G., Samutrtai, P., Connell, S. P., Wilson, S., Vesey, A. T., Fokkens, P. H. B., Boere, A. J. F., Krystek, P., Campbell, C. J., Hadoke, P. W. F., Donaldson, K., Cassee, F. R., Newby, D. E., Duffin, R., & Mills, N. L. (2017). Correction to"Inhaled Nanoparticles Accumulate at Sites of Vascular Disease". *American Chemical Society Nano*, *11*(10), 10623-10624. https://doi.org/10.1021/acsnano.7b06327

Mills, N. L., Miller, M. R., Lucking, A. J., Beveridge, J., Flint, L., Boere, A. J., Fokkens, P. H., Boon, N. A., Sandstrom, T., Blomberg, A., Duffin, R., Donaldson, K., Hadoke, P. W., Cassee, F. R., & Newby, D. E. (2011). Combustion-derived nanoparticulate induces the adverse vascular effects of diesel exhaust inhalation. *European Heart Journal*, *32*(21), 2660-2671. https://doi.org/10.1093/eurheartj/ehr195

Mittal, M., Siddiqui, M. R., Tran, K., Reddy, S. P., & Malik, A. B. (2014). Reactive oxygen species in inflammation and tissue injury. *Antioxidants & Redox Signaling*, *20*(7), 1126-1167. https://doi.org/10.1089/ars.2012.5149

Morawska, L., Keogh, D. U., Thomas, S. B., & Mengersen, K. (2008). Modality in ambient particle size distributions and its potential as a basis for developing air quality regulation. *Atmospheric Environment*, *42*(7), 1617-1628. https://doi.org/https://doi.org/10.1016/j.atmosenv.2007.09.076

Morel, Y., Mermod, N., & Barouki, R. (1999). An autoregulatory loop controlling CYP1A1 gene expression: role of H(2)O(2) and NFI. *Molecular and Cellular Biology*, *19*(10), 6825-6832. https://doi.org/10.1128/mcb.19.10.6825

Murphy, G., Jr., Rouse, R. L., Polk, W. W., Henk, W. G., Barker, S. A., Boudreaux, M. J., Floyd, Z. E., & Penn, A. L. (2008). Combustion-derived hydrocarbons localize to lipid droplets in respiratory

cells. *American Journal of Respiratory Cell and Molecular Biology*, *38*(5), 532-540. https://doi.org/10.1165/rcmb.2007-0204OC

Murray, R. Z., & Stow, J. L. (2014). Cytokine Secretion in Macrophages: SNAREs, Rabs, and Membrane Trafficking. *Frontiers in Immunology*, *5*, 538. https://doi.org/10.3389/fimmu.2014.00538

Obot, C. J., Morandi, M. T., Beebe, T. P., Hamilton, R. F., & Holian, A. (2002). Surface components of airborne particulate matter induce macrophage apoptosis through scavenger receptors. *Toxicology and Applied Pharmacology*, *184*(2), 98-106.

Oesch, F., Fabian, E., & Landsiedel, R. (2019). Xenobiotica-metabolizing enzymes in the lung of experimental animals, man and in human lung models. *Archives of Toxicology*, *93*(12), 3419-3489. https://doi.org/10.1007/s00204-019-02602-7

Pan, X., Qin, P., Liu, R., & Yu, W. (2022). Molecular mechanism of coating carbon black nanoparticles with polycyclic aromatic hydrocarbons on the binding to serum albumin and the related cytotoxicity. *Journal of Molecular Liquids*, *356*, 119013. https://doi.org/https://doi.org/10.1016/j.molliq.2022.119013

Patwa, A., & Shah, A. (2015). Anatomy and physiology of respiratory system relevant to anaesthesia. *Indian Journal of Anaesthesia*, *59*(9), 533-541. https://doi.org/10.4103/0019-5049.165849

Penn, A., Murphy, G., Barker, S., Henk, W., & Penn, L. (2005). Combustion-derived ultrafine particles transport organic toxicants to target respiratory cells. *Environmental Health Perspectives*, *113*(8), 956-963. https://doi.org/10.1289/ehp.7661

Penning, T. M., Burczynski, M. E., Hung, C.-F., McCoull, K. D., Palackal, N. T., & Tsuruda, L. S. (1999). Dihydrodiol Dehydrogenases and Polycyclic Aromatic Hydrocarbon Activation: Generation of Reactive and Redox Active o-Quinones. *Chemical Research in Toxicology*, *12*(1), 1-18. https://doi.org/10.1021/tx980143n

Piekarska, K. (2010). Mutagenicity of airborne particulates assessed by salmonella assay and the SOS chromotest in Wrocław, Poland. *Journal of the Air & Waste Management Association*, *60*(8), 993-1001. https://doi.org/10.3155/1047-3289.60.8.993

Podechard, N., Lecureur, V., Le Ferrec, E., Guenon, I., Sparfel, L., Gilot, D., Gordon, J. R., Lagente, V., & Fardel, O. (2008). Interleukin-8 induction by the environmental contaminant benzo(a)pyrene is aryl hydrocarbon receptor-dependent and leads to lung inflammation. *Toxicology Letters*, *177*(2), 130-137. https://doi.org/10.1016/j.toxlet.2008.01.006

Qazi, F., Shahsavari, E., Prawer, S., Ball, A. S., & Tomljenovic-Hanic, S. (2021). Detection and identification of polyaromatic hydrocarbons (PAHs) contamination in soil using intrinsic fluorescence. *Environmental Pollution*, *272*, 116010. https://doi.org/https://doi.org/10.1016/j.envpol.2020.116010

Refsnes, M., Skuland, T., Jørgensen, R., Sæter-Grytting, V., Snilsberg, B., Øvrevik, J., Holme, J. A., & Låg, M. (2023). Role of different mechanisms in pro-inflammatory responses triggered by traffic-derived particulate matter in human bronchiolar epithelial cells. *Particle and Fibre Toxicology*, *20*(1), 31. https://doi.org/10.1186/s12989-023-00542-w

Renn, O., & Roco, M. C. (2006). Nanotechnology and the need for risk governance. *Journal of Nanoparticle Research*, *8*(2), 153-191. https://doi.org/10.1007/s11051-006-9092-7

Rothen-Rutishauser, B., Blank, F., Mühlfeld, C., & Gehr, P. (2008). In vitro models of the human epithelial airway barrier to study the toxic potential of particulate matter. *Expert Opinion on Drug Metabolism & Toxicology*, *4*(8), 1075-1089. https://doi.org/10.1517/17425255.4.8.1075

Rothen-Rutishauser, B., Gibb, M., He, R., Petri-Fink, A., & Sayes, C. M. (2023). Human lung cell models to study aerosol delivery - considerations for model design and development. *European Journal of Pharmaceutical Sciences*, *180*, 106337. https://doi.org/10.1016/j.ejps.2022.106337

Ryu, Y., Roh, S., & Joung, Y. S. (2023). Assessing the cytotoxicity of aerosolized carbon black and benzo[a]pyrene with controlled physical and chemical properties on human lung epithelial cells. *Scientific Reports*, *13*(1), 9358. https://doi.org/10.1038/s41598-023-35586-7

Schiwy, A., Brinkmann, M., Thiem, I., Guder, G., Winkens, K., Eichbaum, K., Nüßer, L., Thalmann, B., Buchinger, S., Reifferscheid, G., Seiler, T.-B., Thoms, B., & Hollert, H. (2015). Determination of the CYP1A-inducing potential of single substances, mixtures and extracts of samples in the micro-EROD assay with H4IIE cells. *Nature Protocols*, *10*(11), 1728-1741. https://doi.org/10.1038/nprot.2015.108

Schober, W., Belloni, B., Lubitz, S., Eberlein-König, B., Bohn, P., Saritas, Y., Lintelmann, J., Matuschek, G., Behrendt, H., & Buters, J. (2006). Organic extracts of urban aerosol (< or =PM2.5) enhance rBet v 1-induced upregulation of CD63 in basophils from birch pollen-allergic individuals. *Toxicological Sciences*, *90*(2), 377-384. https://doi.org/10.1093/toxsci/kfj092

Shen, B. Q., Finkbeiner, W. E., Wine, J. J., Mrsny, R. J., & Widdicombe, J. H. (1994). Calu-3: a human airway epithelial cell line that shows cAMP-dependent Cl- secretion. *American journal of physiology*, *266*(5), L493-501. https://doi.org/10.1152/ajplung.1994.266.5.L493

Sherwood, E. R., & Toliver-Kinsky, T. (2004). Mechanisms of the inflammatory response. *Best practice & Reseach: Clinical anaesthesiology*, *18*(3), 385-405. https://doi.org/10.1016/j.bpa.2003.12.002

Shi, H., Liu, J., & Gao, H. (2021). Benzo(α)pyrene induces oxidative stress and inflammation in human vascular endothelial cells through AhR and NF-κB pathways. *Microvascular Research*, *137*, 104179. https://doi.org/10.1016/j.mvr.2021.104179

Shiizaki, K., Kawanishi, M., & Yagi, T. (2017). Modulation of benzo[a]pyrene-DNA adduct formation by CYP1 inducer and inhibitor. *Genes and Environment*, *39*, 14. https://doi.org/10.1186/s41021-017-0076-x

Shivanna, B., Jiang, W., Wang, L., Couroucli, X. I., & Moorthy, B. (2011). Omeprazole attenuates hyperoxic lung injury in mice via aryl hydrocarbon receptor activation and is associated with increased expression of cytochrome P4501A enzymes. *Journal of Pharmacology and Experimental Therapeutics*, *339*(1), 106-114. https://doi.org/10.1124/jpet.111.182980

Shvedova, A. A., Pietroiusti, A., Fadeel, B., & Kagan, V. E. (2012). Mechanisms of carbon nanotube-induced toxicity: focus on oxidative stress. *Toxicology and Applied Pharmacology*, *261*(2), 121-133. https://doi.org/10.1016/j.taap.2012.03.023

Singh, D. K., Kawamura, K., Yanase, A., & Barrie, L. A. (2017). Distributions of Polycyclic Aromatic Hydrocarbons, Aromatic Ketones, Carboxylic Acids, and Trace Metals in Arctic Aerosols: Long-Range Atmospheric Transport, Photochemical Degradation/Production at Polar Sunrise. *Environmental Science & Technology*, *51*(16), 8992-9004. https://doi.org/10.1021/acs.est.7b01644

Spurny, K. R. (1998). On the physics, chemistry and toxicology of ultrafine anthropogenic, atmospheric aerosols (UAAA): new advances. *Toxicology Letters*, *96-97*, 253-261. https://doi.org/10.1016/s0378-4274(98)00080-0

Sracic, M. K. (2016). Modeled regional airway deposition of inhaled particles in athletes at exertion. *Journal of Aerosol Science*, *99*, 54-63. https://doi.org/https://doi.org/10.1016/j.jaerosci.2015.12.007

Srogi, K. (2007). Monitoring of environmental exposure to polycyclic aromatic hydrocarbons: a review. *Environmental Chemistry Letters*, *5*(4), 169-195. https://doi.org/10.1007/s10311-007-0095-0

Steiner, S., Bisig, C., Petri-Fink, A., & Rothen-Rutishauser, B. (2016). Diesel exhaust: current knowledge of adverse effects and underlying cellular mechanisms. *Archives of Toxicology*, *90*(7), 1541-1553. https://doi.org/10.1007/s00204-016-1736-5

Steiner, S., Czerwinski, J., Comte, P., Müller, L. L., Heeb, N. V., Mayer, A., Petri-Fink, A., & Rothen-Rutishauser, B. (2013). Reduction in (pro-)inflammatory responses of lung cells exposed in vitro to diesel exhaust treated with a non-catalyzed diesel particle filter. *Atmospheric Environment*, *81*, 117-124. https://doi.org/https://doi.org/10.1016/j.atmosenv.2013.08.029

Stejskalova, L., Dvorak, Z., & Pavek, P. (2011). Endogenous and exogenous ligands of aryl hydrocarbon receptor: current state of art. *Current Drug Metabolism*, *12*(2), 198-212. https://doi.org/10.2174/138920011795016818

Stetefeld, J., McKenna, S. A., & Patel, T. R. (2016). Dynamic light scattering: a practical guide and applications in biomedical sciences. *Biophysical Reviews*, *8*(4), 409-427. https://doi.org/10.1007/s12551-016-0218-6

Stoeger, T., Reinhard, C., Takenaka, S., Schroeppel, A., Karg, E., Ritter, B., Heyder, J. P. D., & Schulz, H. (2005). Instillation of Six Different Ultrafine Carbon Particles Indicates a Surface Area Threshold Dose for Acute Lung Inflammation in Mice. *Environmental Health Perspectives*, *114*, 328 - 333.

Svendsen, E. R., Yeatts, K. B., Peden, D., Orton, S., Alexis, N. E., Creason, J., Williams, R., & Neas, L. (2007). Circulating neutrophil CD14 expression and the inverse association of ambient particulate matter on lung function in asthmatic children. *Annals of Allergy, Asthma & Immunology*, *99*(3), 244-253. https://doi.org/10.1016/s1081-1206(10)60660-6

Swanson, H. I. (2002). DNA binding and protein interactions of the AHR/ARNT heterodimer that facilitate gene activation. *Chemico-Biological Interactions*, *141*(1), 63-76. https://doi.org/https://doi.org/10.1016/S0009-2797(02)00066-2

Tabatabaei, M. S., & Ahmed, M. (2022). Enzyme-Linked Immunosorbent Assay (ELISA). *Methods in Molecular Biology*, *2508*, 115-134. https://doi.org/10.1007/978-1-0716-2376-3_10

Takano, H., Yanagisawa, R., Ichinose, T., Sadakane, K., Inoue, K., Yoshida, S., Takeda, K., Yoshino, S., Yoshikawa, T., & Morita, M. (2002). Lung expression of cytochrome P450 1A1 as a possible biomarker of exposure to diesel exhaust particles. *Archives of Toxicology*, *76*(3), 146-151. https://doi.org/10.1007/s00204-002-0323-0

Terzano, C., Di Stefano, F., Conti, V., Graziani, E., & Petroianni, A. (2010). Air pollution ultrafine particles: toxicity beyond the lung. *European Review for Medical and Pharmacological Sciences*, *14*(10), 809-821.

Totlandsdal, A. I., Cassee, F. R., Schwarze, P., Refsnes, M., & Låg, M. (2010). Diesel exhaust particles induce CYP1A1 and pro-inflammatory responses via differential pathways in human bronchial epithelial cells. *Particle and Fibre Toxicology*, *7*, 41. https://doi.org/10.1186/1743-8977-7-41

Totlandsdal, A. I., Herseth, J. I., Bølling, A. K., Kubátová, A., Braun, A., Cochran, R. E., Refsnes, M., Ovrevik, J., & Låg, M. (2012). Differential effects of the particle core and organic extract of diesel exhaust particles. *Toxicology Letters*, *208*(3), 262-268. https://doi.org/10.1016/j.toxlet.2011.10.025

Totlandsdal, A. I., Låg, M., Lilleaas, E., Cassee, F., & Schwarze, P. (2015). Differential proinflammatory responses induced by diesel exhaust particles with contrasting PAH and metal content. *Environmental Toxicology*, *30*(2), 188-196. https://doi.org/10.1002/tox.21884

Totlandsdal, A. I., Refsnes, M., & Låg, M. (2010). Mechanisms involved in ultrafine carbon black-induced release of IL-6 from primary rat epithelial lung cells. *Toxicology in Vitro*, *24*(1), 10-20. https://doi.org/10.1016/j.tiv.2009.09.016

Totlandsdal, A. I., Refsnes, M., Skomedal, T., Osnes, J. B., Schwarze, P. E., & Låg, M. (2008). Particle-induced cytokine responses in cardiac cell cultures--the effect of particles versus soluble mediators released by particle-exposed lung cells. *Toxicological Sciences*, *106*(1), 233-241. https://doi.org/10.1093/toxsci/kfn162

Totlandsdal, A. I., Øvrevik, J., Cochran, R. E., Herseth, J. I., Bølling, A. K., Låg, M., Schwarze, P., Lilleaas, E., Holme, J. A., & Kubátová, A. (2014). The occurrence of polycyclic aromatic hydrocarbons and their derivatives and the proinflammatory potential of fractionated extracts of diesel exhaust and wood smoke particles. *Journal of Environmental Science and Health*, *49*(4), 383-396. https://doi.org/10.1080/10934529.2014.854586

Turner, M. D., Nedjai, B., Hurst, T., & Pennington, D. J. (2014). Cytokines and chemokines: At the crossroads of cell signalling and inflammatory disease. *International Journal of Biochemistry and Biophysics*, *1843*(11), 2563-2582. https://doi.org/10.1016/j.bbamcr.2014.05.014

Turrens, J. F. (2003). Mitochondrial formation of reactive oxygen species. *Journal of Physiology*, *552*(Pt 2), 335-344. https://doi.org/10.1113/jphysiol.2003.049478

Valderrama, A., Ortiz-Hernández, P., Agraz-Cibrián, J. M., Tabares-Guevara, J. H., Gómez, D. M., Zambrano-Zaragoza, J. F., Taborda, N. A., & Hernandez, J. C. (2022). Particulate matter (PM(10)) induces in vitro activation of human neutrophils, and lung histopathological alterations in a mouse model. *Scientific Reports*, *12*(1), 7581. https://doi.org/10.1038/s41598-022-11553-6

Vijayalakshmi, K. P., & Suresh, C. H. (2008). Theoretical studies on the carcinogenicity of polycyclic aromatic hydrocarbons. *Journal of Computational Chemistry*, *29*(11), 1808-1817. https://doi.org/10.1002/jcc.20939

VITROCELL. (n.d.). *VITROCELL® Cloud Alpha 6. How the Vitrocell Cloud works*. https://www.vitrocell.com/inhalation-toxicology/exposure-systems/vitrocell-cloud-system/vitrocell-cloud-alpha-6/

Westerholm, R. N., Almen, J., Li, H., Rannug, J. U., Egebaeck, K. E., & Graegg, K. (1991). Chemical and biological characterization of particulate-, semivolatile-, and gas-phase-associated compounds in diluted heavy-duty diesel exhausts: a comparison of three different semivolatile-phase samplers. *Environmental Science & Technology*, *25*(2), 332-338. https://doi.org/10.1021/es00014a018

Whitby, K. T. (1978). The physical characteristics of sulfur aerosols. *Atmospheric Environment*, *12*(1), 135-159. https://doi.org/https://doi.org/10.1016/0004-6981(78)90196-8

Whitsett, J. A., Wert, S. E., & Weaver, T. E. (2010). Alveolar surfactant homeostasis and the pathogenesis of pulmonary disease. *Annual Review of Medicine*, *61*, 105-119. https://doi.org/10.1146/annurev.med.60.041807.123500

Wong, P. S., Vogel, C. F., Kokosinski, K., & Matsumura, F. (2010). Arylhydrocarbon receptor activation in NCI-H441 cells and C57BL/6 mice: possible mechanisms for lung dysfunction. *American Journal of Respiratory Cell and Molecular Biology*, *42*(2), 210-217. https://doi.org/10.1165/rcmb.2008-0228OC

Wong, W., Farr, R., Joglekar, M., Januszewski, A., & Hardikar, A. (2015). Probe-based Real-time PCR Approaches for Quantitative Measurement of microRNAs. *Journal of Visualized Experiments*(98). https://doi.org/10.3791/52586

World Health Organization. (2021). *WHO global air quality guidelines: Particulate matter (PM2.5 and PM10), ozone, nitrogen dioxide, sulfur dioxide and carbon monoxide.* int.ezproxy.uio.no/publications/i/item/9789240034228

Yamada, M., Fujino, N., & Ichinose, M. (2016). Inflammatory responses in the initiation of lung repair and regeneration: their role in stimulating lung resident stem cells. *Inflammation and Regeneration*, *36*(1), 15. https://doi.org/10.1186/s41232-016-0020-7

Yang, L., Zhang, L., Zhang, H., Zhou, Q., Zhang, X., Xing, W., Takami, A., Sato, K., Shimizu, A., Yoshino, A., Kaneyasu, N., Matsuki, A., Hayakawa, K., Toriba, A., & Tang, N. (2020). Comparative Analysis of PM(2.5)-Bound Polycyclic Aromatic Hydrocarbons (PAHs), Nitro-PAHs (NPAHs), and Water-Soluble Inorganic Ions (WSIIs) at Two Background Sites in Japan. *International Journal of Environmental Research and Public Health*, *17*(21). https://doi.org/10.3390/ijerph17218224

Zhang, L. P., Zhang, X., Duan, H. W., Meng, T., Niu, Y., Huang, C. F., Gao, W. M., Yu, S. F., & Zheng, Y. X. (2017). Long-term exposure to diesel engine exhaust induced lung function decline in a cross sectional study. *Industrial Health*, *55*(1), 13-26. https://doi.org/10.2486/indhealth.2016-0031

Zhang, Z., Zhang, L., Zhou, L., Lei, Y., Zhang, Y., & Huang, C. (2019). Redox signaling and unfolded protein response coordinate cell fate decisions under ER stress. *Redox Biology*, *25*, 101047. https://doi.org/https://doi.org/10.1016/j.redox.2018.11.005

Zhao, J., Li, M., Wang, Z., Chen, J., Zhao, J., Xu, Y., Wei, X., Wang, J., & Xie, J. (2019). Role of PM(2.5) in the development and progression of COPD and its mechanisms. *Respiratory Research*, *20*(1), 120. https://doi.org/10.1186/s12931-019-1081-3

Zhu, Y., Chidekel, A., & Shaffer, T. H. (2010). Cultured human airway epithelial cells (calu-3): a model of human respiratory function, structure, and inflammatory responses. *Critical Care Research and Practice*, *2010*. https://doi.org/10.1155/2010/394578

Øvrevik, J., Låg, M., Lecureur, V., Gilot, D., Lagadic-Gossmann, D., Refsnes, M., Schwarze, P. E., Skuland, T., Becher, R., & Holme, J. A. (2014). AhR and Arnt differentially regulate NF-κB signaling and chemokine responses in human bronchial epithelial cells. *Cell Communication and Signaling*, *12*, 48. https://doi.org/10.1186/s12964-014-0048-8

Øvrevik, J., Refsnes, M., Låg, M., Holme, J. A., & Schwarze, P. E. (2015). Activation of Proinflammatory Responses in Cells of the Airway Mucosa by Particulate Matter: Oxidant- and Non-Oxidant-Mediated Triggering Mechanisms. *Biomolecules*, *5*(3), 1399-1440. https://doi.org/10.3390/biom5031399

8 Appendices

Appendix A

Table A1. Reagents, chemicals, and equipment used in the study.

Kits	Manufacturer
alarmarBlue™ assay	Invitrogen, Life Technologies Ltd, UK
Cytotoxicity Detection Kit (LDH)	Roche Diagnostics, Mannheim, Germany
IL-6 Cytoset	Invitrogen, Life Technologies Ltd, UK
IL-8 Cytoset	Invitrogen, Life Technologies Ltd, UK
RNeasy miniprep kit	Qiagen GmbH, Hilden, Germany
High-Capacity cDNA Achive kit	Applied Biosystems, CA, USA
DC™ protein assay	BioRad, Hercules, CA, USA
Primers/probes for RT-qpcr	
IL-6 primer/probe	Thermofischer, Waltham, MA, USA
IL-8 primer/probe	Thermofischer, Waltham, MA, USA
CYP1A1 primer/probe	Thermofischer, Waltham, MA, USA
GAPDH	Thermofischer, Waltham, MA, USA
Universal PCR mastermix (Taqman®)	Thermofischer, Waltham, MA, USA
Chemicals	
HEPES	Gibco, Waltham, MA, USA
FCS	Euroclone, Pero, Italy
FBS	Euroclone, Pero, Italy
Penicilin	Gibco, Waltham, MA, USA
Streptomycin	Gibco, Waltham, MA, USA
Non-essental amino acids	Gibco, Waltham, MA, USA
Gentamycin solution	Gibco, Waltham, MA, USA
Na-pyruvate	Sigma-Aldrich, St. Louis, MO, USA
DPBS	Gibco, Waltham, MA, USA
HBSS	Gibco, Waltham, MA, USA
PMA	Merck, Burlington, MA, USA
Accutase	Sigma-Aldrich, St. Louis, MO, USA
Albumin bovine serum (BSA)	Sigma-Aldrich, St. Louis, MO, USA
Trypsin-EDTA	Gibco, Waltham, MA, USA
Triton X-100	Merck, Burlington, MA, United States
B-mercaptoethanol	Sigma-Aldrich, St. Louis, MO, USA
3,3’,5,5’-Tetramethylbenzidine (TMB)	Merck, Burlington, MA, USA
H2O2	Merck, Burlington, MA, USA
Tween 20	Sigma-Aldrich, St. Louis, MO, USA
NaCl	Merck, Whitehouse Station, NJ USA
Tryptan blue Dye 0.4 %	Gibco, Waltham, MA, USA
DMSO	Sigma-Aldrich, St. Louis, MO, USA
Methanol	POCH S.A, Sowinskiego 11, Poland
7-etoxyresorufin	Santa Cruz Biotechnology, Inc., Heidelberg, Germany
Resorufin	Santa Cruz Biotechnology, Inc., Heidelberg, Germany

Table A1 continued

Instuments	
Sunrise Absorbance Reader	Tecan, Männedorf, Switzerland
Clariostar plate reader	BMG Labtech, Ortenberg, Germany
Ultrasonic sonicator	Elma Schmidbauer GmbH, Singen, Germany
LUNA II automated cell counter	Logos Biosystems, Annandale, USA
NanoDrop2000	Thermo Fisher Scientific Inc., Rockford, USA
VITROCELL® Cloud alpha 6 exposure system	Vitrocell, Waldkirch, Germany
CFX96 Touch Real-Time PCR Detection System	BioRad, Hercules, CA, USA
Zetasizer-nano	Malvern Instrument Ltd , UK
Microscope, Zeis LSM510 Meta confocal	Carl Zeiss S.p.A, Italy
Equipments	
Microtiter plates	Nunc A/S, Roskilde, Denmark
Cell culture bottles	Nunc A/S, Roskilde, Denmark
6-well plates	Greiner Bio-One, Kremsmünster, Austria
6-well Thincert® Cell Culture Inserts	Greiner Bio-One, Kremsmünster, Austria
Hard-shell PCR 96-well plates	BioRad, Hercules, CA, USA

Appendix B

Solutions used in the study

Solutions for ELISA

Diluent buffer (Invitrogen, Life technologies)

BSA	5 g
Tween 20	1 ml
DPBS	1000 ml

Blocking solution (Invitrogen, Life techonolgies)

BSA	5 g
DPBS	1000 ml

Citrate buffer

Sodium acetate trihydrate	3 g
Distilled water	200 ml

Citric acid is used to adjust pH to 5.5

TMB solution

Citrate buffer	11 ml
TMB 6 mg/ml	200 µg
30 % H_2O_2	2.2 µl

Stop solution

H2SO4 50 ml

Distilled water 1000 ml

Mastermix for cDNA synthesis

10 x reverse buffer 2.5 µl

25x dNTP 1 µl 10x random primers 2.5 µl

Multiscribe reverse transcriptase 1.25 µl

Nuclease free water 5.25 µl

Appendix C

Table C1 Percentage (%) cytotoxicity/cell viability compared to mean control (mean±SD) in monocultures measured by AlarmarBlue assay after 20 h exposure.

Cell line:	Calu-3		A549		Ea.Hy		THP-1	
P90 (µg/mL)	mean	SD	mean	SD	mean	SD	mean	SD
0	102,772	15,490	100,486	0,668	93,690	0,213	98,781	0,439
12.5	88,532	14,637	102,888	2,166	102,087	1,066	97,801	3,222
25	87,640	15,259	101,559	1,406	95,286	2,027	96,229	4,754
50	87,924	10,972	98,985	3,368	79,556	5,788	96,437	4,514
100	82,062	10,178	93,854	5,325	62,722	0,184	88,374	10,796
200	77,042	16,720	72,735	11,445	40,383	4,067	74,504	13,292
P90+B[a]P (µg/mL)	mean	SD	mean	SD	mean	SD	mean	SD
0	97,228	18,590	99,514	2,981	106,310	12,130	101,219	5,494
12.5	86,861	12,167	99,927	1,166	98,120	15,234	93,446	2,033
25	84,439	17,487	96,796	3,123	96,669	11,187	93,475	2,665
50	76,463	12,623	81,555	16,572	96,325	22,052	94,769	9,115
100	71,049	16,608	75,264	14,396	78,144	7,975	86,540	7,723
200	60,331	11,829	52,288	15,579	65,919	17,774	87,378	3,388

Table C1 continued

Cell line:	Calu-3		A549		Ea.Hy		THP-1	
B[a]P (µM)	mean	SD	mean	SD	mean	SD	mean	SD
0	100,000	26,196	100,000	1,394	100,000	0,105	100,000	0,358
0.05	100,534	24,040	101,087	2,754	98,879	3,064	97,549	3,073
0.1	101,786	26,300	101,645	1,619	98,988	3,331	100,365	3,264
0.2	107,354	30,891	92,202	11,305	97,174	3,672	99,948	1,894
0.6	91,200	19,295	84,623	23,913	96,892	3,103	98,423	1,629
2	94,830	25,501	86,714	20,405	95,181	5,591	100,087	7,676
Cell line:	Calu-3		Ea.Hy		THP-1			
P90+Pyr (µg/mL)	mean	SD	mean	SD	mean	SD		
0	100,000	26,082	100,000	10,238	100,000	5,427		
12.5	84,531	10,968	91,932	11,517	92,321	2,009		
25	88,599	16,636	95,468	11,238	92,349	2,633		
50	86,304	6,259	95,612	12,452	93,628	9,006		
100	85,491	11,064	87,316	5,657	85,498	7,630		
200	11,505	1,782	91,318	7,026	86,326	3,347		

Table C2 Percentage (%) cytotoxicity compared to control (mean±SD) in monocultures measured by LDH assay after 20 h exposure.

Cell line:	Calu-3		A549		Ea.Hy		THP-1	
P90 (µg/mL)	mean	SD	mean	SD	mean	SD	mean	SD
0	5,375	1,527	7,561	1,340	16,535	5,911	59,373	16,300
12.5	5,238	1,394	7,963	1,467	18,719	6,854	60,809	16,518
25	5,591	1,550	8,523	1,129	20,033	7,174	60,666	16,141
50	5,999	1,609	9,315	1,148	24,105	8,261	63,145	15,708
100	6,114	1,241	12,889	3,415	32,748	10,915	63,052	15,823
200	5,786	1,320	22,864	11,707	47,053	15,714	64,702	14,411
P90+B[a]P (µg/mL)	mean	SD	mean	SD	mean	SD	mean	SD
0	5,321	1,239	7,776	1,441	13,590	2,386	63,535	19,946
12.5	5,893	0,722	8,233	1,545	13,960	2,225	60,929	16,677
25	5,357	1,392	8,546	1,217	14,641	1,936	61,580	16,669
50	5,744	1,371	15,364	10,427	15,950	2,469	62,871	18,315
100	5,623	1,447	18,135	11,829	17,433	1,664	64,651	17,253
200	5,383	1,550	26,062	18,204	29,824	8,065	66,062	16,426
B[a]P (µM)	mean	SD	mean	SD	mean	SD	mean	SD
0	6,757	4,340	7,755	1,007	13,510	6,882	51,002	20,916
0.05	7,168	4,715	8,065	1,143	13,894	7,108	52,440	25,649
0.1	7,372	4,832	8,094	1,422	14,070	7,480	54,510	25,156
0.2	7,493	4,667	15,891	14,828	16,465	4,418	54,960	24,717
0.6	7,156	4,651	18,086	18,795	16,594	4,840	54,193	24,651
2	7,897	5,418	17,788	17,769	17,497	4,346	57,349	27,467
Cell line:	Calu-3		Ea.Hy		THP-1			
P90+Pyr (µg/mL)	mean	SD	mean	SD	mean	SD		
0	5,613	1,077	13,536	2,145	62,412	19,798		
12.5	5,703	0,532	13,374	1,895	64,304	18,954		
25	5,489	1,321	13,688	2,108	62,179	17,083		
50	5,650	1,622	15,158	3,571	62,796	18,516		
100	5,733	1,598	15,608	3,695	62,515	17,882		
200	5,861	1,394	16,627	4,115	65,191	15,512		

Table C3 Relative IL-6 concentration (mean±SD) in monocultures measured by ELISA after 20 h exposure.

Cell line:	Calu-3		A549		Ea.Hy	
P90 (µg/mL)	mean	SD	mean	SD	mean	SD
0	392,102	234,091	5,438	2,604	60,043	13,105
12.5	390,458	228,130	4,164	1,743	92,014	24,167
25	372,342	203,679	3,516	3,799	122,526	25,433
50	388,810	179,198	5,436	5,411	168,068	40,448
100	435,443	210,620	10,229	6,888	256,808	42,101
200	439,987	218,355	18,985	13,723	436,620	115,143
P90+B[a]P (µg/mL)	mean	SD	mean	SD	mean	SD
0	404,165	158,262	12,791	8,281	61,443	21,211
12.5	358,955	135,504	13,072	8,406	67,149	22,386
25	382,282	173,725	6,106	5,266	77,503	19,938
50	353,767	166,054	5,529	3,115	91,388	29,390
100	377,637	197,700	5,444	1,853	108,500	36,264
200	349,812	168,939	3,525	0,747	136,934	47,791
B[a]P (µM)	mean	SD	mean	SD	mean	SD
0	51,381	27,675	5,828	5,330	37,743	6,088
0.05	51,186	25,188	8,730	6,928	35,185	7,127
0.1	68,799	30,690	6,267	4,475	37,069	1,801
0.2	81,335	43,277	9,056	6,235	36,879	6,983
0.6	123,338	80,748	11,152	12,817	38,045	6,003
2	134,237	44,701	7,005	4,526	42,548	7,609
0.6	123,338	80,748	11,152	12,817	38,045	6,003
2	134,237	44,701	7,005	4,526	42,548	7,609

Cell line:	Calu-3		Ea.Hy	
P90+Pyr (µg/mL)	mean	SD	mean	SD
0	394,148	178,558	64,051	20,728
12.5	388,372	152,317	70,699	21,024
25	360,532	174,991	71,497	19,073
50	349,775	152,502	81,563	22,695
100	346,253	158,873	79,073	22,449
200	379,215	112,588	87,046	24,245

Table C4 Relative CXCL8 concentration (mean±SD) in monocultures measured by ELISA after 20 h exposure.

Cell line:	Calu-3		A549		Ea.Hy		THP-1	
P90 (µg/mL)	mean	SD	mean	SD	mean	SD	mean	SD
0	5832,700	3755,956	586,342	155,225	384,583	156,243	67,976	26,581
12.5	5417,750	2411,884	697,698	283,873	663,025	184,863	92,669	43,718
25	5635,567	3240,778	780,175	209,607	932,843	167,641	87,223	27,076
50	5650,333	3342,814	802,875	98,978	1248,050	297,470	93,694	23,601
100	2817,930	2300,132	1111,277	169,800	1897,700	219,544	112,045	51,504
200	4995,917	2100,475	1675,533	221,914	2969,833	444,180	119,836	46,823
P90+B[a]P (µg/mL)	mean	SD	mean	SD	mean	SD	mean	SD
0	5898,633	3360,332	659,737	285,522	355,123	137,948	73,986	18,086
12.5	5103,133	1877,856	667,007	205,752	410,128	111,979	72,436	19,100
25	4044,967	2391,280	796,435	350,260	445,410	106,106	82,128	34,978
50	4921,400	3035,269	941,860	650,034	485,772	111,766	95,794	38,932
100	4296,150	2221,703	980,937	590,074	574,170	118,393	103,277	54,448
200	4146,133	1819,462	1074,117	597,099	849,555	210,815	137,250	88,928
B[a]P (µM)	mean	SD	mean	SD	mean	SD	mean	SD
0	5228,900	2673,030	460,777	150,421	149,549	109,255	29,120	4,922
0.05	5385,250	2827,767	524,685	174,991	142,827	75,698	43,561	11,391
0.1	5984,417	3081,154	510,440	213,510	147,103	55,095	44,434	15,496
0.2	7091,000	3699,959	635,352	428,795	214,960	151,283	45,509	9,258
0.6	7330,967	4168,896	812,065	845,997	211,948	166,032	44,519	9,488
2	7986,533	4209,268	709,788	722,318	216,975	138,343	102,357	77,268

Cell line:	Calu-3		Ea.Hy		THP-1	
P90+Pyr (µg/mL)	mean	SD	mean	SD	mean	SD
0	4777,200	2154,955	339,390	163,378	73,438	31,031
12.5	4680,600	2060,761	372,382	164,096	79,294	22,511
25	5276,150	2743,794	386,007	166,382	71,153	9,892
50	6725,817	4392,916	367,077	145,971	97,522	23,995
100	10188,900	9832,284	336,387	138,464	108,880	18,520
200	8271,900	6362,597	317,145	163,044	142,208	29,288

Table C5 Relative IL-6 concentration (mean±SD) in 3D cultures measured by ELISA after 3 and 6 h exposure.

3D model:	Calu-3 (apical)		Calu-3 (basolateral)		A459 (apical)		A549 (basolateral)	
3 hours	mean	SD	mean	SD	mean	SD	mean	SD
H2O	342,163	172,531	204,972	151,461	17,401	20,945	69,545	85,171
P90	366,788	88,657	157,962	36,023	7,822	4,621	41,390	25,935
P90+B[a]P	330,712	138,923	118,759	36,965	14,400	16,195	53,472	47,298
B[a]P	825,482	447,766	412,950	223,702	23,629	32,318	72,816	75,251
6 hours								
H2O	391,557	144,097	307,257	137,042	7,689	6,198	73,940	73,718
P90	354,777	35,272	218,843	12,668	3,149	0,532	39,806	3,529
P90+B[a]P	335,925	98,963	159,865	17,810	11,098	8,027	94,972	96,107
B[a]P	749,002	443,213	477,397	235,855	13,359	6,724	110,520	113,285

Table C6 Relative CXCL8 concentration (mean±SD) in 3D cultures measured by ELISA after 3 and 6 h exposure.

3D model:	Calu-3 (apical)		Calu-3 (basolateral)		A459 (apical)		A549 (basolateral)	
3 hours	mean	SD	mean	SD	mean	SD	mean	SD
H2O	752,147	203,239	2016,083	658,996	863,422	687,209	3317,137	2557,004
P90	885,650	259,441	1757,303	576,011	525,643	94,282	2919,470	1759,466
P90+B[a]P	894,383	177,348	1357,877	506,767	919,258	793,326	3594,207	1869,286
B[a]P	994,752	183,662	1661,737	618,355	1134,307	1329,944	4341,453	3144,135
6 hours								
H2O	965,063	74,620	2908,967	636,068	458,323	365,410	4660,267	2647,257
P90	1009,938	237,511	2521,930	734,982	314,693	86,051	4153,500	197,707
P90+B[a]P	908,417	141,928	2150,993	537,730	574,680	363,020	4991,833	3494,433
B[a]P	916,625	252,150	2212,360	763,456	692,093	371,960	4899,400	2845,904

Table C7 Data from gene expression in 3D cultures estimated by RT-qPCR after 3 and 6 h exposure. Ct values (mean±SD) used in statistical analysis.

Calu-3 (apical)	CYP1A1		CXCL8		IL-6	
3 hours	mean	SD	mean	SD	mean	SD
H2O	33,175	0,857	29,537	2,587	32,972	2,730
P90	33,018	1,685	27,523	1,087	31,311	1,200
P90+B[a]P	32,151	2,197	27,944	1,733	31,626	1,505
B[a]P	24,540	2,696	29,265	3,299	32,390	3,507
Calu-3 (basolateral)						
H2O	29,129	0,754	27,066	1,142	33,617	0,687
P90	29,776	0,091	29,020	0,966	34,711	1,548
P90+B[a]P	28,364	0,181	28,726	0,800	34,220	1,506
B[a]P	27,153	0,668	28,457	1,268	34,594	1,962
Calu-3 (apical)	CYP1A1		CXCL8		IL-6	
6 hours	mean	SD	mean	SD	mean	SD
H2O	30,913	2,528	27,523	1,901	30,702	2,020
P90	33,531	1,687	28,367	0,527	31,746	0,435
P90+B[a]P	32,032	1,695	26,495	1,516	30,414	1,527
B[a]P	23,696	1,264	28,271	1,673	31,355	1,955
Calu-3 (basolateral)						
H2O	32,164	0,976	28,633	0,772	34,409	1,528
P90	30,829	0,380	28,268	1,931	34,030	0,875
P90+B[a]P	30,993	0,544	28,900	1,065	34,474	1,371
B[a]P	28,425	0,115	28,827	1,682	34,048	1,195

Table C7 continued

A549 (apical)	CYP1A1		CXCL8		IL-6	
3 hours	mean	SD	mean	SD	mean	SD
H2O	36,813	0,964	26,049	0,088	36,530	1,138
P90	37,607	0,779	25,196	1,474	35,221	4,966
P90+B[a]P	36,485	1,118	26,232	0,232	36,700	1,575
B[a]P	27,060	0,765	25,927	0,683	36,243	1,728
A549 (basolateral)						
H2O	30,761	2,939	26,843	0,777	33,811	1,235
P90	31,961	3,383	25,832	1,989	32,426	4,015
P90+B[a]P	31,643	3,920	25,613	0,105	33,950	1,460
B[a]P	27,921	0,442	26,223	0,252	35,073	1,827
A549 (apical)	CYP1A1		CXCL8		IL-6	
6 hours	mean	SD	mean	SD	mean	SD
H2O	35,830	1,369	26,705	0,944	37,496	2,109
P90	37,567	1,192	26,310	0,484	37,097	2,691
P90+B[a]P	37,482	0,842	26,614	0,786	37,776	1,885
B[a]P	28,898	1,010	26,491	0,557	36,662	1,700
A549 (basolateral)						
H2O	31,652	2,750	27,798	0,444	34,702	0,763
P90	33,680	2,607	27,475	1,551	34,273	2,112
P90+B[a]P	33,405	2,390	27,797	0,694	35,443	1,560
B[a]P	29,196	1,207	26,856	0,034	34,334	0,683